Advances in soil genesis and morphology and their impact on the water cycle

Aaron Nathaniel Koop

Submitted to the graduate degree program in the Department of Geography and Atmospheric Science and the Graduate Faculty of the University of Kansas in partial fulfillment of the requirements for the degree of Doctor of Philosophy.

Committee members

Nathaniel A. Brunsell, Chairperson

Daniel R. Hirmas

Pamela L. Sullivan

Rolfe D. Mandel

Bing Pu

Terrance D. Loecke, External Reviewer

Date defended: April 26, 2022

The Dissertation Committee for Aaron Nathaniel Koop certifies
that this is the approved version of the following dissertation :

Advances in soil genesis and morphology and their impact on the water cycle

Nathaniel A. Brunsell, Chairperson

Date approved: May 5, 2022

Abstract

Broad-scale approaches to soil genesis and morphology and their impact on the water cycle are critically important to address widespread ecosystem service challenges in the future especially given increasing climatic and land-use pressures on soils. Thus, the general aim of this dissertation was to quantify pedogenic development and examine the impact of soil properties and soil-climate interactions on the water cycle at continental, basin, and ecoregion scales. I utilized continental-scale data to develop and evaluate horizon and profile development indices based primarily on relative horizon properties instead of parent material information. These indices—which reflect generalizable pedogenic processes—are valid proxies of soil development applicable at large geographic scales and may aid in numerous broad-scale applications including pedogenic modeling, use in pedotransfer functions, identification of anomalies, and estimation of surface soil ages, and have the potential to address the impact of climate and land-use changes on pedogenesis. Combined effects of near-surface soil organic carbon (SOC) and ped roundness were used to explain systematic differences in long-term water balance (as represented within the Budyko framework) at a continental scale and explore potentially important feedbacks to climate. Evidence presented across basins of the conterminous US point to the need to include soil structural information in Earth system models. Effective porosity (EP) determined from continental and ecoregion-stratified data show that surface and subsurface macroporosity is strongly influenced by the fraction of clay complexed with SOC. The relationship between EP and this fraction could serve as a framework for understanding soil macropore sensitivity to additions of SOC and its incorporation into hydrologic and Earth system models has the potential to more effectively predict land use- and climate-induced changes to soil hydraulic properties and alterations to water cycling across scales. These findings, associated implications, and future research directions are explored.

Acknowledgements

First, I want to express sincere thanks to my advisors, Dan Hirmas and Pam Sullivan. They have provided steadfast guidance and encouragement in navigating through all aspects of this research and I am grateful for the opportunity to learn from them. I also appreciate Nate Brunsell taking on the role of my department advisor for the last several years. I have a great committee which also includes Rolfe Mandel, Bing Pu, and Terry Loecke, and I have benefitted from their insights while taking courses taught by them and throughout various stages of my dissertation. Many thanks go to each of them for their support, patience, and flexibility during the years undertaking this project.

I also want to acknowledge the support and funding provided by the Department of Geography and Atmospheric Science that also allowed me to gain experience teaching while working on my dissertation. Throughout the last several years I appreciated Pam and Dan's invitations to join their research groups for discussion and a collaborative exchange of thoughts and ideas. I especially want to thank Dan, Pam, Sharon Billings, Hoori Ajami, Lejo Flores, Li Li, Hang Wen, Xi Zhang, and Katie Murenbeeld for their insights shared during group meetings. Thanks also go to Aoesta Rudick for her contributions to Chapter 2 of my dissertation.

I am sincerely and deeply thankful to my parents, Faye and Cleo, and my Koop family, as well as my father-in-law, Jerry, and the Regier family, for their love and support throughout my studies. I especially want to acknowledge my wife, Melanie, for her love and support in helping me persevere through challenging aspects of this project and life in general—you are my rock and I love you. To my kids, Ella and Everett, each time you came around the corner into my office it provided me with a perfect reprieve and the uplifting boost I needed to keep going—I love you both. Finally, as I was completing this dissertation I was reminded of how my Grandpa Sprunger passed down his awe of the natural world and all of its intricacies to my Mom and she passed it down to me—this dissertation is in remembrance of them.

Contents

List of Figures

List of Tables

Chapter 1

Introduction

Advances in our understanding of soil genesis and morphology and their impact on the water cycle are critically important in the current context of increasing climatic and land-use pressures on soils. These advances are especially needed to quantify the impact of these pressures on ecosystem services (e.g., water storage, food security; Janzen et al., 2011). Pedogenic investigations (including those focused on ecosystem services such as water cycling; e.g., infiltration, leaching, evapotranspiration) have often involved either empirical approaches (see Yaalon, 1975; Birkeland, 1999; Schaetzl and Thompson, 2015) or mechanistic approaches (see Hoosbeek and Bryant, 1992; Hoosbeek et al., 2000; Minasny et al., 2008; Bockheim and Gennadiyev, 2010; Vereecken et al., 2016) that have been very useful for decades. However, empirical models have often lacked a theoretical framework limiting their extrapolation to environments outside the region in which they were developed, and mechanistic models that simulate soil processes have often required calibration of empirical parameters that restricts their usefulness outside the regions in which they were calibrated (Koop et al., 2020). To bridge gaps between these approaches and expand their usefulness, large continental-scale datasets (e.g., Critical Zone Observatories [CZO], National Ecological Observatory Network [NEON]) can be used to examine the influence of broad-scale processes and/or properties on ecosystems. For example, recent applications of broad-scale soil datasets have provided a better understanding of climatic and lithologic controls on soil structural development at continental scales (Panakoulia et al., 2017; Hirmas et al., 2018; Mohammed et al., 2020). Large datasets have also been used to develop generic machine learning-based pedotransfer functions for estimating saturated hydraulic conductivity (K_{sat}) and the sensitivity of K_{sat} to soil structure (Araya & Ghezzehei, 2019). Recent efforts to incorporate the effect of soil structure on hydraulic prop-

erties in land-surface and Earth system models have also been undertaken (Fatichi et al., 2020). Despite these advances, quantifying and predicting the development of soil heterogeneity across a broad range of spatial and temporal scales including components such as soil structural dynamics and preferential flow paths remains a challenge (Vereecken et al., 2016). In light of these efforts, Chapters 2-4 of this dissertation involve broad-scale approaches to soil genesis and morphology with the last two examining the impact of soil properties and their interaction with climate on the water cycle at continental, basin, and ecoregion scales. In total, Chapters 2-4 included analyses of varying subsets of 57,171 horizons from 8,980 pedons (static soils data; approximately late 1960s to the present).

In Chapter 2, I explore and develop generalizable indices of soil development applicable at broad geographic scales in order to lay the groundwork for investigating pedogenic processes at a continental scale. Horizon and profile development indices (HDIs and PDIs, respectively), integrating multiple soil properties, were developed and formalized by Bilzi & Ciolkosz (1977), Harden (1982), and Harden & Taylor (1983) and extensively and effectively used for decades at regional and local scales. However, it can be argued that the greatest limitation to generalizability of these indices is their reliance on parent material information which causes problems with extrapolation outside of the regions in which they were developed and in many soil profiles there is often a lack of access to C horizons (i.e., a proxy for parent material) or remnants of the actual parent material. Therefore, constructing a theoretical foundation for soil development index generalizability and developing a generalizable HDI and PDI that rely primarily on relative horizon properties instead of parent material information are key components of this work. The developed index was applied to a large dataset of soil properties, assessed against taxonomic information and weathering indices, and potential applications of generalizable HDIs and PDIs were explored. One of the applications of these generalizable indices may be their inclusion in pedogenic modeling efforts exploring broad-scale quantitative relationships between soil development, chemical weathering, and climate. In addition, since these indices are independent of parent material, the PDI could be used as a covariate to adjust regression models in broad-scale studies examining the

influence of climate, lithology, or land use on ecosystem services or serve as a variable by which to stratify sampling efforts to minimize known sources of variability in soil investigations. These applications have the potential to bridge gaps and address some of the challenges inherent in varying approaches to quantifying and predicting soil development at continental and regional scales.

Chapter 3 and 4 focus on the impact of soil development and morphology on the water cycle. Chapter 3 focuses on analyzing relationships between near-surface soil properties and scatter within the Budyko space. Although the Budyko framework (Budyko, 1974) established a method for partitioning precipitation into runoff and evapotranspiration as a function of aridity, after decades of research, the most relevant factors controlling the ratio of evapotranspiration to precipitation (ET/P) and the long-term water balance (other than aridity) remains unclear, especially across large spatial scales (Greve et al., 2015; Padrón et al., 2017; Berghuijs et al., 2020). In this chapter I explore which soil properties are most relevant and important to controlling the long-term land-atmosphere water cycle across basins at a continental scale. This work was undertaken in an effort to bridge gaps in our understanding of the role of soils in systematically explaining differences in ET/P.

Emerging evidence at plot, hillslope, and continental scales indicate that soil structural changes are occurring on yearly to decadal timescales in response to shifts in precipitation regimes (Robinson et al., 2016; Hirmas et al., 2018; Caplan et al., 2019). Chapter 4 builds upon these findings to shed light on why more humid conditions appear to promote reductions in both macroporosity and K_{sat} while drier conditions promote an increase in these properties. Specifically, I explore the properties (soil, root, and climate) and mechanisms that control macroporosity in both surface and subsurface horizons under varying land use and management practices across ecoregions of the conterminous US. This research was undertaken with the goal of determining the properties and processes controlling soil structural development and macroporosity that have disproportionate effects on K_{sat} with important implications on water storage, flux, and, thus, the water cycle (Hirmas et al., 2018). In sum, the combination of these studies aim to advance our understanding of soil genesis and morphology and their impact on the water cycle through broad-scale approaches

that have the potential to address widespread ecosystem service challenges in the future. Finally, Chapter 5 summarizes key findings, associated implications, and future research directions.

Chapter 2

A generalizable index of soil development

Koop, A. N., Hirmas, D. R., Sullivan, P. L., & Mohammed, A. K. (2020). A generalizable index of soil development. *Geoderma*, 360, 113898.

Abstract

The growing influence of climatic and land-use pressures on soils across broad geographic extents have revealed a need for generalizable indices of soil development applicable at continental scales. In this study, we present generalizable horizon and profile development indices (HDIs and PDIs, respectively) based primarily on relative horizon properties instead of parent material information and provide an evaluation of these indices at a continental scale. The indices developed in this work combine knowledge of pedogenic processes with selected properties from a large database of predominantly US soils to yield relevant soil morphological, physical, and chemical information on 57,171 horizons arising from 8,980 pedons. We selected four properties from which the generalizable HDI and PDI calculations were based: particle size, calcium carbonate equivalent (CCE), color, and clay films. Modified z-scores were used to assess relative changes between either eluvial and illuvial horizons for particle size and CCE or surface and subsurface horizons for color. These values were then normalized using maximum and minimum values observed in the dataset. Normalized clay film scores were calculated using percent cover along with ordinal values assigned to distinctness categories described in the field. The index values from HDI compared well to both diagnostic horizon designations and chemical index of alteration and PDI values matched the sequence of taxonomic soil orders that represent a development gradient. In addition,

we observed a correspondence between calculated PDIs and a clay mineralogy index representing weathering intensity. Relationships between these generalizable indices, evaluation metrics, and climate (i.e., MAP) explored in this work opens the door to numerous broad-scale applications in the future such as pedogenic modeling, identification of soil anomalies, and estimation of surface soil ages.

2.1 Introduction

Continental-scale, generalizable indices of soil development are needed to elucidate how accelerating climatic and land use changes impact ecosystem services (e.g., water storage, food security; Janzen et al., 2011). The development of these indices is especially relevant in light of recent findings highlighting climate-induced changes in continental-scale soil properties (e.g., Hirmas et al., 2018) and the emergence of large, broad-scale soil and environmental datasets (e.g., Critical Zone Observatories [CZO] and the National Ecological Observatory Network [NEON]). These large datasets provide ample opportunities to explore the integration of multiple soil properties related to pedogenic development at horizon and profile scales across broad geographic extents.

Horizon and profile development indices (HDIs and PDIs, respectively), integrating multiple soil properties, were developed and formalized by Bilzi & Ciolkosz (1977), Harden (1982), and Harden & Taylor (1983), and have been widely used in pedogenic investigations for decades. These indices originated from the need to quantify the collective nature and process of pedogenesis (Harden, 1982; Harden & Taylor, 1983; Birkeland, 1999) and have primarily consisted of weight-averaging normalized scores of various morphological information (e.g., texture, color, ped/void surface features) to represent pedogenic development of either a horizon or a profile in a compact numerical value. Studies using development indices have typically benefited from a wealth of soil morphological information and the ease and versatility provided by integrative semi-quantification of qualitative morphological data. In addition, researchers have combined field-based morphological data with analytical laboratory-based soil data (e.g., physical, chemical, or mineralogical data) into a single development index (e.g., Busacca, 1987; Harrison et al., 1990; Alonso et al., 1994) as

well as kept morphological and analytical indices separate for purposes of comparison and use in soil analyses (e.g., Birkeland, 1984; Birkeland & Burke, 1988; Rodbell, 1990; Harden et al., 1991; Dorronsoro & Alonso, 1994).

At regional and localized scales, these development indices have been validated through general comparisons with soil taxonomy (e.g., Phillips, 1990; Tsai et al., 2007b; Badía et al., 2009; Zielhofer et al., 2009) and statistical analyses of these relationships (e.g., Schaetzl & Mokma, 1988; Verheyen et al., 2001; Calero et al., 2008; Tsai et al., 2016). Development indices have also been used extensively in regional and localized soil chronosequence and soil-geomorphic studies in a variety of contexts including alluvial terraces (e.g., Meixner & Singer, 1981; Busacca, 1987; McFadden & Weldon II, 1987; Dorronsoro & Alonso, 1994; García-García et al., 2016), marine and lake terraces and ridges (e.g., Barrett & Schaetzl, 1993; Huang et al., 2010; May et al., 2015), and alluvial fans and colluvial settings (e.g., Harden & Matti, 1989; Reheis et al., 1989; Berry, 1990; Amit et al., 1996; Turk et al., 2008). In addition, these indices have also been used in geomorphic contexts including glacial outwash and till (e.g., Swanson, 1985; Berry, 1987, 1994; Applegarth & Dahms, 2001; Munroe & Bockheim, 2001), residuum (e.g., Lybrand & Rasmussen, 2015), and loess (e.g., McFadden et al., 1986; Hirmas & Allen, 2007; Layzell et al., 2016).

A number of regional and localized soil chronosequence and soil-geomorphic studies using HDIs and PDIs have also been extended to consider soil development under different climatic conditions (e.g., Harden & Taylor, 1983; McFadden et al., 1986; Miller & Birkeland, 1992; Birkeland, 1994; Lybrand & Rasmussen, 2015) and across geomorphic surfaces in tectonic settings (e.g., Harden & Matti, 1989; Amit et al., 1996; Kendrick & McFadden, 1996; McCalpin & Berry, 1996; Tsai et al., 2007a). Research efforts have also incorporated HDIs and PDIs into pedogenic modeling including regional chronofunctions (e.g., Birkeland, 1984; Reheis et al., 1989; Rodbell, 1990; Alonso et al., 1994; Vidic & Lobnik, 1997), maximum likelihood estimates relating soil development to age (e.g., Switzer et al., 1988; Harden et al., 1991), and deterministic chaos approaches (e.g., Phillips, 1993) (see Bockheim, 1990; Schaetzl et al., 1994; Vidic, 1998; Sauer, 2010, for reviews of models incorporating development indices).

Given the extensive and effective use of soil development indices at regional and localized scales, the development of a generalizable index applicable at a broad geographic scale would be a logical next step in order to investigate pedogenic processes at a continental scale. Here we argue that the greatest limitation to generalizability of these indices, however, is their reliance on parent material information. This is due to problems with extrapolating these indices to environments outside of the region in which they were developed, and because, in many cases, neither C horizons (i.e., a proxy for parent material) nor remnants of the actual parent material are present, although there have been efforts to overcome these limitations (e.g., Bilzi & Ciolkosz, 1977). For example, Langley Turnbaugh & Evans (1994), developed an index that used morphological and micromorphological properties instead of parent material and used it in a paleopedology study to distinguish soil from sediment. Similarly, Schaetzl & Mokma (1988) developed a podzolization index which calculated color differences between E and B horizons without dependence on parent material information. Although they applied their indices to only either paleosols or a specific soil order, these studies highlight the potential for developing a generalizable index independent of parent material information.

The goal of this work, therefore, was to develop a generalizable HDI and PDI that relies primarily on relative horizon properties instead of parent material information. Specific objectives were to (1) construct a theoretical foundation for soil development index generalizability, (2) develop the index based on this foundation and apply it to a large dataset of soil properties, (3) assess the index against taxonomic information and weathering indices, and (4) explore potential applications of generalizable HDIs and PDIs.

2.2 Theory

In order to develop a generalizable index for soil development, we selected commonly recorded soil properties that were assumed to be closely related to pedogenic processes and readily available in large soil datasets. Here, the term *properties* refers to the measured or recorded physical (e.g., particle size), chemical (e.g., calcium carbonate), and morphological (e.g., color, clay films)

attributes of genetically-related soil horizons. These properties can be described by various features which we refer to as *property characteristics*. For example, clay films (soil property) can be described by two property characteristics—distinctness of the clay films observed in the field and their amount (i.e., the percentage of visible surface area covered by clay films).

In the framework of this study, a score (*S*) refers to an individual property that is calculated from either a single characteristic or a combination of characteristics. The *S* for a given horizon can be normalized by either an empirical *S* maximum and minimum or a theoretical *S* maximum to generate a HDI between 0 and 1 (Harden, 1982; Harden & Taylor, 1983). The HDIs of the soil horizons comprising a soil profile can then be depth-weighted and divided by the thickness of the whole profile to generate a PDI representing the pedon.

2.2.1 Principles guiding the selection of properties

In this study, several guiding principles were followed in selecting properties for this generalizable index of soil development. These principles can be articulated as follows:

- Properties selected for the index should have a known relationship to pedogenic development. For example, soil structure was not included in this index because its general relationship with soil development is unknown.
- Property characteristics should reflect a continuous change in pedogenic development where only those characteristics that have known or assumed monotonic relationships with pedogenic development should be used.
- Characteristics should be selected to avoid redundant descriptions of the same property thereby preserving sensitivity of each characteristic to pedogenic development. For example, in this study, only the amount and distinctness of clay films were selected as property characteristics while clay film color was excluded from the index in order to avoid redundancy. This is because color is implicitly used when assigning distinctness. Additionally, clay film color should be avoided since the characteristic does not have a clear relationship with pedogenic

development.

- Property characteristics that are sensitive to the differences between descriptions arising from describers who either tend to lump or split horizons (aka “lumper” vs. “splitter”) should be avoided. For example, one characteristic of soil particle-size distributions that might be useful to a pedogenic development index is the particle-size gradient between adjacent horizons (e.g., the change in clay content divided by the distance between horizon midpoint depths). However, this characteristic should be avoided because it would be sensitive to variations in the number of horizons assigned by different describers of the same pit.

In addition to these principles, if the goal of the index is to (at least partly) examine the depth distribution of soil development, then care should be taken to select properties or characteristics for which a HDI can be calculated. Characteristics that are better understood as attributes of a pedon rather than a horizon, such as a parameter describing the rate of change of soil organic carbon with depth or an index of profile anisotropy (Walker & Green, 1976), should be avoided since these would be calculated across multiple horizons. Given these principles, we selected particle-size distribution (geometric mean particle diameter), pedogenic carbonate (calcium carbonate equivalent, CCE), soil color (CIELAB L* and a* values), and clay films (amount and distinctness of clay films, clay bridges, or organoargillans) as the properties used to develop this generalizable index. These properties were selected since they both aligned with above mentioned principles and were readily available in the dataset used in this study. Calculation of scores for each property are discussed in detail in the sections below.

2.2.2 Soil property scores

2.2.2.1 Particle-size distribution

As pedogenesis proceeds, upper layers of the soil column lose fine particles as percolating meteoric waters translocate and concentrate them at depth (Birkeland, 1999). In addition, secondary minerals form preferentially within the clay size fraction at the low temperature and pressure en-

vironments near the Earth's surface further differentiating the mean particle size of eluvial surface horizons from illuvial subsurface horizons (Cremeens & Mokma, 1986). Thus, by examining the relative differences between these two horizon types (i.e., eluvial and illuvial), rather than comparing a horizon to the particle size of the parent material as is typically done in most development indices, a generalizable index can be created that is theoretically independent of the parent material (e.g., Cremeens & Mokma, 1986). In this study, we use the geometric mean particle diameter of eluvial and illuvial horizons to calculate an index of particle size development.

Particle-size distributions are often reported as compositional class data (e.g., the mass fraction of clay, coarse silt, medium sand, etc.). In order to convert these data into numeric values representing particle size, the geometric mean particle diameters, $\{d_1, d_2, \ldots, d_j, \ldots, d_m\}$, corresponding to the lower, $\{l_1, l_2, \ldots, l_j, \ldots, l_m\}$, and upper, $\{u_1, u_2, \ldots, u_j, \ldots, u_m\}$, particle diameters at the boundaries of the respective particle-size class bins can be calculated as:

$$d_j = \exp\left[\frac{\ln[l_j + a] + \ln[u_j + a]}{2}\right] \tag{2.1}$$

where a is a constant added to the boundary of each size bin to avoid taking the logarithm of zero at the minimum boundary of the smallest size bin and m is the total number of particle-size bins recorded for a horizon. The geometric mean was used as opposed to other central tendency values (e.g., arithmetic mean or median) both because particle sizes are commonly log-normally distributed and to account for the full-range of information in the fine-earth particle size distribution (e.g., as opposed to just using clay content). These d_j values can be used to calculate the geometric mean particle diameter of the ith horizon, D_i, using Eq. 2.2:

$$D_i = \exp\left[\frac{\sum_{j=1}^{m} f_j \ln d_j}{\sum_{j=1}^{m} f_j}\right] \tag{2.2}$$

where f_j is the particle mass or volume fraction of the jth particle-size bin.

Using reference particle diameters, it is possible to assess the relative change between eluvial (E) and illuvial (I) horizons. For instance, eluvial horizons can be compared against the depth-weighted mean particle diameter of the illuvial horizons, ${}^{I}\overline{D}$, and illuvial horizons against the depth-weighted mean particle diameter of eluvial horizons, ${}^{E}\overline{D}$, both of which can be calculated as:

$$ {}^{E}\overline{D} = \frac{\sum_{k=1}^{n} t_k D_k}{\sum_{k=1}^{n} t_k} \quad \text{or} \quad {}^{I}\overline{D} = \frac{\sum_{g=1}^{p} t_g D_g}{\sum_{g=1}^{p} t_g} \tag{2.3} $$

where t_k and t_g refer to the kth eluvial and gth illuvial horizon thickness, respectively, and D_k and D_g represent the geometric mean particle diameters of the kth eluvial and gth illuvial horizon, respectively. In Eq. 2.3 above, n is the total number of eluvial horizons and p is the total number of illuvial horizons in the profile. Horizons that have been morphologically described as A and E horizons are eluvial with respect to particle size since these horizons leach clay-size particles to lower horizons. By contrast, B horizons are illuvial since fines translocate to and accumulate within these horizons (Turk et al., 2012).

Using D_i, ${}^{E}\overline{D}$, and ${}^{I}\overline{D}$, a modified depth-weighted standard deviation of the geometric mean particle diameter for the combined eluvial and illuvial horizons in the profile, $\tilde{s}_D$, can be calculated following Bevington & Robinson (2003):

$$ \tilde{s}_D = \sqrt{\frac{N \sum_{i=1}^{N} t_i (D_i - {}^{h}\overline{D})^2}{(N-1) \sum_{i=1}^{N} t_i}} \tag{2.4} $$

and used to calculate the distance, $\tilde{z}_{D_i}$, of the particle-size value of the ith horizon from its reference particle diameter in modified standard deviation units as:

$$ \tilde{z}_{D_i} = \frac{D_i - {}^{h}\overline{D}}{\tilde{s}_D} \tag{2.5} $$

In the above equations, N is the total number of horizons in the pedon, t_i is the thickness of the ith horizon, and h represents either dominantly eluvial or illuvial horizons as appropriate. That is, in the calculation of $\tilde{s}_D$, when D_i corresponds to an eluvial horizon, ${}^{E}\overline{D}$ is used; when D_i corresponds to an illuvial horizon, ${}^{I}\overline{D}$ is used. However, in the calculation of $\tilde{z}_{D_i}$, when D_i corresponds to an eluvial horizon, ${}^{I}\overline{D}$ is used as the reference particle diameter; when D_i corresponds to an illuvial horizon, ${}^{E}\overline{D}$ is used as the reference particle diameter. C horizons are not included in the calculation of ${}^{I}\overline{D}$ or $\tilde{s}_D$ since these horizons are little affected by soil formation processes (Buol et al., 2011). However, $\tilde{z}_{D_i}$ can be calculated for C horizons using the ${}^{E}\overline{D}$ as a reference. In addition, we note that the $\tilde{z}_{D_i}$ represents a modified z-score differing slightly in how the means and standard deviations are calculated from the normal meaning of a z-score.

The $\tilde{z}$-scores can be used to generate a score from the geometric mean particle diameter of the ith horizon, S_{D_i}, for horizons in a profile described as dominantly A, E, B, or C horizons as follows:

$$S_{D_i} = \begin{cases} \tilde{z}_{D_i} & : \text{ horizon } i \text{ is A or E and } \tilde{z}_{D_i} > 0 \\ -\tilde{z}_{D_i} & : \text{ horizon } i \text{ is B or C and } \tilde{z}_{D_i} < 0 \\ 0 & : \text{ otherwise} \end{cases} \tag{2.6}$$

Finally, a HDI can be calculated for particle size, HDI_{D_i}, using an empirical S_D maximum and minimum in a large dataset to scale the S_{D_i} value for a given horizon between 0 and 1 following Eq. 2.7:

$$\text{HDI}_{D_i} = \frac{\log S_{D_i} - \min(\log S_D)}{\max(\log S_D) - \min(\log S_D)} \tag{2.7}$$

where $\max(S_D)$ is two standard deviations above and $\min(S_D)$ is two standard deviations below the mean value for a distribution of log-transformed S_{D_i} values in the dataset. S_{D_i} values are log-transformed to reduce skewness and approximate a normal distribution. Two standard deviations above and below the mean are used as a maximum and minimum, respectively, because the majority of the data ($> 94\%$) fall between these values. Values below or above the minimum or maximum S_D scores were assigned values of 0 or 1, respectively. Generalizability of this HDI

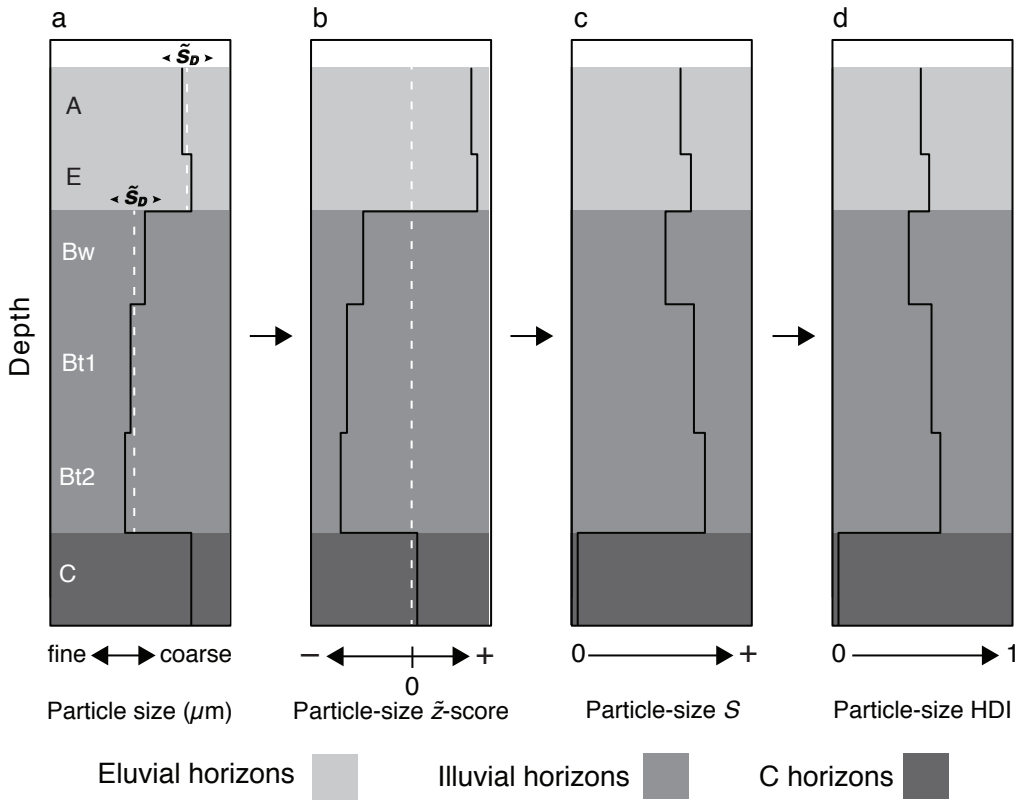

Figure 2.1: For this hypothetical example of particle size, (a) the particle size of each horizon as well as mean particle sizes of eluvial and illuvial horizons (Eq. 2.3) can be used to calculate a modified standard deviation ($\tilde{s}_D$; Eq. 2.4). (b) This information can be used to generate modified $\tilde{z}$-scores (Eq. 2.5) that are then (c) scored (S) as shown in Eq. 2.6. (d) Finally, a horizon development index (HDI) for particle size can be calculated using empirical maximum and minimum scores in a large dataset to scale the value for a given horizon between 0 and 1 (Eq. 2.7).

should be proportional to the degree that the dataset (from which the $\max[S_D]$ and $\min[S_D]$ are determined) represents a broad geographic and taxonomic distribution of soils. Figure 2.1 shows a hypothetical example of the progression from particle size to the HDI for this property as outlined in the calculations above.

2.2.2.2 Pedogenic carbonate

As with particle-size distributions, a similar eluvial-illuvial relationship occurs with respect to the leaching and removal of carbonate and its accumulation at depth in areas that lack sufficient effective precipitation to leach carbonate completely through the soil column (Turk et al., 2012). This

eluvial depletion and illuvial accumulation of carbonate in soils presents an opportunity to examine relative differences in carbonate content between these types of horizons rather than relying on parent material information to calculate accumulation indices as in previous studies (e.g., Harden et al., 1991; Hall & Shroba, 1995). Using reference CCE values, eluvial horizons can be compared against the depth-weighted mean CCE of illuvial horizons and vice versa. The depth-weighted mean CCE of eluvial horizons, ${}^{E}\overline{\text{CCE}}$, and the depth-weighted mean CCE of illuvial horizons, ${}^{I}\overline{\text{CCE}}$, can be calculated as:

$$ {}^{E}\overline{\text{CCE}} = \frac{\sum_{k=1}^{n} t_k \text{CCE}_k}{\sum_{k=1}^{n} t_k} \quad \text{or} \quad {}^{I}\overline{\text{CCE}} = \frac{\sum_{g=1}^{p} t_g \text{CCE}_g}{\sum_{g=1}^{p} t_g} \tag{2.8} $$

where t_k, t_g, n, and p are defined in Eq. 2.3, CCE_k is the CCE of the kth eluvial horizon, and CCE_g is the CCE of the gth illuvial horizon. Morphological descriptions of A, E, and B horizons without a subordinate distinction of "k" or "kk" in the horizon name occurring in soils that have visible accumulations of $CaCO_3$ in the profile are considered eluvial with respect to CCE as these horizons leach carbonate to lower horizons. By contrast, B or C horizons that have been described with "k" or "kk" subordinate distinctions are illuvial with respect to CCE due to the accumulation of carbonate within these horizons (Buol et al., 2011).

A modified depth-weighted standard deviation of the CCE for the combined eluvial and illuvial horizons in a profile, $\tilde{s}_{\text{CCE}}$, can be calculated similar to Eq. 2.4 as:

$$ \tilde{s}_{\text{CCE}} = \sqrt{\frac{N \sum_{i=1}^{N} t_i (\text{CCE}_i - {}^{h}\overline{\text{CCE}})^2}{(N-1) \sum_{i=1}^{N} t_i}} \tag{2.9} $$

and used to calculate the distance of the CCE value of the ith horizon from its reference CCE in

modified standard deviation units as:

$$\tilde{z}_{\mathrm{CCE}_i} = \frac{\mathrm{CCE}_i - {}^{h}\overline{\mathrm{CCE}}}{\tilde{s}_{\mathrm{CCE}}} \tag{2.10}$$

where N, t_i, and h are defined previously (Eq. 2.4). As mentioned above, h represents either dominantly eluvial or illuvial horizons as appropriate. That is, in the calculation of $\tilde{s}_{\mathrm{CCE}}$, when CCE_i corresponds to an eluvial horizon, ${}^{E}\overline{\mathrm{CCE}}$ is used; when CCE_i corresponds to an illuvial horizon, ${}^{I}\overline{\mathrm{CCE}}$ is used. In the calculation of $\tilde{z}_{\mathrm{CCE}_i}$, however, when CCE_i corresponds to an eluvial horizon, ${}^{I}\overline{\mathrm{CCE}}$ is used as the reference CCE value; when CCE_i corresponds to an illuvial horizon, ${}^{E}\overline{\mathrm{CCE}}$ is used as the reference CCE value. C horizons without a subordinate designation of "k" are not included in the calculation of ${}^{I}\overline{\mathrm{CCE}}$ or $\tilde{s}_{\mathrm{CCE}}$ since these horizons exhibit little or no pedogenic alteration. However, $\tilde{z}_{\mathrm{CCE}_i}$ can be calculated for C horizons using the ${}^{E}\overline{\mathrm{CCE}}$ as a reference.

These $\tilde{z}$-scores can be used to calculate a development score from the CCE of the ith horizon, S_{CCE_i}, for horizons comprising a profile described as dominantly A, E, B, or C horizons as follows:

$$S_{\mathrm{CCE}_i} = \begin{cases} -z_{\mathrm{CCE}_i} & : \text{ horizon } i \text{ is A, E, or B without "k" or "kk" and } \tilde{z}_{\mathrm{CCE}_i} < 0 \\ z_{\mathrm{CCE}_i} & : \text{ horizon } i \text{ is Bk, Bkk, or Ck and } \tilde{z}_{\mathrm{CCE}_i} > 0 \\ 0 & : \text{ otherwise} \end{cases} \tag{2.11}$$

A HDI can be calculated for CCE, $\mathrm{HDI}_{\mathrm{CCE}_i}$, using an empirical S_{CCE} maximum and minimum in a large dataset to scale the S_{CCE_i} value for a given horizon between 0 and 1 as follows:

$$\mathrm{HDI}_{\mathrm{CCE}_i} = \frac{\log S_{\mathrm{CCE}_i} - \min(\log S_{\mathrm{CCE}})}{\max(\log S_{\mathrm{CCE}}) - \min(\log S_{\mathrm{CCE}})} \tag{2.12}$$

where $\max(S_{\mathrm{CCE}})$ represents two standard deviations above and $\min(S_{\mathrm{CCE}})$ two standard deviations below the mean value of a distribution of log-transformed S_{CCE_i} values in the dataset. As mentioned for particle-size distributions, S_{CCE_i} values are log-transformed to reduce skewness and approximate a normal distribution. Since the majority of the data ($> 94\%$) fall between two stan-

dard deviations above and below the mean, these values are used as the maximum and minimum. Values falling below or above the minimum or maximum S_{CCE} were assigned values of 0 or 1, respectively. For pedons that do not record any accumulation of secondary carbonates (i.e., no "k" or "kk" subordinate distinction in any horizon in the profile), $\mathrm{HDI}_{\mathrm{CCE}_i}$ are given NA values to avoid arbitrarily scoring soils low that have non-calcareous parent materials or those whose environments prevent the accumulation of carbonate due to excessive leaching (e.g., humid environments) or a lack of calcareous dust inputs. As discussed for particle-size distributions, generalizability of this HDI should be proportional to the degree that the dataset (from which the $\max[S_{\mathrm{CCE}}]$ and $\min[S_{\mathrm{CCE}}]$ are determined) is representative of a broad distribution of soils.

2.2.2.3 Soil color

Darkening of soil horizons (aka melanization) from the addition of organic matter and humus, occurs when the development of dark, humus-rich coatings on ped faces and mineral grains render horizons dark brown or black in color (Schaetzl & Thompson, 2015). While this melanization process predominantly occurs in A horizons at or near the soil surface, the process of soil reddening (aka rubification) predominantly occurs in subsurface B horizons where brown to red colors generally indicate the release of iron from primary minerals followed by the dispersion of iron oxide particles occurring during pedogenesis (Birkeland, 1999; Schaetzl & Thompson, 2015).

With few exceptions (e.g., Torrent et al., 1983; Schaetzl & Mokma, 1988; Thompson & Bell, 1996), most development indices incorporating color have typically relied on comparing the color of a soil horizon to that of the parent material. However, by comparing the relative differences in color of organic matter-enriched surface horizons against subsurface horizons, a pedogenic development index can be derived without the need to rely on parent material color. This surface-subsurface approach is similar to that of the eluvial-illuvial indices for particle-size distribution and pedogenic carbonate development described above.

In this work, dominant moist matrix Munsell colors of horizons were converted to the CIELAB color space using the Algorithms for Quantitative Pedology (AQP) package (Beaudette et al.,

2013). By converting Munsell color to the CIELAB color space, the L^* (darkening) and a^* (reddening) values can be used to assess melanization and rubification in this surface-subsurface context (Barrón & Torrent, 1986; Turk et al., 2008). Surface horizon L^* values compared against the depth-weighted mean L^* color of subsurface horizons in combination with the a^* values of subsurface horizons compared against the depth-weighted mean a^* color of surface horizons provide a method for scoring pedogenic development as represented by soil color. The depth-weighted mean color of either surface or subsurface horizons can be calculated as:

$$ {}^{A}\overline{x} = \frac{\sum_{k=1}^{n} t_k x_k}{\sum_{k=1}^{n} t_k} \quad \text{or} \quad {}^{EBC}\overline{x} = \frac{\sum_{g=1}^{p} t_g x_g}{\sum_{g=1}^{p} t_g} \tag{2.13} $$

where x refers to either L* or a*, and t_k and t_g refer to the kth A horizon and gth E, B, or C horizon thickness, respectively. Here, the superscript A refers to surface A horizons and EBC refers to subsurface E, B, or C horizons.

Similar to particle-size distribution and pedogenic carbonate, a modified depth-weighted standard deviation of soil color, $\tilde{s}_x$, can be generated for the combined surface and subsurface horizons in a profile and calculated as:

$$ \tilde{s}_x = \sqrt{\frac{N \sum_{i=1}^{N} t_i (x_i - {}^{h}\overline{x})^2}{(N-1) \sum_{i=1}^{N} t_i}} \tag{2.14} $$

Equation 2.14 can be used to calculate the distances of L^* and a^* values of a horizon from each respective reference L^* and a^* in modified standard deviation units representing a soil color score for the ith horizon, S_{c_i}, as:

$$ S_{c_i} = \begin{cases} \frac{{}^{EBC}\overline{\mathrm{L}^*} - \mathrm{L}^*_i}{\tilde{s}_{\mathrm{L}^*}} & : \text{ horizon } i \text{ is A and } \mathrm{L}^*_i < {}^{EBC}\overline{\mathrm{L}^*} \\ \frac{\mathrm{a}^*_i - {}^{A}\overline{\mathrm{a}^*}}{\tilde{s}_{\mathrm{a}^*}} & : \text{ horizon } i \text{ is E, B, or C and } \mathrm{a}^*_i > {}^{A}\overline{\mathrm{a}^*} \\ 0 & : \text{ otherwise} \end{cases} \tag{2.15} $$

where the definitions of the variables in Eq. 2.15 follow from Eqs. 2.13 and 2.14. It is important to note that h in Eq. 2.14 represents either dominantly surface or subsurface horizons as appropriate. That is, in the calculation of $\tilde{s}_x$, when x_i corresponds to a surface horizon, ${}^{A}\overline{x}$ is used; when x_i corresponds to a subsurface horizon, ${}^{EBC}\overline{x}$ is used. However, in the calculation of S_{c_i} in Eq. 2.15, $\mathrm{L}^*{}_i$ corresponds to a dominantly surface horizon (i.e., A horizon) and ${}^{EBC}\overline{\mathrm{L}^*}$ is used as the reference L^* value; conversely, $\mathrm{a}^*{}_i$ corresponds to a dominantly subsurface horizon (i.e., E, B, or C horizon) and ${}^{A}\overline{\mathrm{a}^*}$ is used as the reference a^* value.

A HDI can be calculated for soil color of the ith horizon, HDI_{c_i}, using an empirical S_c maximum and minimum in a large dataset to scale the S_{c_i} value in Eq. 2.15 between 0 and 1 as shown in Eq. 2.16:

$$\mathrm{HDI}_{c_i} = \frac{\log S_{c_i} - \min(\log S_c)}{\max(\log S_c) - \min(\log S_c)} \tag{2.16}$$

where $\max(S_c)$ is two standard deviations above and $\min(S_c)$ is two standard deviations below the mean value for a distribution of log-transformed S_{c_i} values in the dataset. As discussed for particle-size distributions and CCE, S_{c_i} values are log-transformed to reduce skewness and approximate a normal distribution. Two standard deviations above and below the mean are used as a maximum and minimum because most of the data ($> 90\%$) fall between these values. In addition, values below or above the minimum or maximum S_c scores were assigned values of 0 or 1, respectively. As mentioned previously for geometric mean particle diameter and CCE, generalizability of this HDI should be proportional to the degree that the $\max(S_c)$ and $\min(S_c)$ values are representative of a broad distribution of soils.

2.2.2.4 Clay films

As illuvial accumulation of phyllosilicate clays occurs during pedogenesis, this process results in films or coatings of oriented clay on the surfaces of pores or peds, or bridging sand grains (Schaetzl & Thompson, 2015). Since oriented clay films or coatings are generally observable in the field, this morphological property has often been included in soil development indices in a variety of settings (e.g., Harden & Matti, 1989; Vidic & Lobnik, 1997; Tsai et al., 2007b; Sauer, 2010). Here we

follow a similar approach to that of Harden (1982) and Harden & Taylor (1983) and use estimated amounts (% of surface area) and distinctness classes as property characteristics of clay films.

Distinctness of clay films in the *i*th horizon, F_{d_i}, can be scored as:

$$F_{d_i} = \begin{cases} 10 & : \quad \text{horizon } i \text{ has faint clay films} \\ 20 & : \quad \text{horizon } i \text{ has distinct clay films} \\ 30 & : \quad \text{horizon } i \text{ has prominent clay films} \end{cases} \tag{2.17}$$

Scores for clay film amount, $S_{F_{a_i}}$, and clay film distinctness, $S_{F_{d_i}}$, can be calculated for A, E, B, and C horizons as follows:

$$S_{F_{a_i}} = \frac{F_{a_i}}{\max(F_a)} \tag{2.18}$$

$$S_{F_{d_i}} = \frac{F_{d_i}}{\max(F_d)} \tag{2.19}$$

where clay film amount, F_{a_i}, and distinctness, F_{d_i}, are divided by the maximum scores possible for these property characteristics (i.e., $\max(F_a) = 100\%$ and $\max(F_d) = 30$, respectively) to scale the value for a given horizon between 0 and 1. The scores for clay films amount, $S_{F_{a_i}}$, and clay films distinctness, $S_{F_{d_i}}$, can be combined into a HDI for clay films, HDI_{F_i}, by taking the mean of these property characteristic scores. As previously mentioned, the scoring of clay films also includes amount and distinctness of clay bridges and organoargillans where present in the dataset. In addition, it is important to note that if a horizon does not have a "t" subordinate designation nor information on clay films/clay bridges/organoargillans, a HDI_{F_i} of 0 is assigned. If a horizon does have a "t" subordinate designation, but no information on clay films/clay bridges/organoargillans, a HDI_{F_i} of NA is assigned. Lastly, HDI_{F_i} can be calculated from either $S_{F_{a_i}}$ or $S_{F_{d_i}}$ or both by calculating the mean of these property characteristic scores. Given this clay films scoring framework, we selected soil orders of broad geographic extent that are found in areas where environmental conditions would allow for lessivage.

2.2.3 HDI and PDI

Following the logic of Harden (1982), a final HDI of the *i*th horizon, HDI_i, is calculated by taking the mean of the property HDI scores (i.e., HDI_{D_i}, $\text{HDI}_{\text{CCE}_i}$, HDI_{c_i}, HDI_{F_i}) for that horizon. HDIs calculated in this work include scores for only those properties that are recorded for profiles in the dataset with the exception of clay films (see discussion of clay films scoring above); an NA value is given otherwise. The final PDI is calculated by taking the depth-weighted mean of the HDIs as shown in Eq. 2.20:

$$\text{PDI} = \frac{\sum_{i=1}^{n} t_i \text{HDI}_i}{\sum_{i=1}^{n} t_i} \tag{2.20}$$

For reference, see Table 2.1 for an explanation of variables used in this study and Table 2.2 for empirical and theoretical maximum and minimum scores for properties/property characteristics used in the normalization of HDIs. In addition, see Tables A2 and A3 for example calculations of our approach outlined above.

2.3 Methods

2.3.1 Dataset

In this study, we assembled field-based pedon information and laboratory data collected through the USDA NRCS National Cooperative Soil Survey (NCSS). The complex nature of these data files required pre-processing to put them into an easily accessible format. After organizing and cleaning the two datasets, we merged them with climate data from WorldClim 2 (Fick & Hijmans, 2017).

Entisols, Inceptisols, Mollisols, Aridisols, Alfisols, and Ultisols were selected from the dataset; poorly drained soils and soils with lithologic discontinuities were removed. We avoided soil orders with low number of pedons in our dataset, orders that tend to be expressed in more localized environments, or orders that represent unique pedogenic pathways limiting their generalizabilty

Table 2.1: Explanation of variables used in this study listed in order of occurrence.

Variable	Explanation
d	Geometric mean particle diameter of a particle-size class bin
l	Lower particle diameter at the boundary of a particle-size class bin
u	Upper particle diameter at the boundary of a particle-size class bin
a	Constant (0.01) added to the boundary of each particle-size class bin
D	Geometric mean particle diameter of a horizon
f	Particle mass or volume fraction of a particle-size class bin
$\overline{D}$	Depth-weighted mean particle diameter of a horizon
t	Thickness of a horizon
$\tilde{s}$	Modified depth-weighted standard deviation of a property for specified horizons in a profile
h	Represents either dominantly eluvial or illuvial horizons as appropriate
$\tilde{z}$	Modified z-score of a specified horizon property
S	Non-normalized development score of a specified horizon property
HDI	Empirical maximum and minimum-normalized or theoretical maximum-normalized horizon development index
$\max(S)$	Empirical maximum development score of a specified horizon property that is two standard deviations above the mean value for a logged distribution of property scores or theoretical maximum development score of a specified horizon property
$\min(S)$	Empirical minimum development score of a specified horizon property that is two standard deviations below the mean value for a logged distribution of property scores
CCE	Calcium carbonate equivalent of a horizon
$\overline{\text{CCE}}$	Depth-weighted mean CCE of a horizon
x	CIELAB L* or a* color of a horizon
$\overline{x}$	Depth-weighted mean L* or a* color of a horizon
F	Clay films or clay bridges or organoargillans of a horizon
PDI	Depth-normalized profile development index

Table 2.2: Empirical and theoretical maximum scores [max(S)] and minimum scores [min(S)] for properties/property characteristics used to calculate a generalizable horizon development index (HDI) between 0 and 1 in this study.

Property/Property characteristic	**Empirical or theoretical max(S)**	**Empirical or theoretical min(S)**
Particle size	1.46	−1.06
CCE	1.54	−0.45
Color	1.37	−0.92
Clay films amount	100	NA
Clay films distinctness	30	NA

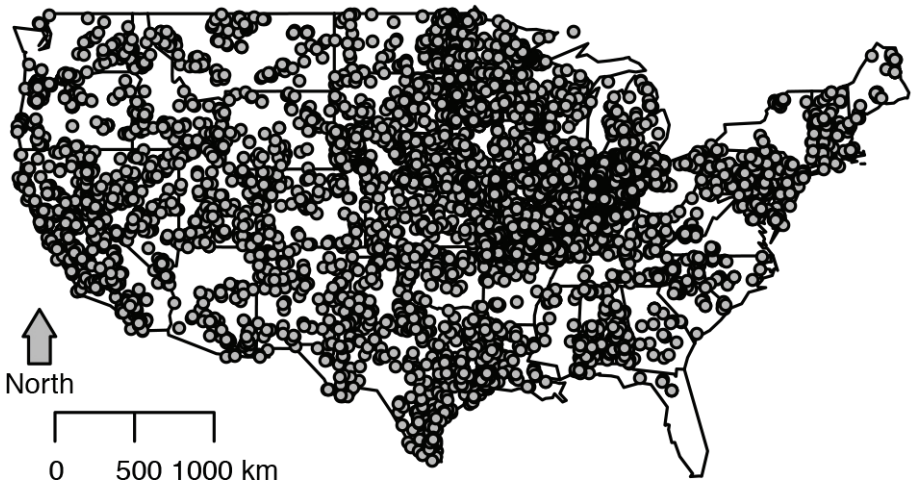

Figure 2.2: Spatial distribution of pedon locations used in this study across the conterminous US.

across broad geographic extents. Thus, if successful, this index would be generalizable only to the soil orders and conditions selected in this study. A total of 57,171 horizons from 8,980 pedons (8,522 pedons in the US; 458 pedons outside of the US) were analyzed (Fig. 2.2).

2.3.2 Evaluation metrics

2.3.2.1 Diagnostic horizons

To assess validity of the HDI, values from two diagnostic subsurface horizons (cambic and argillic horizons) were compared since well-developed argillic horizons should correspond to higher val-

ues of HDI as opposed to cambic horizons which should correspond to relatively low HDI values. In total, 1,022 cambic horizons and 5,985 argillic horizons were used for this comparison. We used the 95% confidence interval around the median of the two distributions to compare these horizons.

2.3.2.2 Geochemical weathering index

As a separate test of validity, we compared HDI values to a geochemical weathering index—chemical index of alteration (CIA). We selected horizons from the dataset that had total soil geochemistry determined by inductively coupled plasma atomic emission spectrophotometry (ICP-AES) on acid-digested bulk samples (Soil Survey Staff, 2014a); we removed anomalous horizons with zero HDI values. In total, 640 horizons from 192 pedons were used to calculate CIA (%) following Nesbitt & Young (1982):

$$\mathrm{CIA} = \frac{\mathrm{Al_2O_3}}{\mathrm{Al_2O_3} + \mathrm{CaO} + \mathrm{Na_2O} + \mathrm{K_2O}} \times 100 \tag{2.21}$$

where the oxides of each element are given in percent. Piecewise linear regression (Muggeo, 2003, 2008) was used to examine the relationship between the CIA and the HDI. We used the associated corresponding mean annual precipitation (MAP) values from WorldClim 2 (Fick & Hijmans, 2017) for these horizons to further evaluate the CIA-HDI relationship. A positive association between CIA, HDI, and MAP was expected for horizons with CIA values above 50% corresponding to samples that represent increasingly weathered material (Nesbitt & Young, 1982).

2.3.2.3 Soil orders

Soil orders (i.e., Entisols, Inceptisols, Mollisols, Aridisols, Alfisols, and Ultisols) were used to assess both overall PDI values and those arising from individual soil properties (i.e., particle size, CCE, color, and clay films). We used the 95% confidence interval around the median of each distribution to evaluate significance and compare the taxonomic orders with respect to their PDIs.

2.3.2.4 Mineralogy

We investigated the relationship between clay mineralogy of B horizons and PDI. Clay mineralogy information was available for 1,534 pedons in the dataset. As part of this evaluation, we developed a clay mineralogy index (CMI) based on the work of Barshad (1966) where changes in clay mineralogy in soils formed from igneous parent material were analyzed along a precipitation gradient. The observed patterns in that work showed a generally increasing relative mineral content of kaolinite (Ka) and halloysite (Ha) with increasing MAP (Birkeland, 1999). Using this relationship, we compared the sum of Ka and Ha to the sum of Ka, Ha, montmorillonite (Mt), illite (Il), vermiculite (Vm), and gibbsite (Gi) as shown in Eq. 2.22 to calculate CMI:

$$\text{CMI} = \frac{\text{Ka} + \text{Ha}}{\text{Ka} + \text{Ha} + \text{Mt} + \text{Il} + \text{Vm} + \text{Gi}} \tag{2.22}$$

where the minerals above are represented by an ordinal value from 1 to 5 corresponding to their relative peak height in the X-ray diffraction pattern determined on oriented clay samples (Soil Survey Staff, 2014a). PDI values were expected to be positively correlated with CMI.

2.4 Evaluation and Interpretation

2.4.1 HDI

2.4.1.1 Diagnostic horizons

As shown in Fig. 2.3, HDI values for argillic horizons were significantly greater than that of cambic horizons as indicated by the 95% confidence interval around the median of each diagnostic subsurface horizon. The relationship between HDI and these diagnostic subsurface horizons was mainly driven by particle-size and clay film differences between argillic and cambic horizons. Argillic horizons form from pedogenic processes such as lessivage, translocation of dissolved components at depth which leads to the neosynthesis of clay, and clay production from primary minerals in subsurface horizons (Buol et al., 2011). These horizons are characterized by illuvial accumulation

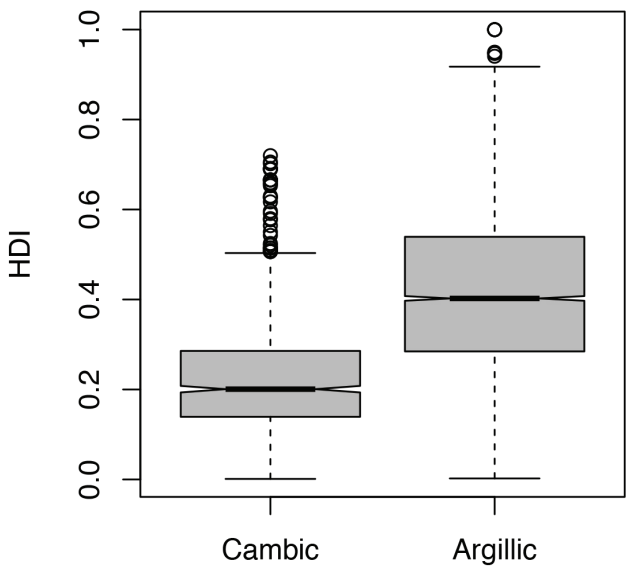

Figure 2.3: Boxplots of the HDI grouped by cambic and argillic diagnostic subsurface horizons. Boxes display the upper and lower quartiles with center bars indicating median HDI values. Whiskers indicate extreme HDI values and points represent very extreme HDI values ($>$ 1.5 times the interquartile range). In addition, notches represent the approximate 95% confidence interval around each median.

of phyllosilicate clays with specific requirements about the total clay increase from an overlying eluvial horizon, minimum thickness of the horizon, and morphological evidence of clay illuviation (e.g., clay films, clay bridging) (Soil Survey Staff, 2014b). This diagnostic subsurface horizon often corresponds to moderate to strong soil development and a Bt horizon designation (Birkeland, 1999; Soil Science Division Staff, 2017). Cambic horizons, however, are characterized by physical alterations, chemical transformations, or removals (or a combination of these processes) with properties such as very fine sand or finer texture, soil structure or the absence of rock structure, and/or additional properties that generally do not meet the requirements of other diagnostic horizons (Soil Survey Staff, 2014b). Cambic horizons, therefore, correspond to weak soil development and often a Bw horizon designation (Birkeland, 1999; Soil Science Division Staff, 2017). Thus, the higher HDI values of argillic horizons and the lower values of cambic horizons align with the definitions of these horizons providing evidence of HDI as a valid proxy of soil horizon development.

2.4.1.2 Geochemical weathering index

Figure 2.4 shows the relationship between CIA and HDI and supports the validity of HDI as a proxy representing varying degrees of soil development in addition to its generalizability across a broad geographic scale. Although the coefficient of determination ($r^2 = 0.08$) was relatively low, the piecewise linear regression shows a highly significant ($P < 0.001$) positive linear trend between CIA and HDI at values of CIA greater than 53% (dotted line; Fig. 2.4). Above this value, HDI represented increasing pedogenic development. This data-derived breakpoint corresponds to the theoretical chemically unweathered fresh material cutoff (50%; dashed line; Nesbitt and Young, 1982). As was expected, below this cutoff, there was no significant relationship between CIA and HDI. When MAP was mapped to this relationship, results showed that elevated MAP corresponded to greater CIA and HDI values, while lower MAP values corresponded to lower CIA and HDI values where the CIA-HDI relationship was significant.

2.4.2 PDI

2.4.2.1 Soil orders

Boxplots of PDIs for particle size, CCE, color, and clay films are shown for each soil order in Fig. 2.5. Median values of the PDI for particle size increased significantly (i.e., 95% confidence intervals around each median) in the following order: Entisols–Inceptisols–Mollisols–Aridisols–Alfisols–Ultisols (Fig. 2.5a). This progression was expected for Entisols, Inceptisols, Alfisols, and Ultisols and it suggests that the scoring of particle size in the PDI based on relative differences between the eluvial and illuvial horizons within a pedon is a valid proxy of soil development. Thus, the modified z-score framework used in the PDI for particle size was able to capture and quantify both the increasing eluvial coarsening and illuvial fining (i.e., lessivage) represented by these orders. However, besides falling between Inceptisols and Alfisols, the appropriate soil development order of Mollisols and Aridisols is unclear.

Figure 2.5b shows median values of the PDI for CCE generally increasing from Entisols to

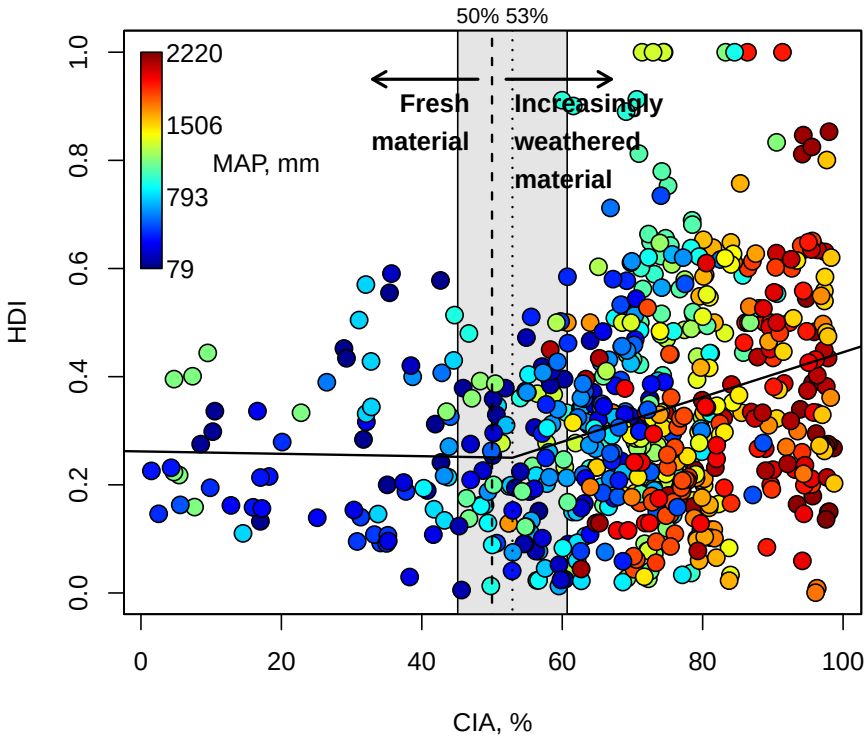

Figure 2.4: Piecewise linear regression of HDI vs. CIA colored by MAP. A significant ($P < 0.001$) positive linear trend between HDI and CIA at values of CIA greater than 53% (dotted line; increasingly weathered material) was observed. This breakpoint approximately corresponds to the chemically unweathered fresh material cutoff of 50% (dashed line; Nesbitt and Young, 1982). The shaded bar at 53% represents one standard error distance around the breakpoint value.

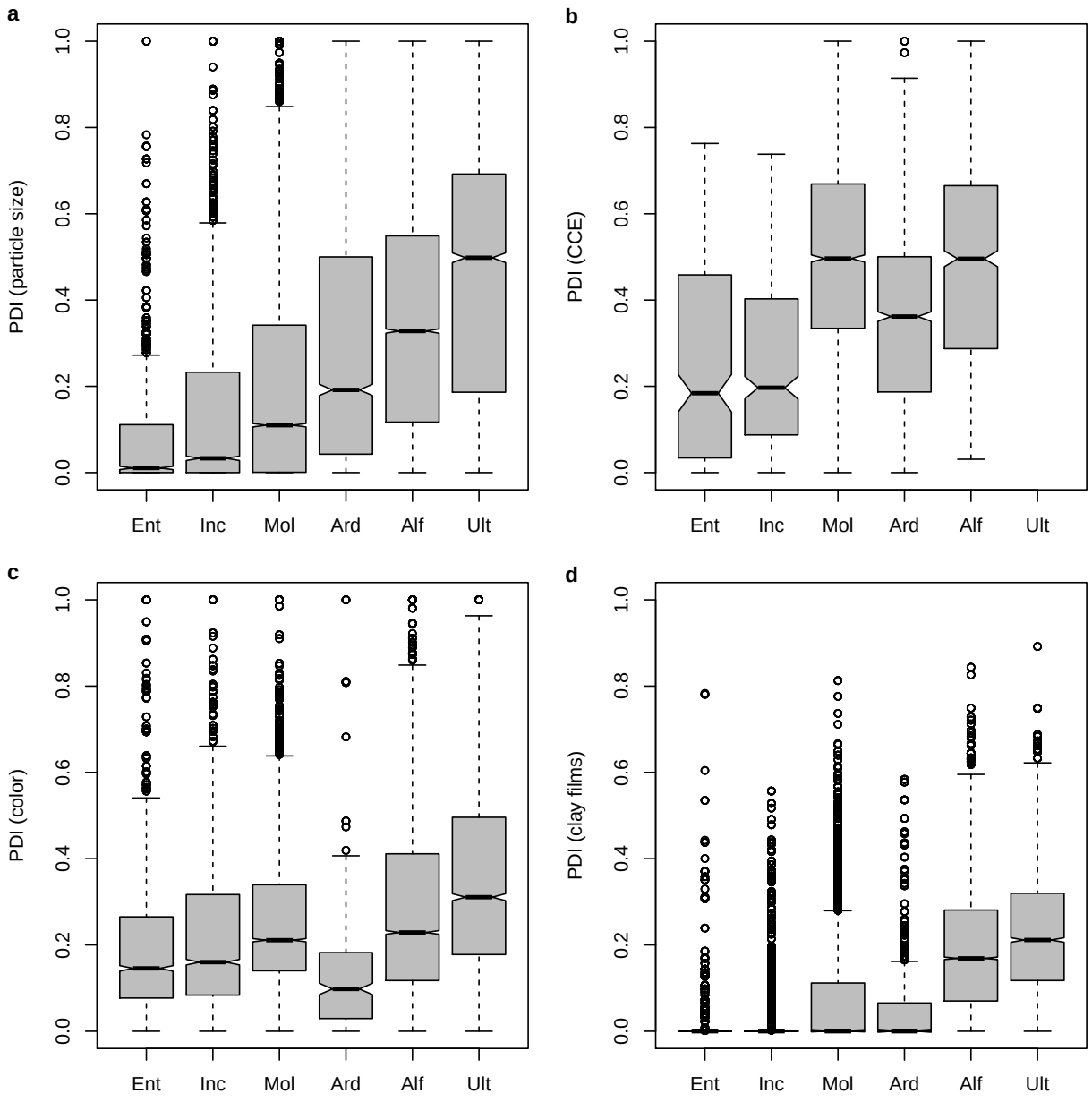

Figure 2.5: Boxplots of PDIs for (a) particle size, (b) CCE, (c) color, and (d) clay films for Entisols (Ent), Inceptisols (Inc), Mollisols (Mol), Aridisols (Ard), Alfisols (Alf), and Ultisols (Ult). Boxes show the upper and lower quartiles with center bars indicating median PDI values for each soil order. Whiskers display extreme PDI values and points represent very extreme PDI values ($>$ 1.5 times the interquartile range) for each soil order. Notches represent the approximate 95% confidence interval around each median.

Alfisols. Median values for Entisols and Inceptisols were not significantly different from each other although both were significantly lower than Aridisols. Mollisols and Alfisols were also not significantly different from each other but both were significantly higher than Aridisols.

Higher median values for Mollisols and Alfisols is perhaps partly attributable to the greater degree of translocation of carbonate from eluvial to illuvial horizons given that Mollisols and Alfisols occur in areas with greater MAP compared to Aridisols (Buol et al., 2011). In addition, the lower median value of Aridisols compared to Mollisols and Alfisols can perhaps be explained by the combination of more continuous delivery of carbonate to soil surfaces associated with dust inputs in arid environments and the lower MAP that reduces the potential for translocation of carbonate from eluvial to illuvial horizons. In general, the maximum separation between soil inorganic carbon (SIC) in surface horizons (upper 20 cm) and deeper layers (upper 100 and 200 cm) occurs in areas with MAPs between approximately 100 and 850 mm (Guo et al., 2006). Both the total SIC and the difference in eluvial and illuvial horizons declines considerably above and below that MAP range and corresponds to the lower CCE PDI median value observed for Aridisols compared to Mollisols and Alfisols in this study (Fig. 2.5b). Ultisols are not displayed in Fig. 2.5b because of either the absence of soil carbonate or the lack of CCE differences between eluvial and illuvial horizons.

Median values of PDI based on surface-subsurface differences in color increased significantly from Entisols to Ultisols with the exception of Aridisols which had the lowest median color PDI value (Fig. 2.5c). This progression of increasing median values (i.e., except for Aridisols) suggests that the scoring approach for color is a valid description of soil development across the broad scales investigated in this study. The lower median value for Aridisols is likely due to the low melanization of surface horizons due to lower soil organic carbon compared to surface horizons of orders that span semi-arid to humid environments. In addition, the low MAP in areas where Aridisols develop limits mineral weathering in these soils and, thus, the rubification of subsurface horizons. Although abundant calcium carbonate has a distinct effect on hue, value, and chroma (Harden & Taylor, 1983), it is unclear to what extent this effect controls soil color in other orders

that may contain horizons with significant CCE (i.e., Mollisols and Alfisols).

Figure 2.5d shows boxplots of the PDI for clay films where significant increases in median values were only observable for Alfisols and Ultisols. The near-zero median values observed for Entisols and Inceptisols were expected due to the taxonomic criteria by which they were classified; these soils are poorly developed and can occur across a range of climates. Although the median values for Mollisols and Aridisols were not significantly different from zero, there is a considerable increase in the upper quartile range for these soil orders likely reflecting increased soil ages compared to Entisols and Inceptisols which have allowed for increased soil development as represented by clay translocation.

Overall, the median PDI values that incorporate particle size, CCE, color, and clay films increased significantly from Entisols to Inceptisols to Mollisols to Aridisols to Alfisols, and finally to Ultisols (Fig. 2.6). This progression of increasing median values was expected for Entisols, Inceptisols, Alfisols, and Ultisols and demonstrates the validity of the approach taken in this study for calculating PDIs in investigations at a broad continental scale and with large soil taxonomic diversity.

2.4.2.2 Mineralogy

A positive correlation was observed between PDI values and the CMI developed in this study which generally followed increasing MAP (Fig. 2.7). Exceptions included CMI values of 0.05 and 0.15 as well as 0.55 and 0.75 which were switched in terms of the expected progression of increasing MAP associated with these values. In general, lower values of the CMI indicate lower relative concentrations of kaolinite and halloysite in the clay fraction (Eq. 2.22) corresponding with lower PDI values and lower MAP. Conversely, higher CMI values indicate higher kaolinite and halloysite concentrations which corresponded to higher PDI values and higher MAP. Clay mineralogy index, therefore, provides additional evidence, independent of taxonomy, for the validity and generalizability of the developed PDI.

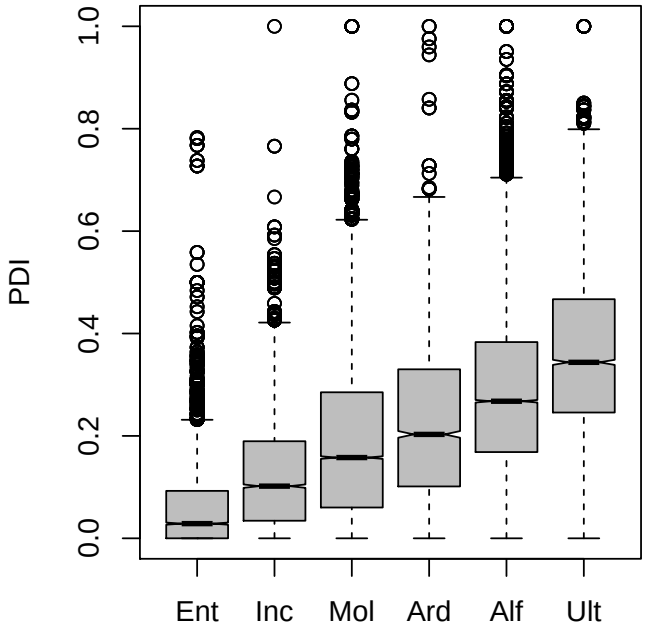

Figure 2.6: Boxplots of the PDI integrating the four properties shown in Fig. 2.5 for Entisols (Ent), Inceptisols (Inc), Mollisols (Mol), Aridisols (Ard), Alfisols (Alf), and Ultisols (Ult). Boxes indicate the upper and lower quartiles with center bars representing median PDI values for each soil order. Whiskers indicate extreme PDI values, points display very extreme PDI values ($>$ 1.5 times the interquartile range), and notches represent the approximate 95% confidence interval around the median for each soil order.

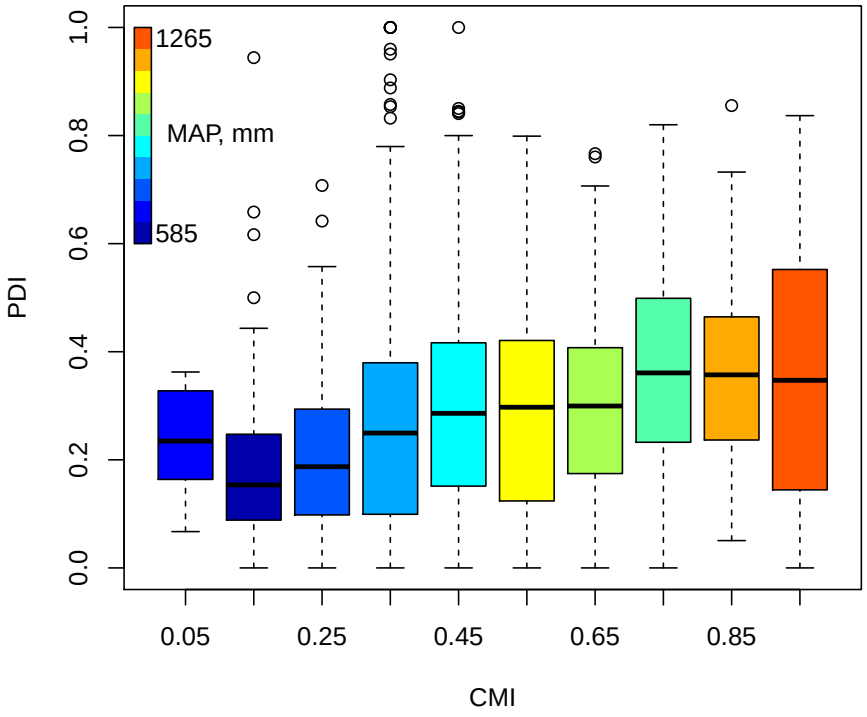

Figure 2.7: Boxplots of PDI for binned CMI values colored by MAP. Boxes display the upper and lower quartiles with center bars indicating median PDI values for each aggregated CMI bin. Whiskers show extreme PDI values and points indicate very extreme PDI values ($>$ 1.5 times the interquartile range).

2.5 Applications

The relationships between HDI, diagnostic horizons, and CIA and between PDI, soil orders, and CMI support the validity and generalizability of indices based on relative horizon properties instead of parent material information. This approach, therefore, represents a potentially powerful new tool for examining and quantifying soil development. In addition, modified z-scores provide a standardized basis within an eluvial-illuvial or surface-subsurface context (e.g., particle-size coarsening and fining, carbonate depletion and accumulation, melanization and rubification) to quantify and represent degrees of property-integrated pedogenic alteration. This use of z-scores provides a framework for assessing soil development in regional or localized pedogenic studies (e.g., Berry, 1994) as well as broad-scale pedogenic investigations as shown in this work. Below, we discuss several potential applications where the use of generalizable soil development indices may advance pedogenic studies.

2.5.1 Continental-scale pedogenic modeling

Empirical pedogenic modeling approaches have been useful in many soil investigations and interpretations, but these models have often lacked a rigorous theoretical underpinning that limits their extrapolation to other environments outside the region in which they were developed even when soil conditions and contexts are similar (see Yaalon, 1975; Birkeland, 1999; Schaetzl and Thompson, 2015 for reviews of empirical models). While more mechanistic pedogenic models that simulate soil processes exist, they often require the calibration of empirical parameters that restricts their usefulness outside the regions in which they were calibrated (see Hoosbeek and Bryant, 1992; Hoosbeek et al., 2000; Minasny et al., 2008; Bockheim and Gennadiyev, 2010; Vereecken et al., 2016 for reviews of mechanistic models). Therefore, the generalizable indices developed in this work have the potential to bridge gaps in various pedogenic modeling approaches especially with the emergence of large continental-scale datasets (e.g., CZO and NEON).

The relationships shown between the HDI, CIA, and MAP as well as between PDI, CMI, and

MAP highlight the potential for exploring quantitative relationships between soil development, chemical weathering, and climate at broad scales as part of pedogenic modeling efforts. For example, recent applications of broad-scale soil datasets have yielded new insights into the role of climatic and lithologic forcing on the evolution of soil structure at continental scales (Panakoulia et al., 2017; Hirmas et al., 2018; Mohammed et al., 2020). The indices developed in this work could serve as a tool to select research sites in furthering similar future research efforts. For instance, PDI could be used as a covariate to adjust regression models in observational studies examining the influence of broad-scale processes or properties (e.g., climate, lithology, or land use) on ecosystem dynamics. PDI could also serve as a variable by which to stratify sampling efforts to minimize known sources of variability in both pedogenic and soil-geomorphic investigations.

2.5.2 Identification of anomalies

Although pedons were removed from the dataset where lithologic discontinuities were described, the HDI approach used in this work has the potential to be used to identify sedimentological, geomorphic, biotic, or anthropogenic anomalies in soil development such as burial, lithologic discontinuities, bioturbation, or human-altered human-transported (HAHT) material. For example, if the $\tilde{z}$-score for a property does not match the depth pattern assumed to result from the pedogenic processes examined in this study, its HDI is cutoff at zero rather than allowing the value to become negative (Eqs. 2.6, 2.11, and 2.15). Future work could modify this index to allow for negative values in order to identify these types of anomalies in soil-geomorphic investigations and interpretations as well as in digital soil mapping efforts.

2.5.3 Estimation of surface soil ages

In future investigations, the generalizable PDI developed in this work may provide a means to estimate surface soil ages across broad spatial expanses, especially with the emergence of broad-scale datasets of soil age (e.g., International Soil Radiocarbon Database–ISRaD; https://international-soil-radiocarbon-database.github.io/ISRaD/; accessed February 21, 2019). Methods similar to

those used to develop regional chronofunctions (e.g., Switzer et al., 1988; Reheis et al., 1989; Harden et al., 1991; Vidic & Lobnik, 1997; Calero et al., 2009) could potentially be used to relate the generalizable PDI to soil age, which would aid in determining the spatial distribution and drivers of surface soil stability as well as the effect of time on pedogenesis across broad geographic and taxonomic distributions of soils.

2.6 Conclusions

In this work, we present generalizable indices of soil development (HDI and PDI) based primarily on relative horizon properties instead of parent material information and evaluate these indices at a continental scale. The novelty of this approach is the development of indices that reflect an understanding of generalizable pedogenic processes for the soil orders and conditions studied and that integrate relative soil morphological, physical, and chemical information within eluvial-illuvial and surface-subsurface contexts. Our findings show that both HDI and PDI are valid proxies of soil development and applicable across large geographic scales. These indices open the door to numerous broad-scale applications (e.g., pedogenic modeling, identification of anomalies, estimation of surface soil ages) and may aid in understanding how climatic and land-use pressures influence soil development.

Chapter 3

Soil structure and organic carbon give rise to the ecohydrological conditions critical to water cycling at a continental scale

Abstract

Increasing climatic and land-use pressures across broad geographic extents are prompting the need to better understand the role of soils in the water cycle at a continental scale. In this work, we assess the influence of near-surface soil properties on long-term land-atmosphere water cycling and examine systematic differences in $>$ 200 basins across the US. We compiled soil properties from the uppermost horizons of $>$ 6,900 pedons from a large database of US soils and merged these data with vegetation indices and corresponding climate data [mean annual precipitation, actual evapotranspiration (ET), potential ET] where all variables were basin-aggregated. Basin climate data were fit with a parametric model of the Budyko equation and used to generate an empirical parameter (n) for each basin. Our results indicate that the combined effects of higher soil organic carbon (SOC) and ped roundness are related to enhanced ET by increasing total porosity, hydraulic conductivity, and plant-available water holding capacity. Low ped roundness and SOC values likely correspond to agricultural practices leading to the formation of platy soil structure by mechanical compaction leading to decreases in infiltration and increases in runoff. In arid regions, low ped roundness corresponds to natural platy structure associated with vesicular horizons which increases runoff towards shrub islands and ephemeral washes. These findings provide evidence that near-

surface soil structure and SOC controls long-term water balance at large spatial scales with potentially important feedbacks to climate pointing towards the need to include soil structure in Earth system models.

3.1 Introduction

Understanding the role of soils in controlling the land-atmosphere water cycle is critical to quantifying the impact of climate and land-use pressures on ecosystem services (e.g., water storage, food security; Janzen et al., 2011; Hirmas et al., 2018). The land-atmosphere water cycle has been studied extensively within the Budyko framework (Budyko, 1974), which established the partitioning of precipitation into runoff and evapotranspiration as a function of aridity. Here, the Budyko curve is a curvilinear function that describes the relationship between an index of mean annual evapotranspiration [i.e., the ratio of evapotranspiration to precipitation (ET/P)] and mean annual aridity [i.e., the ratio of potential evapotranspiration to precipitation (PET/P)]. This curve is constrained by an energy limit (ET $<$ PET) and a water limit (ET $<$ P) (see Greve et al., 2015; Padrón et al., 2017, for reviews of Budyko framework studies). While PET/P is considered to be the primary control of ET/P within the Budyko framework, aridity does not explain all spatial variations in the long-term water balance of catchments; in fact, the ET/P and PET/P indices of certain catchments can be scattered around the Budyko space sometimes falling above or below the curve (Padrón et al., 2017; Berghuijs et al., 2020). Decades of research show this scatter in the Budyko space is systematic and does not arise strictly from data uncertainty, implying that this relationship can be used to deduce measurable physical processes and catchment properties (Berghuijs et al., 2020).

Greve et al. (2015) note that although the original Budyko curve was deterministic and non-parametric, Budyko acknowledged that variations around the curve could emerge depending on local conditions; in some cases, scatter around the curve could be considerable but explainable (Budyko, 1974; Milly, 1994; Koster & Suarez, 1999). Two common approaches to determine variables (other than PET/P) that control long-term water balances were recently outlined by Berghuijs et al. (2020): (1) quantifying how catchments depart from the Budyko curve and assessing rela-

tionships between particular catchment properties and departures above or below the curve; and (2) using a calibrated parametric Budyko equation with a catchment specific parameter correlated to catchment properties. These approaches have yielded widespread evidence for systematic variations of scatter around the curve, explaining that scatter in terms of various catchment and climate characteristics (Greve et al., 2015; Padrón et al., 2017). Studies have focused on factors controlling ET/P which include vegetation (e.g., Zhang et al., 2001; Donohue et al., 2007, 2010; Williams et al., 2012; Li et al., 2013), soil properties (e.g., Sankarasubramanian & Vogel, 2002; Porporato et al., 2004; Yokoo et al., 2008; Wang et al., 2009a; Donohue et al., 2012), and topography (e.g., Yang et al., 2007; Shao et al., 2012; Xu et al., 2013; Zhou et al., 2015; Rouholahnejad Freund & Kirchner, 2017). Studies have also examined streamflow characteristics (e.g., Potter & Zhang, 2009; Wang & Wu, 2013; Berghuijs et al., 2014a; Trancoso et al., 2016) and groundwater (e.g., Wang et al., 2009a; Istanbulluoglu et al., 2012; Condon & Maxwell, 2017; Condon et al., 2020) in relation to this scatter. Other research has assessed factors controlling ET/P related to climate characteristics such as seasonality (e.g., summer-dominant rainfall, non-seasonal, winter-dominant rainfall; e.g., Dooge et al., 1999; Potter et al., 2005; Hickel & Zhang, 2006; Gerrits et al., 2009; Chen et al., 2013) and climate change (e.g., Koster & Suarez, 1999; Arora, 2002; Jones et al., 2012; Berghuijs et al., 2014b; Creed et al., 2014). Many of these studies have also focused on multiple catchment and climate controls (e.g., Milly, 1994; Gentine et al., 2012; Troch et al., 2013; Carmona et al., 2014; Greve et al., 2015). Despite this research, the combined causes of systematic variations of scatter around the Budyko curve including the most relevant factors controlling ET/P and long-term water balance (other than PET/P), remains unclear (Greve et al., 2015; Padrón et al., 2017; Berghuijs et al., 2020).

With respect to soil properties controlling ET/P, previous studies have often incorporated soil parameters into Budyko framework models where these variables were developed from mathematical representations of known or hypothesized mechanisms that are solved numerically (e.g., Milly, 1994; Porporato et al., 2004; Potter et al., 2005; Troch et al., 2013). These soil parameters are often estimated as a function of plant-available soil water holding capacity or other soil wa-

ter storage capacity terms for both mechanistic and empirical components of studies (e.g., Milly, 1994; Sankarasubramanian & Vogel, 2002; Yang et al., 2007; Yokoo et al., 2008; Donohue et al., 2012). Studies have also incorporated parameters related to soil hydraulic properties for varying soil textures (e.g., Yokoo et al., 2008), assessed relationships between catchment parameters and soil textures (e.g., Wang et al., 2009a), and developed parameters representing other ecohydrological controls on soil water balance (e.g., Donohue et al., 2012; Gentine et al., 2012).

Because a number of these Budyko framework studies incorporate soil water balance and storage changes into models, finer spatial and temporal scales are therefore considered as long-term mean changes in terrestrial water storage at large spatial scales are assumed to be negligible (Zhang et al., 2008; Du et al., 2016; Padrón et al., 2017). In addition, while these types of models have a strong theoretical basis, and, thus, overcome problems with extrapolation, they are often extremely complicated, difficult to apply without expert knowledge, and require specific site measurements for model calibration; thus, the usefulness of such approaches are often restricted to the region where they were developed. Furthermore, since soil properties are parameterized in these Budyko framework models, these properties are often not accounted for explicitly with respect to their role in controlling ET/P and long-term water balance. Indeed, our understanding of the role of soil properties in controlling ET/P and specifically which soil properties are most relevant and important in controlling the long-term land-atmosphere water cycle is currently unclear, especially across large spatial scales (Padrón et al., 2017). The objective of this work, therefore, was to: (1) analyze relationships between near-surface soil properties and scatter around the Budyko space to determine if systematic variations in ET/P for basins were present across broad geographic extents; and (2) develop an empirical model that explains the role of these near-surface soil properties in controlling the long-term land-atmosphere water cycle at a continental scale.

3.2 Methods

3.2.1 Datasets

To better understand the role of near-surface soil properties in controlling land-atmosphere water cycling, we obtained field-based pedon information and laboratory data collected through the United States Department of Agriculture–Natural Resources Conservation Service (USDA–NRCS) National Cooperative Soil Survey (NCSS) Characterization Database. We merged ET products based on Moderate Resolution Imaging Spectroradiometer (MODIS) and meteorology data (Mu et al., 2007, 2011) and P products from the Parameter-elevation Regressions on Independent Slopes Model (PRISM; PRISM Climate Group, Oregon State University, 2021) with the NCSS data in order to use the Budyko framework (Budyko, 1974) in analyses. MODIS Normalized Difference Vegetation Index (NDVI) products were also merged with the NCSS data. Pedons distributed across broad geographic extents in the US and with large and widespread soil taxonomic diversity were selected for the dataset, while poorly drained soils and soils with lithologic discontinuities were removed. In total, 8,262 pedons were selected along with their corresponding mean annual ET, PET, P, and NDVI (2000-2014) (Fig. 3.1).

These mean annual ET, PET, and P data were used to generate the Budyko indices (Budyko, 1974) including mean annual ET/P, runoff ratio (1-ET/P), and PET/P values for each of these pedons. Subsequently, these values were aggregated by basin using the United States Geological Survey (USGS) Watershed Boundary Dataset (WBD) hydrologic unit code (HUC) 6 basins. Mean annual Budyko indices for each pedon location were averaged across each HUC 6 basin for each year; basins that had 15 year (2000-2014) mean annual ET/P values above 1 (i.e., above the water limit), indicating additional inputs of water beyond precipitation, were removed from the dataset. This resulted in a total of 255 basins where curvilinear functions relating mean annual ET/P to mean annual PET/P were generated for each basin using each respective 15 years (2000-2014) of data (the blue and red basins in Fig. 3.1). In this study, we used a parametric model of the Budyko equation based on the work of Mezentsev (1955), Choudhury (1999), and Yang et al.

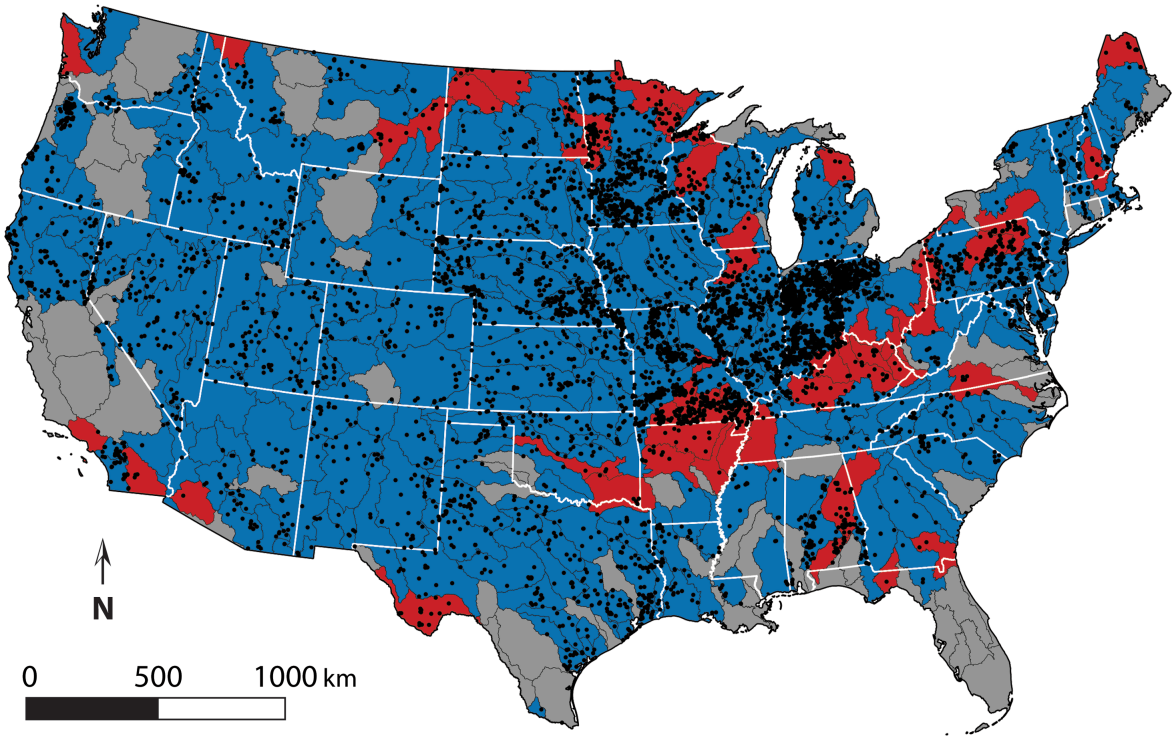

Figure 3.1: Spatial distribution of pedon locations (black dots) and basins (blue and red) used in this study across the conterminous US. Data from 6,962 pedons across 209 basins (blue) as well as an additional 1,300 pedons (i.e., 8,262 in total) corresponding to 46 basins (red; i.e., 255 in total) comprised the datasets used in this study.

(2008), referred to as the Mezentsev–Choudhury–Yang (MCY) model (Sposito, 2017; Daly et al., 2019):

$$\frac{ET}{P} = \frac{1}{(1+(\frac{PET}{P})^{-n})^{1/n}} \tag{3.1}$$

where $n > 0$ is an empirical parameter (Daly et al., 2019). Using the 255 basins selected for this study, the nonlinear fit of Eq. 3.1 using each respective 15 years (2000-2014) of data resulted in an n value for each basin (Fig. 3.2).

To understand the degree to which near-surface soil properties control variability in land-atmosphere water cycling, measured and calculated or derived properties from only the uppermost soil horizons were included in our analyses. Measured properties included particle-size distribution (PSD), soil organic carbon (SOC), field capacity (FC), and wilting point (WP), while calculated/derived properties included soil structural metrics (i.e., size, grade, ped solidity, and ped roundness), total porosity (TP), effective porosity (EP), saturated hydraulic conductivity (K_{sat}), horizon development index (HDI), and root class densities (i.e., corresponding to very fine, fine, medium, coarse, and very coarse roots). For individual soil horizons that contained multiple structure sizes or grades, soil properties were aggregated using either the geometric midpoint of the recorded size classes or by the ordinal-value converted grade classes (0 = structureless to 3.5 = very strong), respectively (Hirmas & Giménez, 2017; Mohammed et al., 2020). One of these properties, ped solidity, is a proxy for ped roughness with values close to unity indicating a smooth surface and lower values indicating increasing roughness (Mohammed et al., 2016). Another property, ped roundness (aka angularity), varies between 0 and 1 with higher values indicating a tendency towards a perfect circle and lower values indicating angular shapes (Mohammed et al., 2016).

Total porosity for each horizon was derived using the measured dry bulk density at a water content corresponding to a matric potential of -33 kPa. Effective porosity was calculated as the difference between TP and FC and considered to be a proxy of macroporosity representing the volume fraction of the largest pores in the soil (Rawls et al., 1998; Hirmas et al., 2018). In addition, the K_{sat} of each horizon was calculated from the EP using a form of the Kozeny-Carman equation proposed by Rawls et al. (1998). Particle-size HDIs for horizons relied on measured PSD and were

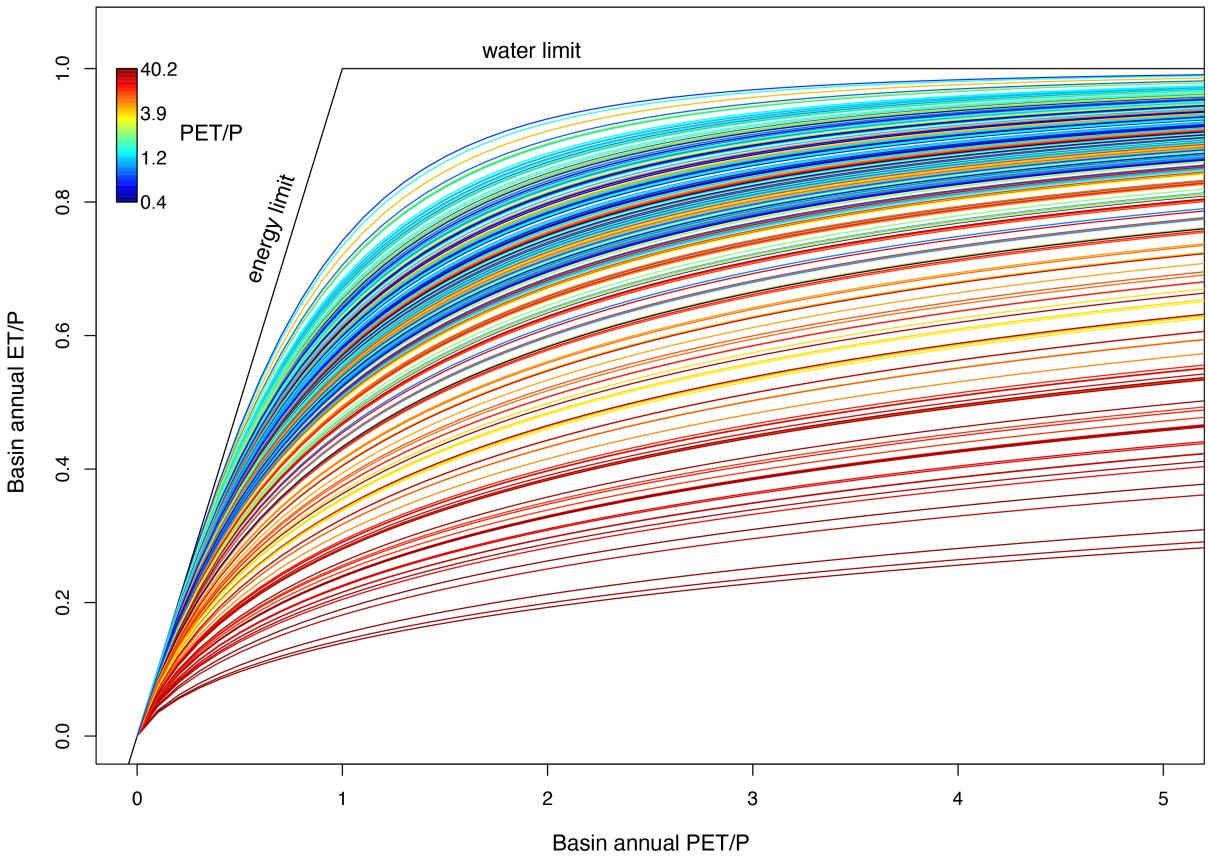

Figure 3.2: Data from 8,262 pedons across 255 basins (blue and red basins in Fig. 3.1) were used to generate curvilinear functions relating annual ET/P to annual PET/P. For condensed viewing, the x-axis only includes annual PET/P values up to 5. The nonlinear fit of Eq. 3.1 using each respective 15 years (2000-2014) of data resulted in an n value for each basin. Each curve is colored by 15 year (2000-2014) mean annual PET/P with the maximum value of 40.2 similar to that of other arid basins as summarized in Du et al. (2016).

calculated using modified z-scores to assess relative changes between eluvial and illuvial horizons following Koop et al. (2020). Lastly, root densities for five root-size classes (i.e., very fine, fine, medium, coarse, and very coarse) were calculated from visual descriptions of root distributions made in the field (Mohammed et al., 2020).

To undertake continental-scale analyses, horizon data for each pedon location were aggregated and averaged across each HUC 6 basin and merged with the corresponding Budyko indices and n values for each basin. This resulted in a total of 6,962 pedons across 209 basins (with no missing data) that were analyzed in initial statistical analyses (the blue basins in Fig. 3.1). Prior to statistical analyses, distributions of all of the variables for each basin were visually inspected and a number of variables were transformed to reduce skewness and approximate a normal distribution. For logarithmic transformations of variables, a constant was added to the values prior to the transformation to avoid taking the logarithm of zero. For angular transformations, the arcsine of the square root was applied to the values of the variables; for ped solidity, this angular transformation was applied twice after dividing the first transformation by $\pi/2$.

3.2.2 Statistical analyses

Principal components analysis (PCA) was used to reduce 19 basin horizon variables into a smaller set of uncorrelated variables (i.e., principal components, PCs) that retained as much information contained in the original basin data as possible (Kabacoff, 2015). We used y-aware PCA to rescale the basin horizon input variables to correspond to the units of the dependent variable n. Y-aware PCA works by fitting a linear regression model between each x and y. Thus, a unit change in the x variables corresponds to a unit change in the y variable (transformed x variables are centered at a mean of zero). Under this rescaling, all of the independent variables were in the same units to facilitate characterizing their effect on the dependent variable (Zumel, 2016a; Mount & Zumel, 2020; Zumel & Mount, 2020).

Following the rescaling of the initial horizon input variables, we selected the final horizon input variables using a significance pruning threshold of the inverse of the number of variables

considered for the y-aware PCA (1/19 = 0.053) following the recommendation given by Zumel (2016b). The selected horizon variables that exhibited a significant relationship with n at the continental scale considered in this study included ped solidity, ped roundness, SOC, and very fine, fine, medium, and coarse root density.

Using these selected basin horizon variables, we performed y-aware PCA where weights used to form the linear composites were chosen to maximize the explained variance of horizon variables used in this study while keeping the horizon PCs uncorrelated (Kabacoff, 2015; Zumel, 2016a). Similar to the selection of significant horizon variables, PCs were selected via a significance pruning threshold calculated as the inverse of the number of PCs generated during the y-aware PCA (1/7 = 0.14) (Zumel, 2016b). In order to assess significance of variable loading values for each PC, t-tests were used to compare the absolute value of each loading to the mean absolute value of all loadings for each corresponding PC.

Three variables were chosen (i.e., ped solidity, ped roundness, and SOC) based on the t-test results. Because there were more samples with this information in the NCSS dataset, we selected an additional 1,300 pedons (i.e., 8,262 in total) corresponding to 46 basins (i.e., 255 in total) to continue the analysis (the red basins in Fig. 3.1). This slightly larger dataset aided in the analysis and interpretation of spatial patterns across the conterminous US. Based on updated visual inspections of the distributions of the variables from the larger dataset, ped roundness values were square root transformed. Horizon variables that loaded highly on the significant PCs were z-score transformed and related to n using weighted regression where the number of pedons in each basin were used as the weightings. Variance inflation factors (VIFs) were used to assess multicollinearity between horizon variables; a VIF ≥ 10 was used as an indication of collinearity between variables as recommended by Logan (2010). Multiple linear regression was run to determine which horizon variables were significant predictors of n. β–weights from the multiple linear regression model were used to compare the relative importance of each horizon variable to n. The resulting n regression model was evaluated by regressing actual against predicted n.

Table 3.1: Selected near-surface horizon variables exhibiting a significant relationship with n ($p < 0.053$) and each respective variable transformation (an angular transformation was applied twice for ped solidity). Also included below are y-aware PCA (i.e., scaled by n) variable loading values, standard deviation, proportion of variance, and cumulative proportion for each of the significant PCs, 1 and 2 ($p < 0.14$). Asterisks indicate variable loading absolute values that are significantly greater than the mean of the variable loading values for each PC ($p < 0.05$).

Variable	**Transform.**	**PC 1**	**PC 2**
Ped solidity	angular	0.69*	−0.07
Ped roundness	angular	0.69*	−0.16
SOC	log	0.18	0.97*
Very fine root density	log	0.09	−0.15
Fine root density	log	0.07	−0.009
Medium root density	log	0.01	0.07
Coarse root density	log	0.02	0.03
Standard deviation		0.13	0.07
Proportion of variance (%)		62.33	19.13
Cumulative proportion (%)		62.33	81.46

3.3 Results

3.3.1 Relationships between soil structure, SOC, and n

The pruning threshold determined during the y-aware PCA and an assessment of the proportion of explained variance resulted in the selection of two PCs that had a significant relationship with n. Table 3.1 shows y-aware PCA (i.e., scaled by n) variable loading values, standard deviation, proportion of variance, and cumulative proportion for PC 1 and PC 2 with asterisks indicating variable loading absolute values that were significantly greater than the mean of the variable loading values for each PC based on t-test results ($p < 0.05$). These t-test results highlighted several significant variables including ped solidity (PC 1), ped roundness (PC 1), and SOC (PC 2).

As shown in Table 3.1, PC 1 accounted for 62.3% of the variance in n across the 209 basins included in the y-aware PCA (blue basins in Fig. 3.1); only ped solidity (0.69) and ped roundness (0.69) loaded significantly on this PC. Using the larger dataset (255 basins) with just the significant variables from PC 1 and PC 2, Fig. 3.3a and b show the geographic distribution of ped solidity and

ped roundness, respectively. In large part, soil structure aligned with aridity index values, where basins with lower PET/P (humid to sub-humid) correlated with increased ped solidity (increasingly smooth surfaces) and increased ped roundness (increased circularity) (Fig. 3.3a, b, and f). In contrast, soil structure across basins with increasing PET/P (increasingly arid) trended towards decreased ped solidity (increased roughness) and decreased ped roundness (increasingly angular shapes) especially in extremely arid basins (Fig. 3.3a, b, and f). Solidity and roundness values for basins in Fig. 3.3a and b exhibited these general relationships, where higher values occurring across central, midwestern, southeastern, eastern, and coastal parts of the US, for the most part, corresponded to increased ped solidity and roundness. In contrast, lower values corresponding to decreased solidity and roundness occurred across the interior western and southwestern US. To a predominant extent, increased ped solidity and roundness corresponded to higher n values with tendencies towards n values approaching the energy and water limits (Fig. 3.2; Fig. 3.3a, b, and g). In contrast, decreased solidity and roundness were associated with increasingly lower n values and corresponding departures from the energy and water limits (Fig. 3.2; Fig. 3.3a, b, and g). Especially across the southwestern US, decreased solidity and roundness associated with decreased ET/P (increased runoff ratio) corresponded to increasingly lower n values to a predominant extent (Fig. 3.2; Fig. 3.3a, b, e, and g).

Soil organic carbon loaded significantly (0.97) on PC 2; PC 2 explained 19.1% of the variance in n across the 209 basins that were part of the y-aware PCA (Table 3.1). Soil organic carbon generally increased from south to north across the US (Fig. 3.3c). The general south to north trend of increasing SOC was more pronounced in basins associated with mountain ranges and forests. Similar to soil structure, increased SOC corresponded to higher n values with tendencies towards decreased distances from the energy and water limits (Fig. 3.2; Fig. 3.3c and g). Decreased SOC largely corresponded to increasingly lower n values and corresponding departures from the energy and water limits especially in increasingly arid settings (Fig. 3.2; Fig. 3.3c, f, and g).

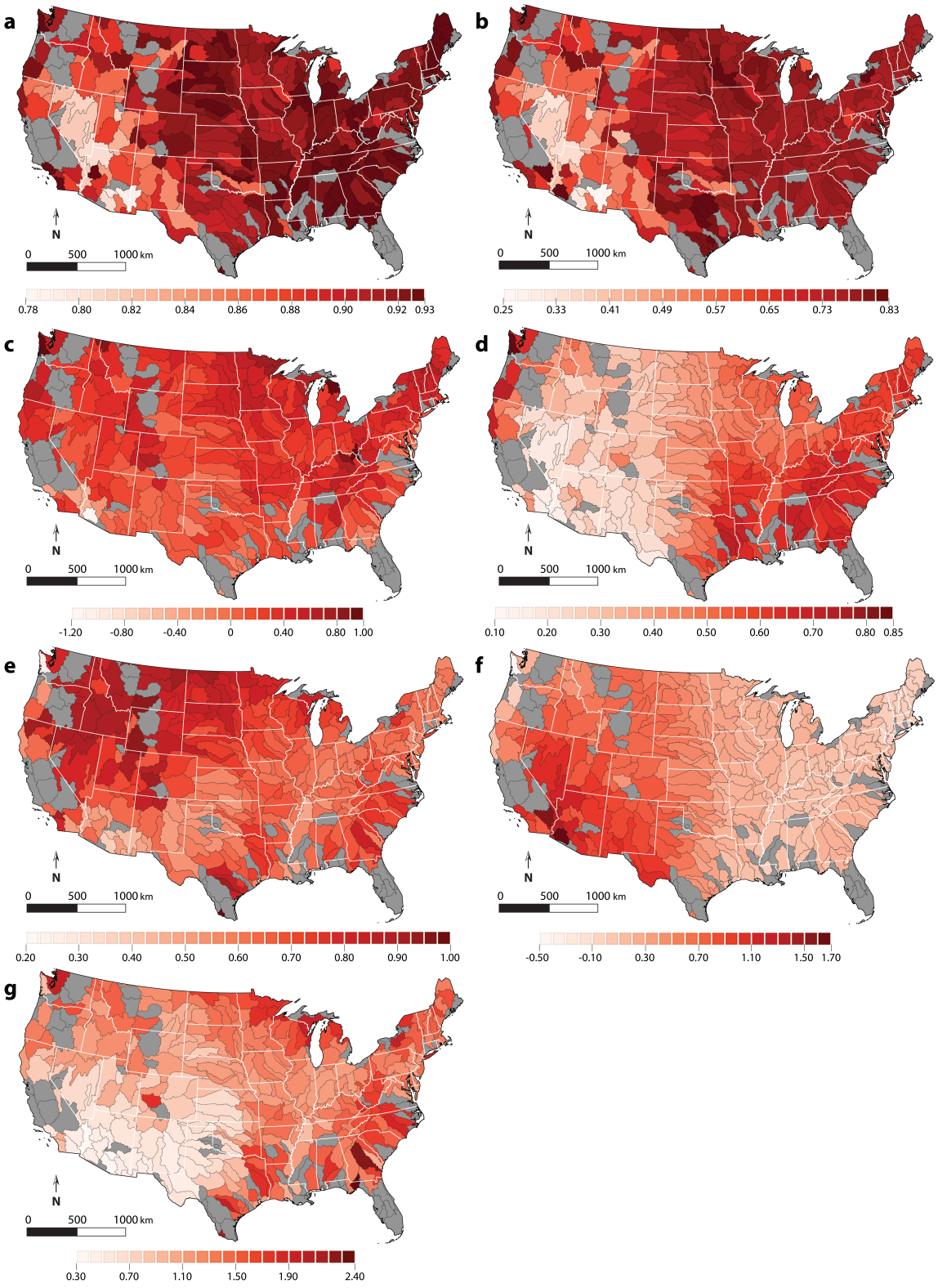

Figure 3.3: Spatial distribution of near-surface horizon (a) ped solidity, (b) ped roundness, and (c) SOC as well as (d) NDVI, (e) ET/P, (f) PET/P, and (g) *n* for 255 basins (8,262 pedons) used in this study across the conterminous US. For NDVI, ET/P, and PET/P, 15 year (2000-2014) mean annual values are displayed. Values for SOC and PET/P are log transformed.

Table 3.2: β–weights, intercept, standard errors, and P values for near-surface horizon ped roundness and SOC comprising the n regression model equation used in this study. This multiple linear regression included 255 basins (8,262 pedons) where the number of pedons in each basin were used as weightings.

Statistic	**Ped roundness**	**SOC**	**Intercept**
Estimate	0.295	0.425	-0.090
Std. error	0.047	0.058	0.036
P	1.51×10^{-9}	2.41×10^{-12}	0.015

3.3.2 Assessing relative importance of soil structure and SOC on n

Table 3.2 shows β–weights, intercept, standard errors, and P values for ped roundness and SOC comprising the n regression model equation used in this study. Ped solidity was not included in the model due to a high correlation with roundness ($r = 0.90$). This multiple linear regression included the 255 basins (8,262 pedons) from the larger dataset with the number of pedons in each basin used as weightings. Roundness and SOC explained a significant proportion of n ($R^2 = 0.342$, $P < 2.20 \times 10^{-16}$) (Table 3.2; Fig. 3.4). Soil organic carbon was the strongest predictor of n explaining 2.07 times the variation compared to roundness as determined by the squares of the β–weights in Table 3.2.

Fig. 3.5a and b show actual and predicted n, respectively, corresponding to the 255 basins (8,262 pedons) included in the multiple linear regression in Table 3.2 and Fig. 3.4. As shown in Fig. 3.5a and b, the actual n map displays a greater range of n values than the predicted n map. For the most part, differences between actual and predicted n values largely corresponded to either increases or decreases towards extremes with respect to the partitioning of P into runoff and ET (Fig. 3.3e; Fig. 3.5a and b). For example, across unclosed basins of the southwestern US, lower ET/P values (higher runoff ratio values) associated with lower ped roundness and SOC values were likely the result of other compounding factors as well (e.g., precipitation and seasonality characteristics, topography) that corresponded to increasingly lower n values (Fig. 3.3e; Fig. 3.5a and b). Towards the other extreme, higher ET/P values (lower runoff ratio values; generally associ-

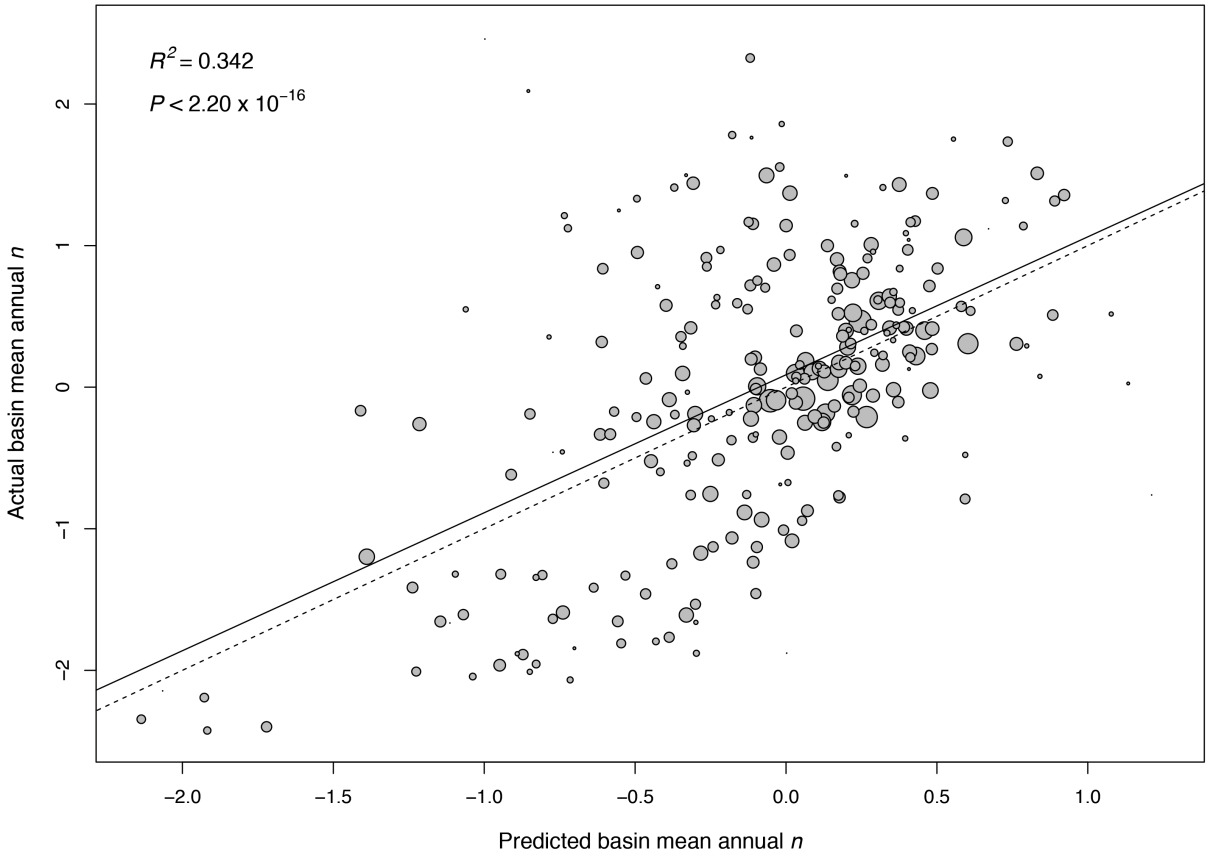

Figure 3.4: Actual n regressed against predicted n from the multiple linear regression model including 255 basins (8,262 pedons) and near-surface horizon ped roundness and SOC in Table 3.2. Displayed values for actual and predicted n are square root transformed and z-score transformed in the regression plot. The size of the gray dots represent the number of pedons in each basin which were used as weightings in the regression. The solid line represents the regression line and the dashed line represents the 1:1 line.

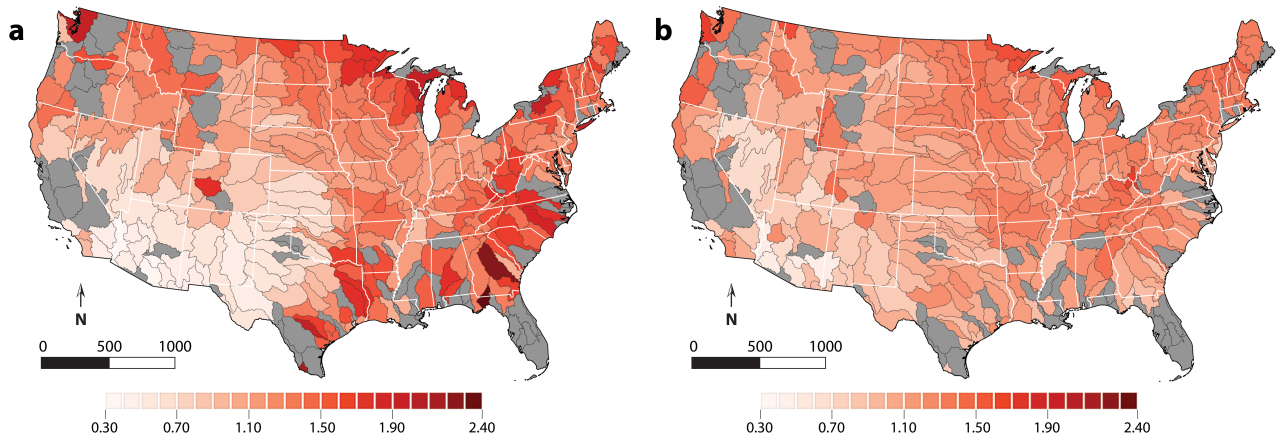

Figure 3.5: (a) Actual and (b) predicted n for the 255 basins (8,262 pedons) used in this study across the conterminous US. The predicted n values displayed were generated from the multiple linear regression model including near-surface horizon ped roundness and SOC in Table 3.2 and Fig. 3.4.

ated with higher ped roundness and SOC values) that corresponded to higher n values occurred in basins that were either more forested or had additional inputs of water (e.g., irrigation) resulting in these higher n values (Fig. 3.3d and e; Fig. 3.5a and b). As previously mentioned, basins that had 15 year (2000-2014) mean annual ET/P values above 1 (i.e., above the water limit) were removed from the dataset. Thus, the extremes of the actual n values were not captured to the same extent in the predicted n values implying there were other compounding factors not included in the model (e.g., precipitation and seasonality characteristics, topography, vegetation, irrigation). However, overall, SOC and roundness controls of ET/P across basins were generally consistent as shown in Fig. 3.4 and Fig. 3.5a and b.

3.4 Discussion

3.4.1 SOC, ped roundness, and ET

Soil organic carbon generally increased from south to north across the US and was more pronounced in basins associated with mountain ranges and forests (Fig. 3.3c). Basins with lower PET/P (humid to sub-humid) generally correlated with increased ped roundness (Fig. 3.3b and f).

Soil organic carbon strongly influences soil aggregation and pore formation (see Six et al., 2004; Bronick & Lal, 2005; Rabot et al., 2018, for relevant reviews). The process of soil aggregation often begins with soil organic matter (SOM) binding primary particles into microaggregates (20–250 μm) which are themselves bound together to form macroaggregates ($>$ 250 μm); alternatively, macroaggregates can form around particulate organic matter with microaggregates forming during the breakdown of macroaggregates (Tisdall & Oades, 1982; Oades, 1984; Angers et al., 1997; Stamati et al., 2013; Rabot et al., 2018). These aggregates contribute to the physical protection of SOC against decomposition and disintegration by disruptive forces (Six et al., 2000; Abiven et al., 2009; Panakoulia et al., 2017). At the ped scale, SOM contributes to increasing ped roundness (Dexter, 1985) and warmer and wetter climates tend to promote aggregation via biological and chemical mechanisms producing peds that are smaller and more equidimensional with smoother surfaces (Mohammed et al., 2020). In these climates, separation of the soil groundmass into finer peds can be the result of increasing root density and biological activity reflected in the production of SOM (Mohammed et al., 2020). In addition, tendencies towards reduced ped size may be the product of combined effects of dense patterns and networks of weakness planes by roots and subsequent soil wetting and drying cycles (Oades, 1993; Angers & Caron, 1998; Ghezzehei, 2012; Mohammed et al., 2020).

As precipitation and subsequent infiltration of water into soil occurs, aggregates with increased SOM are less prone to slaking (i.e., the breaking apart of aggregates) due to the slight hydrophobicity of organic residues which prevent rapid and even wetting of outer surfaces; in addition, moist aggregates are typically less susceptible to slaking due to less air in voids and more continuous coverage of water films leading to a diffuse wetting front (Ghezzehei, 2012). Since some organic materials are inherently hydrophobic (or become so as they dehydrate), SOM can promote aggregate stability by reducing wettability and swelling in addition to increasing strength and stability of intra-aggregate bonding (Hillel, 2004). In general, increased SOM promotes increased water holding capacity (Hudson, 1994; Saxton & Rawls, 2006) and affects the total porosity of soils with its effect on water retention diminishing with decreasing pore size (Rawls et al., 2003). In addition,

increased SOM promotes macroaggregate formation and stability which increases pore volume and decreases bulk density resulting in an increase in plant-available water holding capacity (Eden et al., 2017).

For humid to sub-humid basins largely corresponding to higher n values with tendencies towards n values approaching the energy and water limits, the combined effects of higher SOC and ped roundness contributed to increasing total porosity, hydraulic conductivity, and plant-available water holding capacity (Fig. 3.2; Fig. 3.3b, c, f, and g). Thus, water that percolates into these near-surface horizons is more accessible for uptake by plant roots thereby enhancing ET (Fig. 3.3d and e). As previously mentioned, separation of the soil groundmass into peds via increasing root density and biological activity reflected in the production of SOM (Mohammed et al., 2020) is certainly an important component contributing to increased total porosity, hydraulic conductivity, and plant-available water holding capacity corresponding to higher n values across humid to sub-humid basins (Fig. 3.3b, c, d, f, and g).

3.4.2 Platy soil structure controls effective soil moisture

As mentioned previously, near-surface soil structure in basins with increasing PET/P (i.e., increasingly arid) exhibited decreased ped roundness (Fig. 3.3b and f). Decreased roundness predominantly occurred across the interior western and southwestern US. A general south to north trend of increasing SOC also occurred across these interior western and southwestern basins. Across basins in agricultural regions such as the central, midwestern, and southeastern US, slightly lower values for roundness likely correspond to the occurrence of platy soil structure associated with tillage practices as indicated by the presence of Ap horizons (plowed) in these soils (Fig. 3.3b and d). This mechanical compaction resulting in platy soil structure results in a pronounced horizontal anisotropy of the hydraulic conductivity and intensifies lateral water and solute movement enhancing soil erosion and nutrient export via runoff processes (Horn & Peth, 2012). In addition to the compaction of soil structure in some of these basins, decreased SOC in these agricultural regions also contributes to decreased water retention and the potential for increased runoff (Eden et al.,

2017, Fig. 3.3b, c, and e).

Much lower values of ped roundness, predominantly occurring across basins of the interior western and southwestern US, correspond to the presence of platy soil structure associated with vesicular horizons (V horizons) (Soil Science Division Staff, 2017). These surface or near-surface horizons are characterized by the predominance of vesicular pores and are common across soils in arid and semi-arid environments including approximately 152,000 km^2 of the western US (Turk & Graham, 2011, 2020). Pedogenesis of V horizons is characterized by 1) eolian accumulation beneath a physical or biological surface seal; 2) wet/dry cycles resulting in entrapment of air pockets that develop into vesicular pores; 3) shrink/swell processes resulting in the formation of prismatic and columnar structure; and 4) growth, merging, and collapse of vesicular pores resulting in the formation of platy structure (Turk & Graham, 2011, 2014, 2020). With respect to surface seals, embedded gravels of desert pavement and reg surfaces are especially effective at promoting widespread V horizon formation and generating high runoff (Valentin & Casenave, 1992; Valentin, 1994; Turk & Graham, 2014). Less developed V horizons can be massive (i.e., structureless) or platy, but with increased soil development a primary structure of prisms or columns often parts to a secondary platy structure (McFadden et al., 1998; Anderson et al., 2002; Dietze et al., 2012; Turk & Graham, 2014). Across arid and semi-arid environments, V horizons have much lower infiltration rates compared to non-vesicular soils of shrub islands, ephemeral washes, and young alluvial deposits with negative correlations observed between the abundance of vesicular pores in surface horizons and infiltration rates (Blackburn, 1975; Valentin, 1994; Lebedeva et al., 2009; Turk & Graham, 2011, 2014). Therefore, V horizons promote runoff over infiltration which limits plant water supply, decreases leaching of salts, and consequently increases plant osmotic stress due to high soil salinity (Musick, 1975; Wood et al., 2005; Graham et al., 2008; Turk & Graham, 2014). Thus, with increasing development of V horizons, vegetation becomes increasingly restricted to shrub islands and ephemeral washes where run-on accumulates (Noy-Meir, 1973; Musick, 1975; McAuliffe, 1994; Graham et al., 2008; Turk & Graham, 2014). In addition, incipient V horizons can form within a year in disturbed soils; however, post-disturbance V horizons have lower vesicle

and vugh porosity and lower K_{sat} (Turk & Graham, 2020).

Low ped roundness due to platy structure associated with V horizons in arid and semi-arid basins correlates with increasingly lower n values (Fig. 3.2; Fig. 3.3b, f, and g). Especially across the southwestern US, these lower n values are associated with the widespread occurrence of V horizons which increases runoff and decreases effective soil moisture (i.e., water that infiltrates) as described above (Fig. 3.3b, e, and g). Increased runoff due to platy soil structure associated with V horizons is likely compounded by other factors such as precipitation and seasonality characteristics as well as topography in these arid and semi-arid environments. However, generally increasing SOC from south to north across these interior western and southwestern basins appeared to decrease runoff, increase water retention in near-surface horizons, and increase ET with increasingly higher n values observed (Fig. 3.3c, e, and g).

3.5 Conclusion

This study highlights the role of near-surface soil structure and SOC and the combined effects of these properties in explaining systematic variations of scatter in the Budyko space and points to the importance of these soil properties in controlling ET/P and long-term water balance at a continental scale. Specifically, we observed higher n values (i.e., tendencies towards n values approaching the energy and water limits) for humid to sub-humid basins where the combined effects of higher SOC and ped roundness were related to enhanced ET by increasing total porosity, hydraulic conductivity, and plant-available water holding capacity. Where agriculture was a predominant land use under humid to sub-humid conditions, ped roundness and SOC values decreased and n values were lower. This decline in ped roundness likely corresponds to the presence of platy soil structure that is associated with mechanical compaction and a concomitant reduction in aggregate stability exposing SOC to decomposition; the overall impact of these mechanisms is a decrease in water retention and an increase in runoff. With increasingly arid basins we observed that lower n values were related to lower values of ped roundness. In arid and semi-arid systems, these lower values of ped roundness were also related to the presence of platy soil structure but derived through

mechanisms that form V horizons (and often embedded desert pavement). The platy structure in these environments results in horizontal anisotropy of hydraulic properties that can intensify lateral water movement (Horn & Peth, 2012) and promote an increase in runoff, often shunting water towards shrub islands and ephemeral washes. Overall, this trend was especially pronounced across the southwestern US where ET/P values were lower (runoff ratio values were higher). As SOC generally increased from south to north across these arid and semi-arid basins, we also observed corresponding increases in n values which were associated with an increase in ET driven by the effect of SOC to decrease runoff and increase water retention in near-surface horizons.

Effects of near-surface soil structure and SOC on the long-term water balance at large spatial scales may have cascading and important feedbacks to climate. For example, under a climate scenario of enhanced precipitation, increased soil moisture reduces the frequency of wet-dry cycles and associated shrink-swell behavior minimizing both the abiotic stabilization of soil aggregates and the protection of SOM in aggregate interiors (Bronick & Lal, 2005; Hirmas et al., 2018). The reduction of aggregate stability and the concomitant increase in aggregate SOM decay under higher rainfall conditions could cause a loss of interaggregate macropores, thereby reducing soil K_{sat}. Therefore, mechanisms of macropore "collapse" corresponding to a decline in soil aggregate stability can decrease soil macroporosity and K_{sat} in increasingly energy-limited environments. In contrast, under a climate scenario of increasingly arid conditions associated with water-limited environments, V horizons tend to be more developed which may generate a positive feedback promoting desertification in semi-arid areas by reinforcing hydrologic and ecological patterns characteristic of desert shrublands (Lebedeva et al., 2009; Turk & Graham, 2011). Both of these climate scenario shifts towards extremes may result in catchments becoming subjected to increased runoff. Thus, soil structure-SOC controls on the long-term water balance under changing climate conditions are important to consider in future research efforts. This is especially important given emerging evidence indicating that soil structure is changing faster than previously thought–potentially on decadal timescales–in response to shifts in precipitation regimes (Robinson et al., 2016; Hirmas et al., 2018; Caplan et al., 2019). In addition, soil structure has the potential to

be an important component in Earth system models (e.g., Fatichi et al., 2020) and based on this study we specifically point to the potential of including near-surface SOC and ped roundness in soil parameterization of Budyko models across a wide range of spatial and temporal scales.

Chapter 4

Complexed clay and soil organic carbon control macroporosity across ecoregions

Abstract

Multi-scale evidence of climate-induced soil structural changes occurring at yearly to decadal timescales is mounting. As a result, it has become increasingly important to identify the properties and mechanisms controlling the development and maintenance of soil structure and associated macroporosity. This is especially relevant since macroporosity has disproportionate effects on saturated hydraulic conductivity (K_{sat}) which strongly influences water storage and flux, thus, affecting the water cycle (Hirmas et al., 2018). In this study, we assess the influence of soil, root, and climate properties on effective porosity (EP; a proxy of macroporosity) in both surface and subsurface horizons under varying land use and management practices. Data from 1,491 pedons (3,679 horizons) spanning five ecoregions across the conterminous US were used to show that the EP of surface (A) and subsurface (B) horizons is strongly dependent on the fraction of complexed clay and soil organic carbon (hereafter, 'CCSOC') at a continental scale. We use the relationship between EP and CCSOC to distinguish between undersaturated and oversaturated conditions which refer to the amount of soil organic carbon (SOC) available to complex with clay. In undersaturated conditions (mostly B horizons), steeper increases in EP due to larger amounts of SOC and/or reductions in clay result in a greater proportion of complexed clay leading to stronger organo-mineral bonds and the concomitant development and maintenance of soil structure. In oversaturated conditions (mostly A horizons), the slope describing the EP-CCSOC relationship was positive but

was considerably reduced compared to undersaturated conditions due to all or most of the clay being effectively complexed with SOC. These oversaturated conditions, which are often characterized by increasing accumulations of non-complexed SOM can have varying effects on macroporosity and, as a result, mute the sensitivity of EP to changes in CCSOC creating asymptotical behavior in the relationship between EP and CCSOC. In surface horizons, indirect factors such as mean annual precipitation and land use were important predictors of EP, whereas CCSOC was more influential in controlling EP within the subsoil. The EP-CCSOC relationship also holds within ecoregions but its effect is mitigated by soil and climate interactions suggesting that climate influences this relationship in a complex manner. We found that plowed soils—whether directly influenced by cultivation or underlying plowed horizons—are subject to numerous disturbance effects (e.g., tensile, shear, and/or compressive stresses, clay saturation, and subsoil compaction) that result in increased homogenization of horizons and reduction in the magnitude and rate of change of EP as a function of CCSOC compared to undisturbed horizons. Our findings suggest that the complexed fraction of clay and SOC is important for controlling macroporosity and K_{sat} at ecoregion scales and that the EP-CCSOC relationship may be an important framework in understanding and predicting future land use- and climate-induced changes to soil hydraulic properties.

4.1 Introduction

Emerging evidence at the plot, hillslope, and continental scales indicates that soil structure (i.e., the arrangement of soil particles and pores) is changing faster than previously thought—potentially on decadal timescales—in response to shifts in precipitation regimes (Robinson et al., 2016; Hirmas et al., 2018; Caplan et al., 2019). These structural changes alter soil macroporosity and saturated hydraulic conductivity (K_{sat})—properties in soil that control water storage and flux (e.g., $> 70\%$ of water flux through soil can be controlled by macropores; Watson & Luxmoore, 1986)—and, thus, the water cycle. Specifically, more humid conditions appear to promote a reduction in both macroporosity and K_{sat}, while drier conditions promote an increase in these properties (Hirmas

et al., 2018). The mechanisms governing these rapid responses of soil structure to changing precipitation regimes remain elusive. Biotic processes are the most likely explanation for changes in soil structure on such short timescales, but given the suite of plant and microbial dynamics governing the depth distribution of water, organic carbon, CO_2 fluxes (root and microbe), organic acid production, oxygen availability, and physical mixing via bioturbation by macrofauna, it is difficult to know which specific biologically-controlled processes are most responsible for these changes and how they are coupled to alterations of soil fabric (Sullivan et al., 2022).

Since macroporosity is strongly dependent on particle-size distribution (PSD) and soil organic carbon (SOC) content (Nemes et al., 2005), mechanisms involved in biophysical processes responsible for soil structural changes and alterations of soil material also appear likely to operate in the context of soil texture-SOC interactions. While it is known that macroporosity and K_{sat} exhibit a positive relationship (Ahuja et al., 1984; Watson & Luxmoore, 1986), soil organic matter (SOM) and K_{sat} exhibit a more complex relationship (i.e., both positive and negative relationships) (Nemes et al., 2005; Araya & Ghezzehei, 2019). In general, increases in SOM have been linked to increased K_{sat} due to the influence of SOM on soil aggregation (and stability) and associated pore-size distribution (Hudson, 1994; Saxton & Rawls, 2006). The reason for this positive association is that increases in SOM content promote soil aggregation and lower bulk density which leads to greater porosity resulting in larger K_{sat} (Nemes et al., 2005). Explanations for the negative association between high SOM and K_{sat} have included: (1) that SOM retains water well and this retention acts as part of a complex effect on soil hydraulic conditions where SOM enhances potential hydraulic conductivity by creating larger porosity in the soil, while simultaneously reducing hydraulic conductivity by allowing less water to flow freely due to the ability of SOM to absorb water and (2) that SOM can affect the pore-size distribution of soil through the development of soil structure which influences hydraulic conductivity, although this modification of structure may allow more aggregated material to replace larger cracks and clods resulting in more tortuous and thin pathways for water to go (Nemes et al., 2005). Other studies have attributed negative relationships between SOM and K_{sat} to SOM causing transient sub-critical soil water repellency and inhibiting

water flow due to reduced wettability (Wang et al., 2009b, 2013; Jarvis et al., 2013; Jorda et al., 2015). Thus, SOM can have varying effects on hydraulic properties and mobile organic colloids may clog the soil (Nemes et al., 2005).

Recent work has shown the importance of soil texture for understanding the direction of the association between SOM and K_{sat}. For example, using a machine learning approach, Araya & Ghezzehei (2019) predicted increasing K_{sat} with increasing SOC content for all soil textures except the two coarsest classes (i.e., loamy sand and sand). Their trends suggest that SOC-induced aggregation increases the relative proportion of large pores (inter-aggregate pores such as biopores and macropores) in fine and medium textured soils but increases fine intra-aggregate pores in coarse-textured soils thereby shrinking larger pores and reducing K_{sat}; decreases in K_{sat} at SOC $\geq 3\%$ were predicted for loamy sand and sand textures (Araya & Ghezzehei, 2019). Similar effects of SOC in reducing K_{sat} of coarser soils while increasing that of finer textured soils were found by Rawls et al. (2004) and Nemes et al. (2005) where soils with 50% sand and clay contents ranging between approximately 25 to 45% resulted in lower predicted K_{sat} for soils with higher SOC (5%) compared to those with lower SOC ($1\% \leq$ SOC $\leq 3\%$). Both Araya & Ghezzehei (2019) and Nemes et al. (2005) note the importance of better understanding this complex relationship between SOC content, K_{sat}, and soil texture.

The goal of this study was to build upon the findings in Hirmas et al. (2018) by (1) determining the properties (soil, root, and climate) and mechanisms that control macroporosity in both surface and subsurface horizons under varying land use and management practices with special attention given to the direct and interaction effects of soil texture and SOC, and (2) assessing the importance of these properties and mechanisms at continental and ecoregion scales to explain the reduction in both macroporosity and K_{sat} under humid conditions and their increase under drier conditions. We aim to shed light on the properties and processes controlling soil structural development and macroporosity that have disproportionate effects on K_{sat} (Hirmas et al., 2018).

4.2 Methods

4.2.1 Datasets

In this study, we acquired field-based pedon information and laboratory data collected through the United States Department of Agriculture–Natural Resources Conservation Service (USDA–NRCS) National Cooperative Soil Survey (NCSS) Characterization Database. We selected pedons distributed across broad geographic extents in the US including soils with large and widespread taxonomic diversity (i.e., Entisols, Inceptisols, Mollisols, Aridisols, Alfisols, and Ultisols); poorly drained soils and soils with lithologic discontinuities were removed. These pedons were grouped into United States Environmental Protection Agency (US EPA)/United States Geological Survey (USGS) level I ecoregions (Omernik & Griffith, 2014). Following Hirmas et al. (2018), soil samples were also grouped into surface layers (A horizons) that occurred in the upper 25 cm and subsurface layers (B horizons) that occurred within 25–100 cm of the land surface. Additionally, horizon data were grouped into Ap (plowed) and Bp horizons (defined here as B horizons that occur within a profile that contained a shallower Ap horizon) resulting in four categories of horizons (i.e., A, Ap, B, and Bp) analyzed in this study. In this study, Ap horizons exhibited evidence of plowing (e.g., platy soil structure) at the time of sampling (or in the past), but are not necessarily under current agricultural production. To minimize effects from confounding variables, morphological horizons containing concentrations of aggregating agents, such as carbonate (e.g., Bk), or horizons that were indurated (e.g., Bqm) were not considered in this study. In addition, mean annual precipitation (MAP) and mean annual temperature (MAT) products from the Parameter-elevation Regressions on Independent Slopes Model (PRISM; PRISM Climate Group, Oregon State University, 2021) were merged with the NCSS data.

To better understand soil, root, and climate controls on macroporosity at a continental scale and across ecoregions (including varying land use and management practices), measured, calculated, and/or derived properties from A, Ap, B, and Bp horizons as well as MAP and MAT were included in the analyses. These included PSD, SOM (which was converted from SOC using the standard

SOM:SOC mass ratio of 1.72), field-capacity volumetric water content (FC), complexed clay (CC), complexed SOC (CSOC), mass fraction of water-stable aggregates (WSA), ped size, very fine and fine root class volumetric fractions, total porosity (TP), and effective porosity (EP).

CC and CSOC were calculated following Dexter et al. (2008):

$$\mathrm{CC} = \mathrm{IF}\left[n\mathrm{SOC} < \mathrm{clay}\right]\mathrm{THEN}\left[n\mathrm{SOC}\right]\mathrm{ELSE}\left[\mathrm{clay}\right] \tag{4.1}$$

$$\mathrm{CSOC} = \mathrm{IF}\left[\mathrm{SOC} < \frac{\mathrm{clay}}{n}\right]\mathrm{THEN}\left[\mathrm{SOC}\right]\mathrm{ELSE}\left[\frac{\mathrm{clay}}{n}\right] \tag{4.2}$$

where it was assumed that n g of clay complex with 1 g of SOC where n was set to 10 following Dexter et al. (2008). In this study, we combined CC and CSOC into a single variable (CCSOC) representing the complexed fraction of clay and SOC:

$$\mathrm{CCSOC} = \frac{\mathrm{CC} + \mathrm{CSOC}}{\mathrm{TC} + \mathrm{TSOC}} \tag{4.3}$$

where TC is the total clay and TSOC is the total SOC.

Values of WSA were estimated using an artificial neural network pedotransfer function (Rivera & Bonilla, 2020). Horizons with multiple ped sizes were aggregated using the geometric midpoint of the recorded size classes (Hirmas & Giménez, 2017; Mohammed et al., 2020). Root densities for two root-size classes (i.e., very fine and fine) were calculated from visual descriptions of root distributions made in the field (Mohammed et al., 2020). Lastly, TP for each horizon was derived using the dry bulk density measured at a water content corresponding to a matric potential of -33 kPa. Effective porosity was calculated as the difference between TP and FC; EP was considered to be a proxy of macroporosity representing the volume fraction of the largest pores in the soil (Rawls et al., 1998; Hirmas et al., 2018).

4.2.2 Variable transformations and statistical analyses

Prior to statistical analyses, distributions of all of the variables were visually inspected and transformed to reduce skewness and approximate a normal distribution as needed. Given the compositional and bounded nature of the data used in this study, we transformed and standardized variables as shown in Table 4.1. In order to reduce zero values in the data, several variables were amalgamated including sand and coarse fraction, CC and CSOC (CCSOC; Eq. 4.3), and very fine and fine roots. We used a modified Aitchison procedure (Pawlowsky-Glahn & Egozcue, 2006) to replace the remaining zero values to prepare the variables for a centered log ratio (CLR) transformation. The final variables selected as predictors of EP were sand and coarse fraction (SCF), clay, SOM, CCSOC, WSA, ped size, very fine and fine roots (VFFR), MAP, and MAT. We also selected level I ecoregions that had all four categories of horizons (i.e., A, Ap, B, and Bp) which included Eastern Temperate Forests (ETF), Great Plains (GP), Mediterranean California (MC), North American Deserts (NAD), and Northwestern Forested Mountains (NWFM). For each of these five ecoregions we generated EP models using the selected predictor variables for A, Ap, B, and Bp horizons (i.e., twenty EP models).

To generate these EP models we first detected outliers using an adjusted Mahalanobis distance (Korkmaz et al., 2014) and then used the glmnet R package to fit generalized linear models via penalized maximum likelihood; regularization paths were computed for least absolute shrinkage and selection operator (LASSO) penalties at a grid of values for the regularization parameter λ (Friedman et al., 2010). Although elastic net regularization was initially undertaken, we ultimately used LASSO which resulted in improved prediction across all of the EP models. We also used the glmnet R package to generate cross-validated fits at λ min—that is, the value of λ that gives the minimum mean cross-validated error (Friedman et al., 2010). Following these LASSO regressions, predictors with coefficients of zero were removed and variance inflation factors (VIFs) were used to assess multicollinearity between variables; a VIF $\geq$ 10 was used as an indicator of collinearity between predictor variables as recommended by Logan (2010). A bootstrap procedure was used to determine which variables were significant predictors of EP and β–weights from the LASSO re-

Table 4.1: Below is information on the transformation of variables included in this study. Prior to transformation, CC and CSOC were amalgamated to form a new single complexed clay and SOC variable (CCSOC; Eq. 4.3). This amalgamation was also conducted for sand and coarse fraction (SCF), and very fine and fine roots data (VFFR). In addition, zero values were replaced using a modified Aitchison procedure following Pawlowsky-Glahn & Egozcue (2006) before applying the centered log ratio (CLR) transformation as indicated below. All of the variables below were standardized prior to analyses.

Variable	**Reason for transform**	**Transform**
SCF, clay, SOM, CCSOC, VFFR	Compositional data	Modified Aitchison + CLR
WSA, EP	Compositional and bounded data	Logit
Ped size, MAP, MAT	Bounded data	Log

gression models were used to compare the relative importance of each predictor to EP. In addition, predictions based on the cross-validated fits at λ min were also generated (Friedman et al., 2010) and EP regression models were evaluated by regressing actual against predicted EP.

The LASSO regressions were used to reveal the most important (and significant) predictors of EP across the five ecoregions and four horizon types. The variables identified by LASSO were then analyzed with decision trees (DTs) to assess their relative importance in explaining differences in EP. Prior to the DT analyses, we detected outliers using an adjusted Mahalanobis distance (Korkmaz et al., 2014) across each of the five ecoregions and each of the four respective horizon types. We added two categorical variables—horizon type and land use—with the levels A/B and plowed/non-plowed, respectively. We incorporated both categorical variables and continuous variables in the DT analyses. The rpart and rpart.plot R packages were used to generate DTs and trees were pruned using the default complexity parameter (i.e., 0.01). This parameter represents the overall threshold by which R^2 must increase at each step/node of the splitting process to prevent

Table 4.2: Number of pedons and horizons used in the DT analyses across the Eastern Temperate Forests (ETF), Great Plains (GP), Mediterranean California (MC), North American Deserts (NAD), and Northwestern Forested Mountains (NWFM) ecoregions. Also included below are MAP and MAT $\pm$ one standard deviation for the pedon locations across each of the ecoregions.

Ecoregion	**Number of pedons**	**Number of horizons**	**MAP (mm)**	**MAT (°C)**
ETF	479	1314	1114 ± 167	12.2 ± 3.82
GP	503	1259	661 ± 217	11.5 ± 4.26
MC	92	220	490 ± 278	15.8 ± 2.21
NAD	304	596	310 ± 125	10.4 ± 3.98
NWFM	113	290	638 ± 299	6.84 ± 3.05

overfitting (Therneau et al., 2019; Milborrow, 2021). The complexity parameter at each step/node of the DT represents a minimization of the standard deviation of the errors calculated from cross-validation predictions generated from a set of cost-complexity prunings (Therneau et al., 2019).

4.3 Results and Discussion

4.3.1 Continental-scale relationships

The variables identified from LASSO were SCF, clay, SOM, CCSOC, WSA, MAP, and MAT while the variables of ped size and VFFR appeared to have a more minor role in controlling EP based on the dataset we analyzed (see Table B1 and Fig. B.1). A total of 1,491 pedons fit our criteria across the five ecoregions and were used in the DTs (Fig. 4.1). The number of horizons with complete cases for all variables included in the DT analyses (i.e., EP, SCF, clay, SOM, CCSOC, WSA, MAP, and MAT) ranged from 220 to 1,314 across the ecoregions in this study (Table 4.2). These locations captured a wide range in MAP and MAT, spanning 310–1,114 mm and 6.8–15.8 °C, respectively (Table 4.2).

EP was predicted by clay, CCSOC, ecoregion, and land use at a continental scale across all of the sites in this study (Fig. 4.2; $R^2 = 0.484$). Clay occurred at the first, second, and third split levels all of which showed a negative relationship with EP; this is not surprising given soil texture

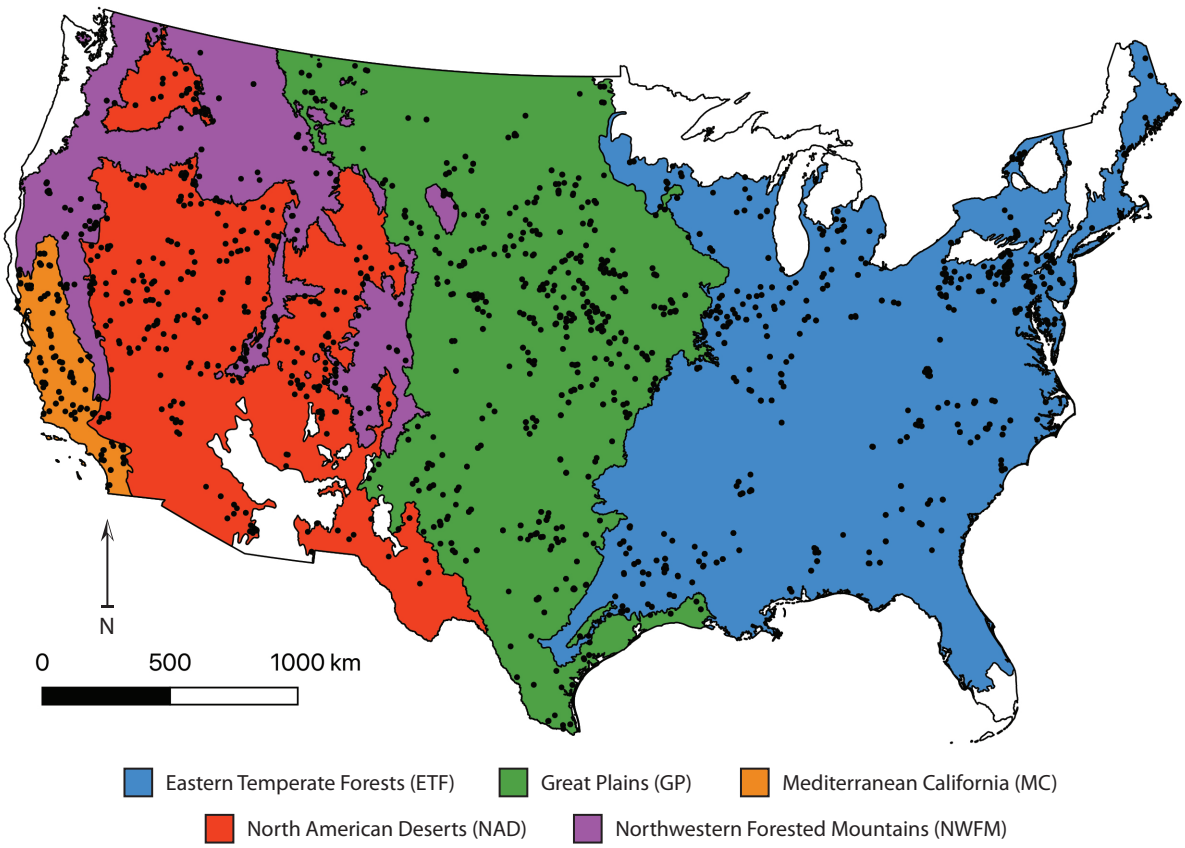

Figure 4.1: Spatial distribution of pedon locations used in DT analyses across the Eastern Temperate Forests (ETF; blue), Great Plains (GP; green), Mediterranean California (MC; orange), North American Deserts (NAD; red), and Northwestern Forested Mountains (NWFM; purple) ecoregions of the conterminous US.

is known to be a primary control of EP (Rawls et al., 1982, 1998; Nemes et al., 2005; Hirmas et al., 2018). For the bulk soil properties of the first DT split, higher clay (left branch) was represented by an elevated mean clay content (36.1%) and a lower mean SOC content (0.661%) across horizons, while lower clay (right branch) was represented by a lower mean clay content (17.0%) and an elevated mean SOC content (1.21%) across horizons. Lessivage is a ubiquitous process that is likely responsible for this clay separation between the two branches as fines translocate from surface A horizons and accumulate within subsurface B horizons (Buol et al., 2011; Turk et al., 2012). The differences in SOC content between the two branches also suggest this first split is governed by horizon development as A horizons accumulate more humified organic matter compared to B horizons (Buol et al., 2011; Turk et al., 2012).

4.3.1.1 Relationships between EP and CCSOC

CCSOC was the second factor that emerged in predicting EP, and exhibited a strong positive relationship with EP across horizons that contained a higher clay content. To better understand this relationship we directly regressed EP and CCSOC (Fig. 4.3a and b). We fit a piecewise linear regression (Muggeo, 2003, 2008) to the data based on their shape and estimated a breakpoint value of -0.250. Using the segmented R package, a standard linear model is fitted at each iteration with a 'gap' parameter (γ) that re-parameterizes the difference-in-slopes parameter (ψ) between two fitted straight lines such that when the algorithm converges, the 'gap' should be small and one standard error distance around the breakpoint value can be obtained; at each step, every breakpoint estimate is updated through the relevant 'gap' and 'difference-in-slope' coefficients (Muggeo, 2003, 2008). EP was more sensitive to changes in CCSOC below the breakpoint (higher clay content, lower SOC/SOM content), and less sensitive above the breakpoint (Fig. 4.3a and b). Below the breakpoint, any additional SOC and/or reduction in clay (such that a greater fraction of the clay is complexed) will cause a steep increase in EP. However, above the breakpoint, when all of the clay is already complexed, any additional organic matter does not cause EP to change very much. Several studies have shown that organo-mineral complexes (i.e., chemically protected organic matter

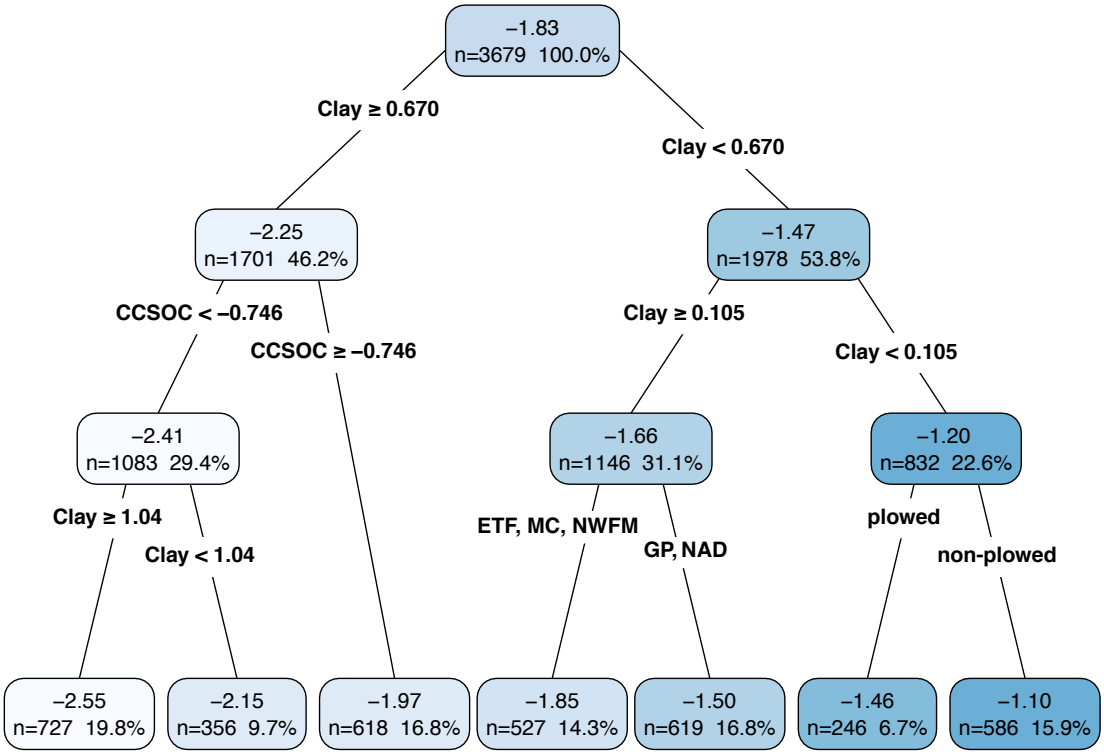

Figure 4.2: Pruned DT displaying predicted EP at a continental scale across the conterminous US. All categorical variables (i.e., ecoregion, horizon type, and land use) and continuous (transformed) variables (i.e., SCF, clay, SOM, CCSOC, WSA, MAP, and MAT) were included as predictors. The first values displayed in the blue-shaded nodes correspond to the mean EP (mean transformed EP) of the data subset, whereas the second and third values refer to the number (n) of horizons and the percentage of all horizons that fall in each subset, respectively. These three values are determined by the criteria specified in the previous splits with lighter shades of blue indicating lower mean EP and darker shades of blue indicating higher mean EP.

bound to soil minerals) have a propensity to saturate with SOC likely due to the finite amount of mineral specific surface area onto which SOC can be stabilized (Hassink, 1996; Chung et al., 2008; Gulde et al., 2008; Stewart et al., 2008; Feng et al., 2014). In other words, what really matters for EP is the percentage of clay surface area that is complexed with SOC. When that surface area is not yet saturated, EP can change more readily in response to SOC additions compared to when the surface area is saturated.

Samples below and above the CCSOC breakpoint in Fig. 4.3a and b have in general an effective mineral surface area (represented by the clay fraction) that is either partially or completely complexed with SOC, respectively (*sensu* Dexter et al., 2008). Here, we refer to partial complexation as "undersaturated" (i.e., values of CCSOC lower than the breakpoint) and complete complexation as "oversaturated" (i.e., CCSOC values above the breakpoint). The term "oversaturated" refers to the excess SOC not complexed with soil clay. Additional inputs of SOC in undersaturated conditions lead to increasing complexation and strengthening of organo-mineral bonds and concomitant development and/or maintenance of soil structure which increases EP (Dexter et al., 2008). However, in oversaturated conditions, EP will respond more slowly to increased inputs of SOC. In addition, declines in SOC stabilization and storage efficiency as soils approach saturation may be linked to changes in the type, strength, or turnover time of organo-mineral interactions with increasing SOC inputs (Kleber et al., 2007; Sollins et al., 2009; Feng et al., 2014). For example, as soils approach SOC saturation, weaker organic–organic interactions become relatively more abundant than stronger organo-mineral interactions and it has been hypothesized that the stability and strength of SOC bound to soil minerals decreases with increasing SOC loadings (Kleber et al., 2007; Feng et al., 2014). Thus, while increasing complexation and a strengthening of organo-mineral bonds can occur with these inputs, it is accompanied by an abundance of non-complexed SOM that can have varying effects on macroporosity ultimately muting the sensitivity of EP to changes in CCSOC and resulting in the asymptotical behavior of the EP-CCSOC relationship.

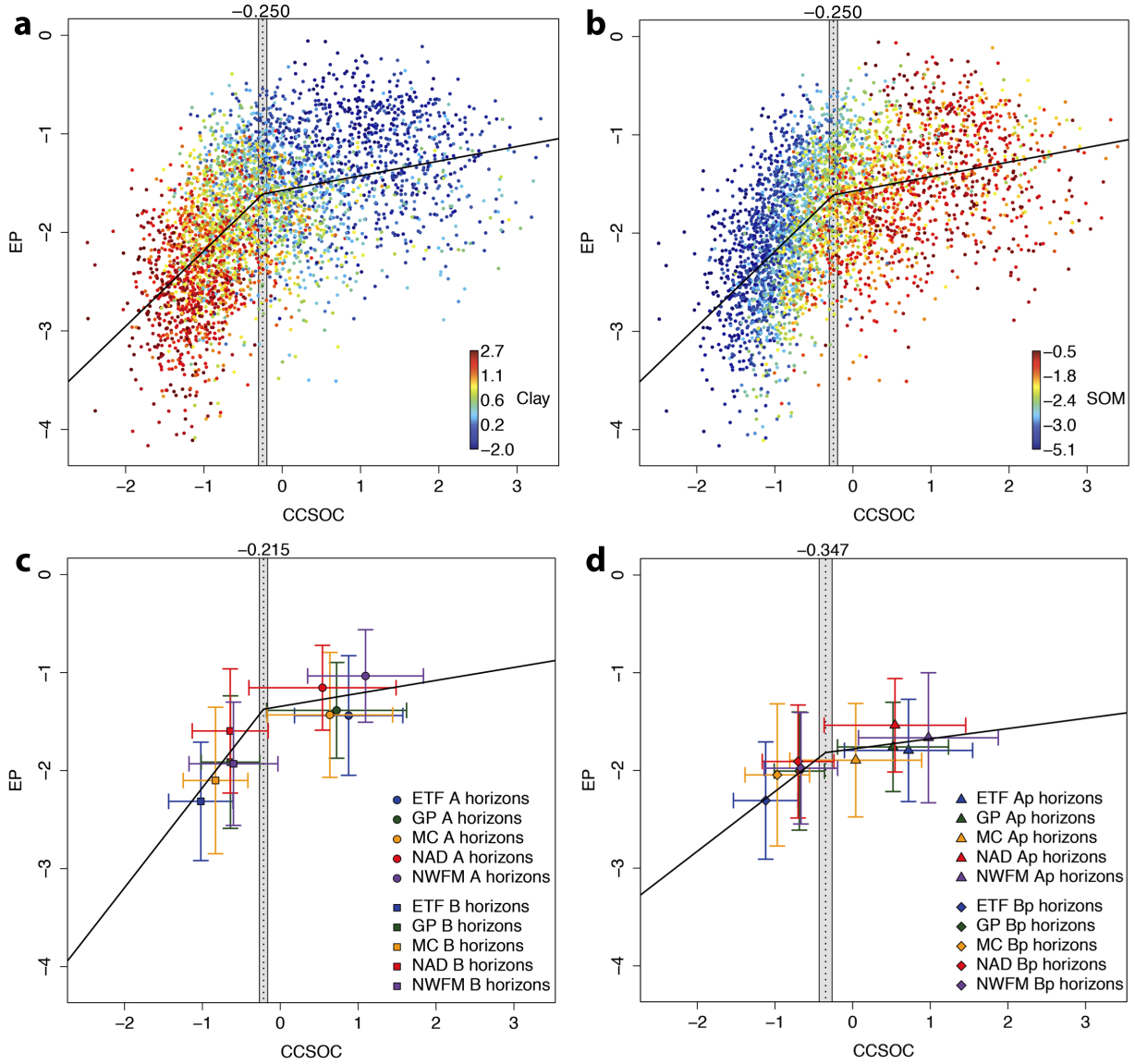

Figure 4.3: (a) and (b) Piecewise linear regression of EP vs. CCSOC colored by clay and SOM, respectively, across all ecoregions and horizon types at a continental scale ($R^2 = 0.339$). The shaded bar at -0.250 represents one standard error distance around the breakpoint value. (c) Centroids and error bars ($\pm$ one standard deviation) for A horizons (circles) and B horizons (squares) across the ETF (blue), GP (green), MC (orange), NAD (red), and NWFM (purple) ecoregions. Piecewise linear regression of EP vs. CCSOC ($R^2 = 0.433$) with the shaded bar at -0.215 represents one standard error distance around the breakpoint value. (d) Centroids and error bars ($\pm$ one standard deviation) for Ap horizons (triangles) and Bp horizons (diamonds) across the ETF (blue), GP (green), MC (orange), NAD (red), and NWFM (purple) ecoregions. Piecewise linear regression of EP vs. CCSOC ($R^2 = 0.244$) with the shaded bar at -0.347 represents one standard error distance around the breakpoint value. All of the variables in this figure were transformed as shown in Table 4.1.

4.3.1.2 Ecoregions and land use trends

When considering both lower and higher CCSOC, we note that the breakpoint value of -0.250 in Fig. 4.3a and b generally corresponds to the clay and SOC differences observed in the first split of the DT in Fig. 4.2. As previously mentioned for the first split, the breakpoint value also largely corresponded to differences between A and B horizons with the former having lower clay content and higher SOC and the latter enriched in clay and lower in SOC. The same was true for a higher breakpoint value separating A and B horizons (-0.215) and a lower breakpoint value separating Ap and Bp horizons (-0.347) (Fig. 4.3c and d, respectively). Thus, B and Bp horizons exhibited lower CCSOC and A and Ap horizons exhibited higher CCSOC (i.e., CCSOC values less or greater than the corresponding breakpoints). However, differences between CCSOC of these horizons (with respect to the breakpoints) emerged when examining ecoregion and land use influences on EP.

For horizons with higher CCSOC (right branch; Fig. 4.2), ecoregion and land use occurred at the third split level of the DT. Specifically, the ETF, MC, and NWFM ecoregions corresponded to decreased EP, whereas the GP and NAD ecoregions corresponded to increased EP (following a second split level of higher clay). Plowed horizons corresponded to decreased EP and non-plowed horizons corresponded to increased EP (following a second split level of lower clay). The potential for increased clay-SOC complexation due to increased mineral surface area likely dictated the higher clay content branch splitting between ecoregions with lower EP (i.e., ETF, MC, and NWFM) and higher EP (i.e., GP and NAD). This ecoregion split could also be attributed to differences in how SOC inputs are stabilized onto mineral surfaces via various organo-mineral bonding reactions (e.g., ligand exchange, cation bridging, H-bonding, van der Waal forces) that depend on a number of factors (e.g., composition of organic inputs, soil mineralogy, environmental factors) (Arnarson & Keil, 2000; Gu et al., 1994; Stevenson, 1994; Feng et al., 2014). Decreased clay-SOC complexation potential due to decreased mineral surface area likely had an impact on the lower clay content branch splitting between plowed and non-plowed horizons. In this case, the split between plowed horizons (decreased EP) and non-plowed horizons (increased EP) likely involved processes occurring in predominantly the non-complexed SOC pool. With respect to crop

production systems, observed losses of SOC induced by cultivation include reduced allocation of organic carbon to soils, reduced belowground allocation of photosynthate, enhanced aggregate disruption and exposure of physically-protected organic carbon, and enhanced rates of decomposition of available organic carbon substrates due to more favorable abiotic conditions (e.g., aeration, temperature, and water content) (Baldock & Broos, 2012). Therefore, disturbance effects such as plowing which reduce SOC in these horizons are likely responsible for the decreased EP. Here we reiterate that due to the lower clay content across horizons, more of the SOC present is not complexed with clay and is therefore subject to more rapid turnover processes associated with the labile non-complexed SOC pool (which is also a factor contributing to decreased EP). Finally, non-plowed horizons would allow for more SOC accumulation and increased EP. The lower clay content across these horizons also corresponds to processes occurring in the non-complexed SOC pool where more of the SOC present is not complexed with clay; however, SOC is more abundant which is a factor contributing to increased EP.

Land use (and management) appears to be driving changes in EP and CCSOC to varying degrees across ecoregions. In general, both EP and CCSOC decreased from A to Ap and B to Bp horizons across ecoregions. This trend was more pronounced from A to Ap horizons as exhibited by differences in mean EP (transformed) for the ETF (A: -1.44; Ap: -1.80), GP (A: -1.39; Ap: -1.76), MC (A: -1.43; Ap: -1.90), NAD (A: -1.15; Ap: -1.54), and NWFM (A: -1.03; Ap: -1.67) (Fig. 4.3c and d). Likewise, differences in mean CCSOC (transformed) also exhibited this trend across surface horizons of the ETF (A: 0.878; Ap: 0.720), GP (A: 0.724; Ap: 0.520), MC (A: 0.637; Ap: 0.0398), and NWFM (A: 1.09; Ap: 0.976) although NAD values were similar (A: 0.542; Ap: 0.545) (Fig. 4.3c and d). This trend was less pronounced from B to Bp horizons as exhibited by differences in mean EP for the GP (B: -1.91; Bp: -2.01) and NWFM (B: -1.93; Bp: -1.98) although NAD values were more pronounced (B: -1.60; Bp: -1.91); in addition, ETF values were similar (B: -2.31; Bp: -2.31) and MC values increased from B to Bp horizons (B: -2.10; Bp: -2.05) (Fig. 4.3c and d). Similarly, differences in mean CCSOC also exhibited a less pronounced trend (however, all were decreasing from B to Bp) across subsurface horizons of the

ETF (B: -1.02; Bp: -1.12), GP (B: -0.640; Bp: -0.686), MC (B: -0.831; Bp: -0.970), NAD (B: -0.643; Bp: -0.703), and NWFM (B: -0.601; Bp: -0.666) (Fig. 4.3c and d). We note that smaller sample sizes for MC Ap and Bp horizons (n = 25 and 37, respectively) as well as NWFM Ap and Bp horizons (n = 11 and 14, respectively) should be taken into account when interpreting these results (see Table B1 for n of A, Ap, B, and Bp horizons by ecoregion).

Although there was overlap of errors associated with centroids in Fig. 4.3c and d, disturbance effects such as plowing generally contributed to decreases in both EP and CCSOC that were more pronounced in surface horizons and less pronounced but nonetheless propagated in subsurface horizons (with some notable exceptions discussed in the following sections). These surface and subsurface horizon changes occurred despite mineral-bound SOC comprising a large majority of total SOC and having longer turnover times (Balesdent et al., 1988; Christensen, 1998; Trumbore, 2000; Kahle et al., 2002; Feng et al., 2014). In general, Ap and Bp centroids were grouped more closely compared to A and B centroids (Fig. 4.3c and d). This appeared to indicate that disturbance effects lead to homogenization of the EP-CCSOC relationship for Ap and Bp horizons including a weakening of this relationship for Bp horizons with relatively low CCSOC values when compared to undisturbed (or less disturbed) conditions across A and B horizons.

4.3.1.3 Impact of disturbance effects on the EP-CCSOC relationship

Comparing A and B centroids (Fig. 4.3c) with Ap and Bp centroids (Fig. 4.3d) does provide some indication of disturbance whereby reduction in the magnitude and rate of change of EP as a function of CCSOC occurs. In general, A and B horizons (undisturbed or less disturbed; hereafter, 'undisturbed') indicate an increase of CCSOC (and soil structure) with increases in EP. Ap and B horizons under Ap (hereafter, 'disturbed') indicate a reduction of CCSOC (and soil structure) with decreases in EP. Czyż & Dexter (2016) estimate that the effective density of clay-organic complexes is very low with a mean value of 0.17 ± 0.04 g ml^{-1} in arable soils; this low value suggests that clay-organic complexes are extremely porous with open structures perhaps in the form of fibers or chains. Therefore, when considering clay-organic complexes as a separate phase in

soils they can account for observed reductions in bulk density with increasing SOM contents as well as disproportionately large effects on soil structure and behavior (Dexter et al., 2008; Czyż & Dexter, 2016). When comparing mean differences between ecoregion median values greater than the breakpoints, undisturbed CCSOC and EP values were 0.429 and 0.380 greater than disturbed values, respectively; for soils below the CCSOC breakpoints, undisturbed CCSOC and EP values were 0.0760 and 0.0897 greater than disturbed values, respectively. Thus, these changes in EP appear to be driven by disturbance effects (e.g., tensile, shear, and/or compressive external forces caused by field operations) which impact the amount and stability of CCSOC with concomitant modifications of soil structure (Dexter, 1988; Ghezzehei, 2012; Horn & Peth, 2012).

Accompanying these general decreases in CCSOC and EP from undisturbed to disturbed settings were general decreases in WSA. When comparing mean differences between ecoregion median values greater than the breakpoints, undisturbed WSA values (untransformed) were 13.4% greater than disturbed values; for less than the breakpoints, undisturbed WSA values were 2.85% greater than disturbed values (Fig. 4.3c and d). Since stress attenuation is greater for increasingly aggregated soils (under in situ conditions for soils with the same internal parameters) (Horn & Peth, 2012), tensile strength associated with CCSOC and WSA of undisturbed soils is likely greater and more effective at attenuating stress than tensile strength of CCSOC and WSA associated with disturbed soils (with corresponding impacts on EP). However, since a combination of shear and compressive stresses generally characterize in situ stress conditions during field operations (e.g., traffic, soil-tool interactions) (Horn & Peth, 2012), a number of other accompanying and compounding factors impacting the EP-CCSOC relationship must be considered. When comparing mean differences between ecoregion median values greater than the breakpoints, undisturbed bulk density, ped size, and clay values were 0.0380 g cm^{-3}, 4.04 mm, and 5.56% less than disturbed values, respectively; for less than the breakpoints, undisturbed bulk density values were 0.0690 g cm^{-3} greater than disturbed values, whereas ped size and clay values were 3.91 mm and 5.09% less than disturbed values, respectively (Fig. 4.3c and d).

For CCSOC values greater than the breakpoints (mainly surface horizons), undisturbed bulk

density values were lower than disturbed values indicating compression and densification in plowed horizons (Ap horizons) likely due to traffic during field operations. However, in B and Bp horizons, which were generally undersaturated with respect to CCSOC, undisturbed bulk densities were greater than those from disturbed horizons. While the reasons for this finding are unclear, this may be due to the effect of shear stresses in disturbed horizons where shearing behavior in aggregated soil depends on the water content and density of the aggregates as well as the geometry of the applied stress system (Dexter, 1988; Ghezzehei, 2012). If the density of the structured soil is above a characteristic critical value, shearing is confined to a well-defined surface or narrow band near the source of the stress where rolling of round particles or alignment of platy clay particles can occur and gross changes in volume take place in only a small proportion of the soil. In contrast, if the density of the structured soil is below the critical value then stress propagates through the whole soil volume resulting in an overall increase in density with disproportionate destruction of larger pores and consequent reductions in air-filled porosity and hydraulic conductivity (Kurtay & Reece, 1970; Hettiaratchi & O'Callaghan, 1980; Dexter, 1988; Ghezzehei, 2012). Therefore, undisturbed bulk densities that were greater than disturbed bulk densities may reflect the former scenario where density of the structured soil is above the critical value and soil-tool interactions cause shearing that is more so confined near the source of the stress with gross changes in volume taking place in a small proportion of the soil.

Clay contents from undisturbed horizons were less than those in disturbed horizons suggesting that deep-loosening or deep-plowing and/or mixing with other soil material not only led to declines in soil stability and strength (Horn & Peth, 2012), but also brought illuvial clay upward and mixed it throughout the disturbed horizons. Peds were smaller for A and B horizons compared to Ap and Bp horizons likely because of the presence of clods in disturbed horizons. Clods are formed due to compaction by agricultural machinery where boundaries between macroaggregates may be lost or remain as microcracks depending on soil wetness and machinery loads during compaction; clods can also be formed during desiccation of large masses of clayey soil (Ghezzehei, 2012). Thus, clods and their formation processes are particularly important in subsoil horizons which typ-

ically do not have aggregates but exhibit similarly complex structure that, in contrast to topsoil (aggregate) structure, can be almost irreversibly damaged when subjected to subsoil compaction (Ghezzehei, 2012). In sum, due to external forces associated with field operations, Ap and Bp horizons not only undergo numerous disturbance effects (e.g., tensile, shear, and/or compressive stresses, clay saturation, subsoil compaction) but through these effects they also become increasingly homogenized and exhibit a reduction in the magnitude and rate of change of EP as a function of CCSOC (Fig. 4.3d) when compared to undisturbed A and B horizons (Fig. 4.3c).

4.3.2 Effects of A and B horizons on EP

As previously mentioned, lessivage and the accumulation of humified organic matter creates either under- or oversaturated conditions that strongly control EP. These conditions are expressed in subsurface (B) and surface (A) horizons, respectively. For example, Fig. 4.4 shows the results of the same DT analysis as in Fig. 4.2 but with clay and CCSOC removed. As can be seen in this figure, EP was predicted by horizon type first, and then by SCF, MAP, SOM, and land use across all sites in this study ($R^2 = 0.379$) confirming that undersaturated conditions largely correspond to B horizons (i.e., lower CCSOC and EP) and oversaturated conditions to A horizons (i.e., higher CCSOC and EP). With clay removed, both A and B horizons were split by SCF in the DT with values of SCF positively correlated to EP (Fig. 4.4). The increase in SCF in A horizons and decrease in B horizons likely indicate the translocation of fines from surface horizons into subsurface layers (Koop et al., 2020).

A horizon EP was predicted by clay, MAP, land use, SCF, SOM, and ecoregion (Fig. 4.5a; $R^2 = 0.397$). Similarly, EP in B horizons was predicted by clay, MAP, SCF, and ecoregion; however, CCSOC was an important predictor while land use was not (Fig. 4.5b; $R^2 = 0.449$). At the first split level, both A and B horizons split by clay with higher clay resulting in decreased EP and lower clay resulting in increased EP. Although differences between A and B horizons emerged at the second split level, both horizon types were dependent on the fraction of clay complexed with SOC. Higher MAP in A horizons correspond with decreases in EP likely due to increased

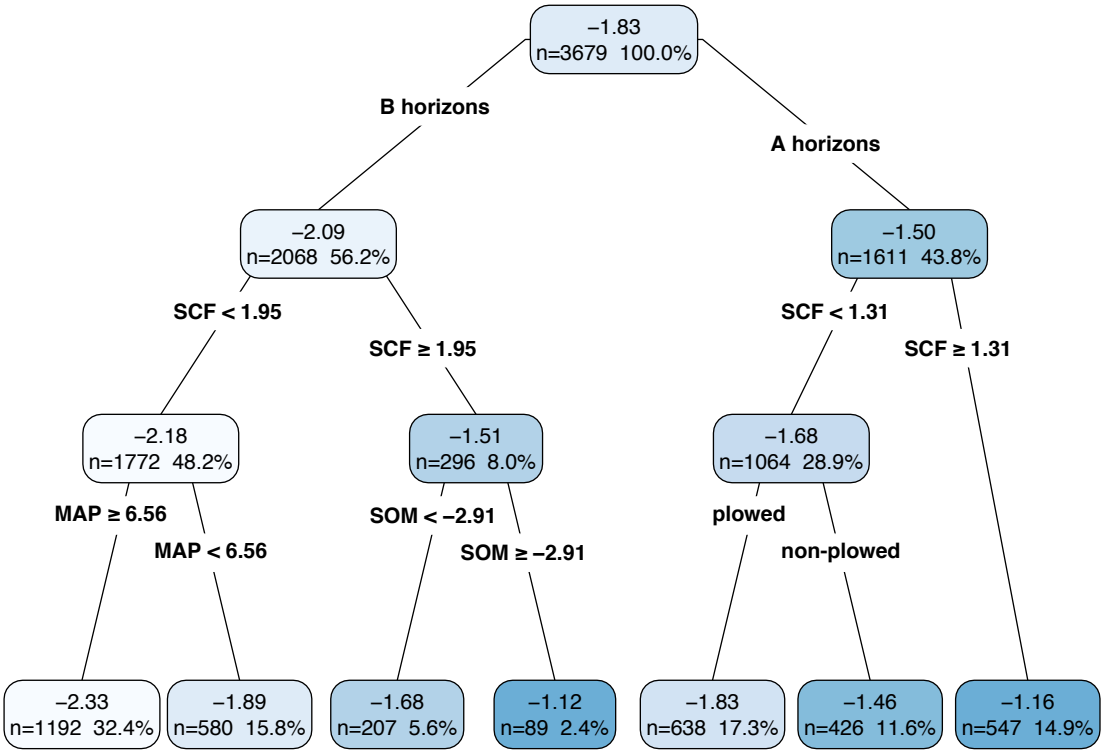

Figure 4.4: Pruned DT showing predicted EP (mean transformed EP) at a continental scale across the conterminous US. All categorical variables (i.e., ecoregion, horizon type, and land use) and continuous (transformed) variables except clay and CCSOC (i.e., SCF, SOM, WSA, MAP, and MAT) were included as predictors. Refer to the Fig. 4.2 caption for general guidance on DT interpretation.

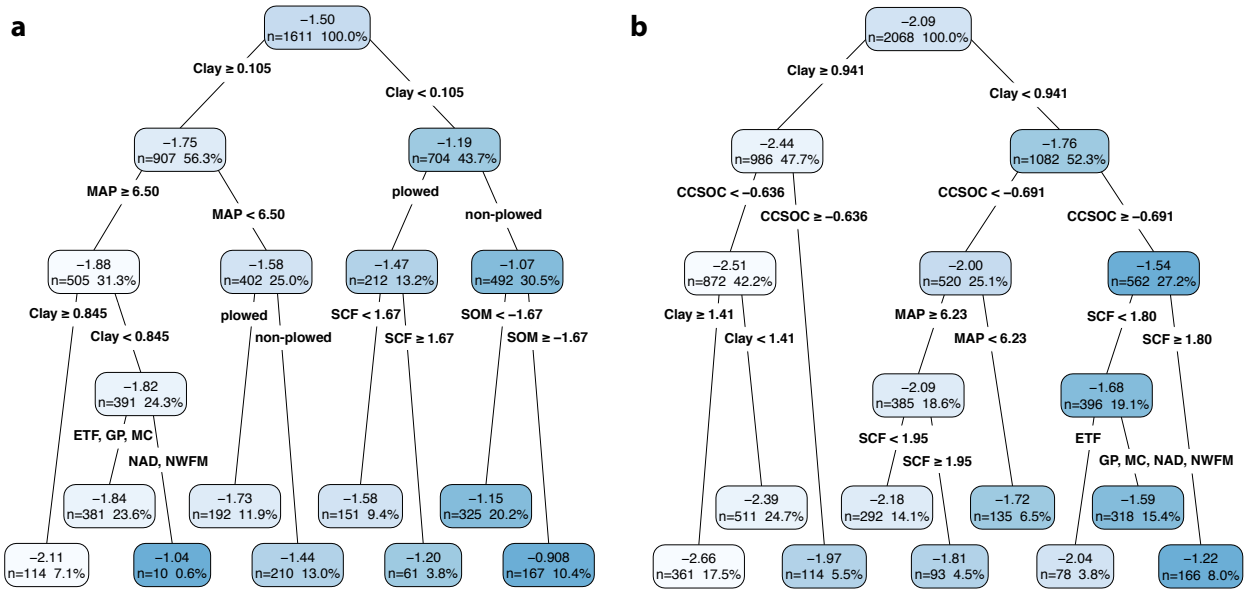

Figure 4.5: Pruned DTs displaying predicted EP at a continental scale across the conterminous US for (a) A horizons and (b) B horizons. For both horizon types, categorical variables (i.e., ecoregion and land use) and continuous variables (i.e., SCF, clay, SOM, CCSOC, WSA, MAP, and MAT) were included as predictors. Refer to the Fig. 4.2 caption for general guidance on DT interpretation.

weathering and production of secondary minerals which corresponded to higher clay and, thus, a reduced fraction of that clay complexed with SOC (Fig. 4.5a). Under lower MAP, decreases in weathering and production of secondary minerals are likely responsible for lower clay contents making a greater proportion of that clay subject to complexation with SOC with, correspondingly, greater potential for aggregation and increases in EP. B horizons, however, more directly reflect the EP-CCSOC relationship at the second split level of the DT (Fig. 4.5b). Since A horizons are typically oversaturated with respect to CCSOC, we observed more indirect factors (i.e., MAP, land use) coming to the forefront as important predictors of EP, whereas since B horizons are typically undersaturated, we observe a more direct influence of CCSOC on EP. In general, clay content in these B horizons was not fully complexed with SOC and, therefore, EP showed a greater response to increased SOC in the subsoil.

Table 4.3: Relationships of variables with EP (+ and − signs indicate the direction of the relationship) and R^2 values for the ETF, GP, MC, NAD, and NWFM ecoregion DTs displayed in Fig. 4.6a, b, c, d, and e, respectively.

Ecoregion	Variable	Relationship with EP	R^2
ETF	Clay	−	0.399
	WSA	+	
	SCF	+	
GP	Clay	−	0.615
	CCSOC	+	
	MAT	−	
	MAP	−	
	SCF	+	
	Plowing	−	
MC	Clay	−	0.771
	MAP	−	
	CCSOC	+	
	MAT	−	
NAD	Clay	−	0.501
	CCSOC	+	
	MAP	−	
	SCF	+	
	Plowing	−	
NWFM	CCSOC	+	0.712
	WSA	+	
	SOM	−	
	SCF	+	

4.3.3 Ecoregion influences on EP

All of the DTs by ecoregion also first split into under- and oversaturated conditions with respect to the proportion of clay complexed with SOC, with the left and right branches largely representing B and A horizons, respectively (Fig. 4.6). This ecoregion behavior was similar to the behavior observed in the continental-scale DTs (Fig. 4.2 and Fig. 4.4). Overall, the ability of the DTs to predict EP across the ecoregions varied from an $R^2 = 0.399$ to $R^2 = 0.771$ with the least confidence in the ETF and the greatest confidence in the MC ecoregion (Fig. 4.6; Table 4.3).

Although the EP-CCSOC relationship holds at a continental scale, differences in how this re-

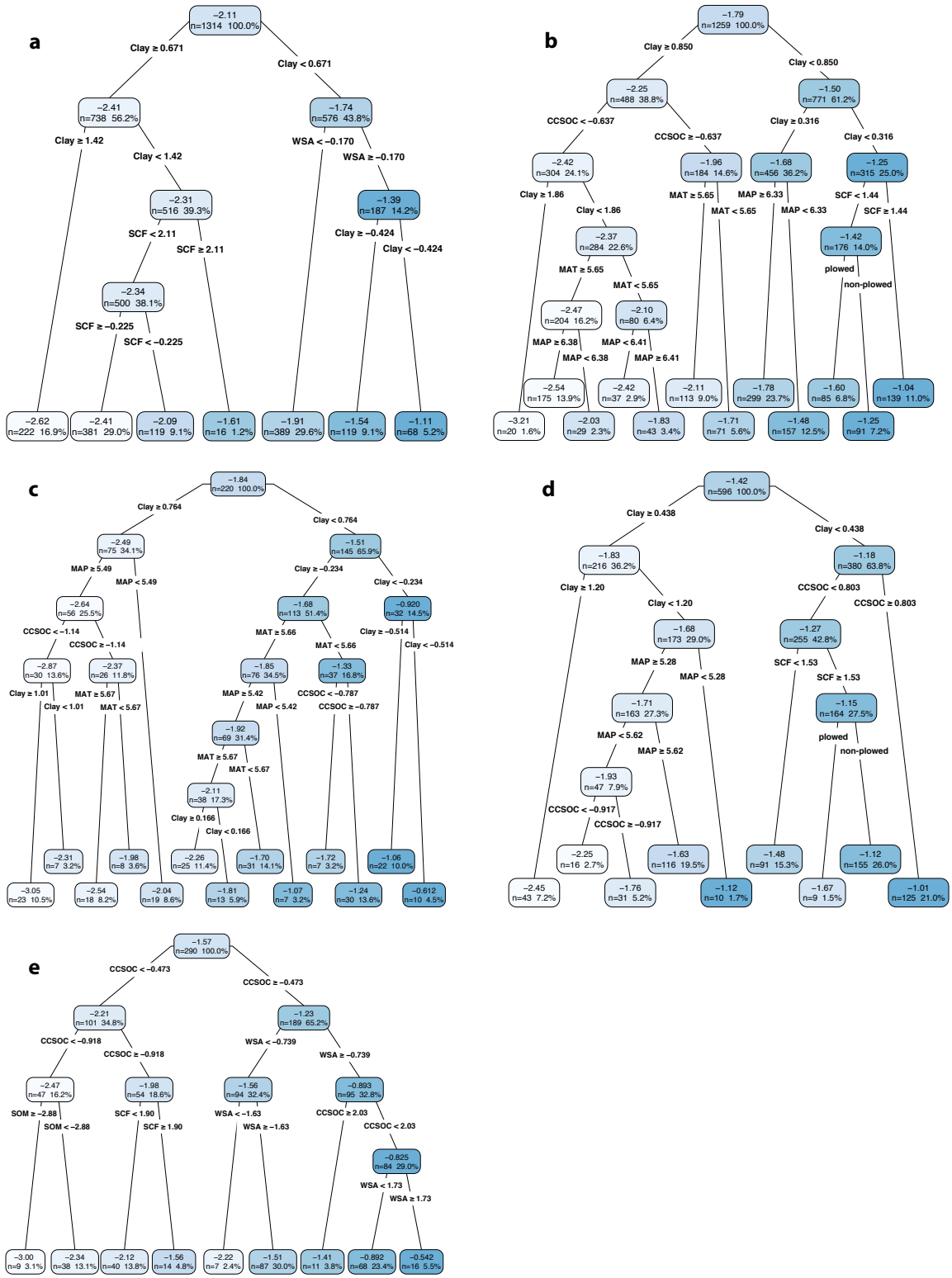

Figure 4.6: Pruned DTs showing predicted EP (mean transformed EP) for (a) ETF, (b) GP, (c) MC, (d) NAD, and (e) NWFM ecoregions of the conterminous US. For each ecoregion, categorical variables (i.e., horizon type and land use) and continuous (transformed) variables (i.e., SCF, clay, SOM, CCSOC, WSA, MAP, and MAT) were included as predictors. Refer to the Fig. 4.2 caption for general guidance on DT interpretation.

lationship is manifested by soil and climate interactions emerge when comparing ecoregions. At the first split level, all of the ecoregions, except NWFM, split between clay content with higher and lower values on the left and right branches largely representing B and A horizons, respectively (Fig. 4.6a, b, c, and d). CCSOC occurred at the first split for NWFM where lower values on the left branch were associated with B horizons, whereas higher values on the right branch corresponded to A horizons (Fig. 4.6e). Thus, EP within the NWFM ecoregion appears to exhibit a propensity to respond to SOC additions for both surface and subsurface horizons. The similarity in the EP-CCSOC relationship between A and B horizons may be due to the increased occurrence of macroaggregation as represented by WSA emerging as the next strongest predictor of EP (Fig. 4.6e). WSA also occurred at the second split level of the ETF DT (right branch; oversaturated A horizons) (Fig. 4.6a). The increased aggregation in forested soils may be caused by both elevated additions of organic matter and increases in acidity. Rivera & Bonilla (2020) observed a positive gradient of macroaggregate stability from arid to humid environments due to increases in SOM and decreases in pH. At lower pH values (< 7), solubility and mobility of cations are higher resulting in the formation of bridges with clay and SOM; in addition, microbial activity under lower pH values increases and promotes macroaggregation and stabilization (Tisdall & Oades, 1982; Bronick & Lal, 2005; Regelink et al., 2015; Wu et al., 2017; Rivera & Bonilla, 2020). Thus, in these forested (or previously forested) environments with higher MAP (Table 4.2) and SOM and lower pH, WSA is an important predictor that is positively associated with EP (Table 4.3).

Where MAP was more limited or where steeper climatic gradients occurred (i.e., GP, MC, NAD; Table 4.2), climate (i.e., MAP, MAT) tended to have an important and negative relationship with EP (Fig. 4.6b, c, and d; Table 4.3). Across the conterminous US, SOC generally increases as MAP increases up to 700–850 mm and then SOC content fluctuates as MAP continues to increase (Guo et al., 2006). However, when considering grassland and forest ecosystems with MAP < 1000 mm, SOC generally decreases as MAT increases across elevations < 600 m and slopes $< 1^{\circ}$ (Guo et al., 2006). The negative correlation between SOC and MAT implies that the relative temperature sensitivity of decomposition is greater than that of net primary productivity although

strong interactions between temperature, water availability, and substrate quantity make it difficult to assess the temperature dependence of decomposition without confounding effects (Baldock & Broos, 2012). The generally negative correlations between climate (i.e., MAP, MAT) and EP likely reflected the positive association between MAP and weathering and production of secondary minerals (and lessivage) (Buol et al., 2011; Schaetzl & Thompson, 2015) and the negative association between MAT and SOC (Guo et al., 2006) which strongly influences the fraction of clay complexed with SOC. However, other than a second split level in the MC ecoregion (left branch; undersaturated B horizons) where higher MAP likely corresponded to increased illuvial clay accumulation (and, thus, lower EP) and lower MAP corresponded to decreased clay illuviation resulting in higher EP (Fig. 4.6c), MAP and MAT occurred at lower split levels with less explanatory power. This suggests that climate influences the EP-CCSOC relationship more indirectly and likely in a complex manner. Additionally, CCSOC occurred at the second split level of the GP DT (left branch in Fig. 4.6b; undersaturated B horizons) which was similar to where it occurred in the continental-scale DTs in Fig. 4.2 and Fig. 4.5b suggesting that the GP ecoregion with its sizable area and steep climatic gradients (north-south MAT; west-east MAP) captured what was occurring in subsurface (B) horizons at a continental scale. That is, EP exhibits a propensity to respond to SOC additions and/or reductions in clay increasing the proportion of complexed clay. EP responding to both SOC additions and reductions in clay was perhaps best exemplified in CCSOC occurring at the first split level of the NWFM DT (right branch) and the second split level of the NAD DT (right branch). The steeper increase in EP of surface (A) horizons was likely linked to coarser textures (and SOC additions) that increased the fraction of complexed clay in these ecoregions of the western US (Fig. 4.6d and e; Table 4.3).

4.4 Conclusion

This work highlights that EP (a proxy of macroporosity) of surface (A) and subsurface (B) horizons is strongly dependent on the fraction of clay complexed with SOC (as represented by CCSOC). In this study, we use the relationship between EP and CCSOC to distinguish between undersaturated

(i.e., low values of CCSOC; largely B horizons) and oversaturated (i.e., high CCSOC values; largely A horizons) conditions; these conditions refer to the amount of SOC available to complex with clay. In undersaturated conditions, steeper increases in EP are associated with larger amounts of SOC and/or reductions in clay that result in a greater fraction of complexed clay leading to stronger organo-mineral bonds and the concomitant development or maintenance of soil structure. In oversaturated conditions, the slope describing the EP-CCSOC relationship was positive but reduced compared to undersaturated conditions. This reduction was likely due to all or most of the clay being already effectively complexed and the varying effects that increasing accumulations of non-complexed SOM can have on macroporosity. Ultimately, these oversaturated conditions mute the sensitivity of EP to changes in CCSOC and result in the observed asymptotical behavior of the EP-CCSOC relationship.

Since surface (A) horizons typically exhibit oversaturated conditions with higher SOC and lower clay contents, indirect factors (e.g., MAP, land use) are important predictors of EP. However, since subsurface (B) horizons are typically associated with undersaturated conditions (i.e., higher clay content and lower SOC), direct influences from CCSOC on EP occurs in the subsoil. We found that the EP-CCSOC relationship was also important for explaining changes in EP within ecoregions but its effect is mitigated by soil and climate interactions. In forested ecoregions (i.e., ETF, NWFM) with higher MAP and SOM and lower pH, increased macroaggregation and stability of these macroaggregates are positively associated with EP. Where MAP is more limited or where steeper climatic gradients occur (i.e., GP, MC, NAD), climate (i.e., MAP, MAT) tends to be negatively correlated with EP likely due to the positive association between MAP and the production or translocation of secondary minerals through weathering and lessivage and the negative association between MAT and SOC. Thus, climate appears to influence the EP-CCSOC relationship in an indirect and complex manner.

We found that EP exhibits strong tendencies to positively respond to SOC additions and/or reductions in clay both of which increase the proportion of complexed clay. This may explain why drier climates (e.g., the western US), which tend to have low to moderate clay contents with low

to moderate SOC contents, lead to increases in the fraction of complexed clay and concomitant increases in macroporosity and K_{sat}. For humid climates (e.g., the eastern US), which tend to have moderate to high clay contents with moderate to moderately high SOC contents, increases in the proportion of complexed clay and concomitant increases in macroporosity and K_{sat} can also occur. However, under humid climates, soils with high SOC/SOM contents where all or most of the clay is complexed create oversaturated conditions such that non-complexed SOM can have varying effects on macroporosity and K_{sat} including reductions of these properties. This may be especially true for coarser textures in humid environments with high SOM where less clay corresponds to a reduced fraction of complexed clay leading to reductions in macroporosity and K_{sat}. Finally, disturbance as represented by the Ap and Bp horizons creates conditions that are more homogenized compared to A and B horizons which reduces the magnitude and rate of change of EP as a function of CCSOC. In sum, the findings of this work point to the importance of complexed clay and SOC in controlling macroporosity and K_{sat} across ecoregions and suggests that the EP-CCSOC relationship provides an important framework for understanding and predicting future land use- and climate-induced changes to soil hydraulic properties.

Chapter 5

Conclusions

Chapters 2-4 of this dissertation represent broad-scale approaches to soil development and morphology coupled with an examination of the impact of soil properties and soil-climate interactions on the water cycle at continental, basin, and ecoregion scales. In Chapter 2, I developed generalizable horizon and profile development indices (HDIs and PDIs, respectively) based primarily on relative horizon properties instead of parent material information and evaluated these indices at a continental scale. These indices reflect general patterns of pedogenesis for several soil orders of broad geographic extent and integrate relative soil morphological, physical, and chemical information by taking into account how eluvial and illuvial processes shape topsoil and subsoil horizons. This work showed that the developed HDIs and PDIs were valid proxies of soil development, applicable across large geographic scales, and may aid in a number of broad-scale applications (e.g., pedogenic modeling, identification of anomalies, estimation of surface soil ages) including a better understanding of how climatic and land-use pressures influence pedogenesis. One promising avenue of future research would be the development of a pedogenic model incorporating the HDI and PDI with a soil climate index and ^{14}C dating to generate quantitative data at the horizon-scale (e.g., degree of parent material preconditioning) and at the pedon-scale (e.g., soil age) that could be extrapolated to produce spatial distributions of these properties. This would likely involve the development of a pedotransfer function that relates MAT and MAP to the soil climate index representing the drivers of soil formation and that distributes the index with depth. The pedogenic model would be calibrated using HDIs from well-studied and documented sites with strongly established temporal and environmental contexts. Finally, the model would be applied to pedons using the dataset from Chapters 2-4 utilizing HDIs to generate quantitative spatial and temporal

data of horizon- and pedon-scale properties across the conterminous US.

The findings in Chapter 3 suggest that the combined effects of higher soil organic carbon (SOC) and ped roundness in humid and sub-humid basins are related to enhanced evapotranspiration by increasing total porosity, hydraulic conductivity, and plant-available water holding capacity. Lower SOC and ped roundness values in these environments likely correspond to agricultural practices that lead to the formation of platy soil structure via mechanical compaction and concomitant decreases in infiltration and increases in runoff. In arid and semi-arid basins, low ped roundness corresponding to natural platy soil structure associated with vesicular horizons lead to decreases in infiltration and increases in runoff which shunt water towards shrub islands and ephemeral washes. This work provides evidence that near-surface soil structure and SOC may explain systematic differences in long-term water balance at a continental scale pointing to potentially important climate feedbacks and the need to include soil structure in Earth system models. To accomplish this goal would require developing a non-stationary pedotransfer function that incorporates the linkage between soil structure, SOC, and climate to derive hydraulic parameters for Earth system models.

Chapter 4 shows that effective porosity (EP; a proxy of macroporosity) of surface (A) and subsurface (B) horizons is strongly dependent on the fraction of clay complexed with SOC (hereafter, 'CCSOC') at both continental and ecoregion scales. The relationship between EP and CCSOC was used to distinguish between undersaturated and oversaturated conditions referring to the amount of SOC available to complex with clay. In undersaturated conditions (largely B horizons), steeper increases in EP were associated with: (1) larger amounts of SOC and/or reductions in clay resulting in a greater proportion of complexed clay, (2) stronger organo-mineral bonds, and (3) concomitant development and maintenance of soil structure. However, in oversaturated conditions, the slope describing the EP-CCSOC relationship was positive but reduced compared to undersaturated conditions due to: (1) all or most of the clay being effectively complexed with SOC, (2) increased accumulations of non-complexed SOM which had varying effects on macroporosity, and (3) resultant muting of the sensitivity of EP to changes in CCSOC creating an asymptotic behavior of the EP-CCSOC relationship.

Additional findings from Chapter 4 indicate that indirect factors such as mean annual precipitation and land use are important predictors of EP in surface horizons, whereas CCSOC is likely more influential in controlling EP within subsurface horizons. Across ecoregions, the effect of the EP-CCSOC relationship appeared to be mitigated by soil-climate interactions suggesting that climate influences this relationship in an indirect and complex manner. Since EP exhibits strong tendencies to positively respond to SOC additions and/or reductions in clay (both of which increase the fraction of complexed clay) this may explain why (1) drier climates (e.g., the western US), which often have low to moderate clay contents with low to moderate SOC contents, exhibit increases in the proportion of complexed clay and associated increases in macroporosity and K_{sat}; and (2) humid climates (e.g., the eastern US), which often have moderate to high clay contents with moderate to moderately high SOC contents, also exhibit increases in the fraction of complexed clay and associated increases in macroporosity and K_{sat}. However, humid climates characterized by soils with high SOC/SOM contents where all or most of the clay is complexed result in oversaturated conditions where non-complexed SOM can have varying effects on macroporosity and K_{sat} including reductions of these properties. Reductions in macroporosity and K_{sat} may be especially prevalent in humid environments characterized by coarser-textured soils with high SOM where less clay corresponds to a reduced fraction of complexed clay. Finally, when comparing Ap and Bp horizons (disturbed) with A and B horizons (undisturbed), the former was characterized by homogenization of soil conditions and a reduction in the magnitude and rate of change of EP as a function of CCSOC. In light of the strong influence of the complexed fraction of clay and SOC on macroporosity and K_{sat} at ecoregion scales, the EP-CCSOC relationship has the potential to be an important framework for understanding and predicting future land use- and climate-induced changes to soil hydraulic properties.

In conclusion, I offer several additional examples of how the broad-scale approaches and findings summarized above might aid future research focused on the impact of soil properties and soil-climate interactions on the water cycle at varying scales. First, in addition to the use of generalizable HDIs and PDIs in pedogenic modeling efforts, as covariates, or as stratifying variables,

these indices could also be used as inputs in pedotransfer functions to aid in the prediction of hydraulic properties. Second, the inclusion of near-surface SOC and ped roundness in soil parameterization of Budyko models across a wide range of spatial and temporal scales could provide confirmation of the role of soils in combining with other factors to explain systematic differences in water balance. Finally, the development of the EP-CCSOC relationship as a framework to understand soil macropore sensitivity to additions of SOC and the incorporation of this framework into hydrologic and Earth system models could capture land use- and climate-induced changes to soil hydraulic properties and more effectively predict alterations to water cycling across scales. Pursuing these directions in future research has the potential to address widespread ecosystem service challenges induced by increasing climate and land-use pressures.

References

Abiven, S., Menasseri, S., & Chenu, C. (2009). The effects of organic inputs over time on soil aggregate stability–A literature analysis. *Soil Biology and Biochemistry*, 41(1), 1–12.

Ahuja, L. R., Naney, J. W., Green, R. E., & Nielsen, D. R. (1984). Macroporosity to characterize spatial variability of hydraulic conductivity and effects of land management. *Soil Science Society of America Journal*, 48(4), 699–702.

Alonso, P., Sierra, C., Ortega, E., & Dorronsoro, C. (1994). Soil development indices of soils developed on fluvial terraces (Peñaranda de Bracamonte, Salamanca, Spain). *Catena*, 23(3-4), 295–308.

Amit, R., Harrison, J. B. J., Enzel, Y., & Porat, N. (1996). Soils as a tool for estimating ages of Quaternary fault scarps in a hyperarid environment—the southern Arava valley, the Dead Sea Rift, Israel. *Catena*, 28(1-2), 21–45.

Anderson, K., Wells, S., & Graham, R. (2002). Pedogenesis of vesicular horizons, Cima Volcanic Field, Mojave Desert, California. *Soil Science Society of America Journal*, 66(3), 878–887.

Angers, D. A. & Caron, J. (1998). Plant-induced changes in soil structure: Processes and feedbacks. *Biogeochemistry*, 42(1), 55–72.

Angers, D. A., Recous, S., & Aita, C. (1997). Fate of carbon and nitrogen in water-stable aggregates during decomposition of $^{13}C^{15}N$-labelled wheat straw in situ. *European Journal of Soil Science*, 48(2), 295–300.

Applegarth, M. T. & Dahms, D. E. (2001). Soil catenas of calcareous tills, Whiskey Basin, Wyoming, USA. *Catena*, 42(1), 17–38.

Araya, S. N. & Ghezzehei, T. A. (2019). Using machine learning for prediction of saturated hydraulic conductivity and its sensitivity to soil structural perturbations. *Water Resources Research*, 55(7), 5715–5737.

Arnarson, T. S. & Keil, R. G. (2000). Mechanisms of pore water organic matter adsorption to montmorillonite. *Marine Chemistry*, 71(3-4), 309–320.

Arora, V. K. (2002). The use of the aridity index to assess climate change effect on annual runoff. *Journal of Hydrology*, 265(1-4), 164–177.

Badía, D., Martí, C., Palacio, E., Sancho, C., & Poch, R. M. (2009). Soil evolution over the Quaternary period in a semiarid climate (Segre river terraces, northeast Spain). *Catena*, 77(3), 165–174.

Baldock, J. A. & Broos, K. (2012). Soil organic matter. In P. M. Huang, Y. Li, & M. E. Sumner (Eds.), *Handbook of Soil Sciences: Properties and Processes* chapter 11, (pp. 11–1—11–52). Boca Raton, FL: CRC Press, 2nd edition.

Balesdent, J., Wagner, G. H., & Mariotti, A. (1988). Soil organic matter turnover in long-term field experiments as revealed by C-13 natural abundance. *Soil Science Society of America Journal*, 52(1), 118–124.

Barrett, L. R. & Schaetzl, R. J. (1993). Soil development and spatial variability on geomorphic surfaces of different age. *Physical Geography*, 14(1), 39–55.

Barrón, V. & Torrent, J. (1986). Use of the Kubelka–Munk theory to study the influence of iron oxides on soil colour. *Journal of Soil Science*, 37(4), 499–510.

Barshad, I. (1966). The effect of a variation in precipitation on the nature of clay mineral formation in soils from acid and basic igneous rocks. In *Proceedings of the International Clay Conference (Jerusalem)*, volume 1 (pp. 167–173).

Beaudette, D. E., Roudier, P., & O'Geen, A. T. (2013). Algorithms for quantitative pedology: A toolkit for soil scientists. *Computers and Geosciences*, 52, 258–268.

Berghuijs, W. R., Gnann, S. J., & Woods, R. A. (2020). Unanswered questions on the Budyko framework. *Hydrological Processes*, 34(26), 5699–5703.

Berghuijs, W. R., Sivapalan, M., Woods, R. A., & Savenije, H. H. (2014a). Patterns of similarity of seasonal water balances: A window into streamflow variability over a range of time scales. *Water Resources Research*, 50(7), 5638–5661.

Berghuijs, W. R., Woods, R., & Hrachowitz, M. (2014b). A precipitation shift from snow towards rain leads to a decrease in streamflow. *Nature Climate Change*, 4(7), 583–586.

Berry, M. E. (1987). Morphological and chemical characteristics of soil catenas on Pinedale and Bull Lake moraine slopes in the Salmon River Mountains, Idaho. *Quaternary Research*, 28(2), 210–225.

Berry, M. E. (1990). Soil catena development on fault scarps of different ages, eastern escarpment of the Sierra Nevada, California. *Geomorphology*, 3(3-4), 333–350.

Berry, M. E. (1994). Soil-geomorphic analysis of late-Pleistocene glacial sequences in the McGee, Pine, and Bishop Creek drainages, East-Central Sierra Nevada, California. *Quaternary Research*, 41, 160–175.

Bevington, P. R. & Robinson, K. D. (2003). *Data reduction and error analysis for the physical sciences*. New York: McGraw-Hill, 3rd edition.

Bilzi, A. F. & Ciolkosz, E. J. (1977). A field morphology rating scale for evaluating pedological development. *Soil Science*, 124(1), 45–48.

Birkeland, P. W. (1984). Holocene soil chronofunctions, Southern Alps, New Zealand. *Geoderma*, 34(2), 115–134.

Birkeland, P. W. (1994). Variation in soil-catena characteristics of moraines with time and climate, South Island, New Zealand. *Quaternary Research*, 42(1), 49–59.

Birkeland, P. W. (1999). *Soils and Geomorphology*. New York: Oxford University Press, 3rd edition.

Birkeland, P. W. & Burke, R. M. (1988). Soil catena chronosequences on eastern Sierra Nevada moraines, California, USA. *Arctic and Alpine Research*, 20(4), 473–484.

Blackburn, W. (1975). Factors influencing infiltration and sediment production of semiarid rangelands in Nevada. *Water Resources Research*, 11(6), 929–937.

Bockheim, J. G. (1990). Soil development rates in the Transantarctic Mountains. *Geoderma*, 47(1-2), 59–77.

Bockheim, J. G. & Gennadiyev, A. N. (2010). Soil-factorial models and earth-system science: A review. *Geoderma*, 159(3-4), 243–251.

Bronick, C. J. & Lal, R. (2005). Soil structure and management: a review. *Geoderma*, 124(1-2), 3–22.

Budyko, M. I. (1974). *Climate and Life*. New York: Academic Press.

Buol, S. W., Southard, R. J., Graham, R. C., & McDaniel, P. A. (2011). *Soil Genesis and Classification*. Hoboken, NJ: Wiley-Blackwell, 6th edition.

Busacca, A. J. (1987). Pedogenesis of a chronosequence in the Sacramento Valley, California, USA, I. Application of a soil development index. *Geoderma*, 41(1-2), 123–148.

Calero, J., Delgado, R., Delgado, G., & Martín-García, J. M. (2008). Transformation of categorical field soil morphological properties into numerical properties for the study of chronosequences. *Geoderma*, 145(3-4), 278–287.

Calero, J., Delgado, R., Delgado, G., & Martín-García, J. M. (2009). SEM image analysis in the study of a soil chronosequence on fluvial terraces of the middle Guadalquivir (southern Spain). *European Journal of Soil Science*, 60(3), 465–480.

Caplan, J. S., Giménez, D., Hirmas, D. R., Brunsell, N. A., Blair, J. M., & Knapp, A. K. (2019). Decadal-scale shifts in soil hydraulic properties as induced by altered precipitation. *Science Advances*, 5(9), eaau6635.

Carmona, A. M., Sivapalan, M., Yaeger, M. A., & Poveda, G. (2014). Regional patterns of interannual variability of catchment water balances across the continental US: A Budyko framework. *Water Resources Research*, 50(12), 9177–9193.

Chen, X., Alimohammadi, N., & Wang, D. (2013). Modeling interannual variability of seasonal evaporation and storage change based on the extended Budyko framework. *Water Resources Research*, 49(9), 6067–6078.

Choudhury, B. J. (1999). Evaluation of an empirical equation for annual evaporation using field observations and results from a biophysical model. *Journal of Hydrology*, 216(1-2), 99–110.

Christensen, B. T. (1998). Carbon in primary and secondary organo-mineral complexes. In M. R. Carter & B. A. Stewart (Eds.), *Structure and Organic Matter Storage in Agricultural Soils* (pp. 97–165). Boca Raton, FL: CRC Press.

Chung, H., Grove, J. H., & Six, J. (2008). Indications for soil carbon saturation in a temperate agroecosystem. *Soil Science Society of America Journal*, 72(4), 1132–1139.

Condon, L. E., Atchley, A. L., & Maxwell, R. M. (2020). Evapotranspiration depletes groundwater under warming over the contiguous United States. *Nature Communications*, 11(1), 873.

Condon, L. E. & Maxwell, R. M. (2017). Systematic shifts in Budyko relationships caused by groundwater storage changes. *Hydrology and Earth System Sciences*, 21(2), 1117–1135.

Creed, I. F., Spargo, A. T., Jones, J. A., Buttle, J. M., Adams, M. B., Beall, F. D., Booth, E. G., Campbell, J. L., Clow, D., Elder, K., et al. (2014). Changing forest water yields in response to climate warming: results from long-term experimental watershed sites across North America. *Global Change Biology*, 20(10), 3191–3208.

Cremeens, D. L. & Mokma, D. L. (1986). Argillic horizon expression and classification in the soils of two Michigan hydrosequences. *Soil Science Society of America Journal*, 50(4), 1002–1007.

Czyż, E. A. & Dexter, A. R. (2016). Estimation of the density of the clay-organic complex in soil. *International Agrophysics*, 30(1), 19–23.

Daly, E., Calabrese, S., Yin, J., & Porporato, A. (2019). Linking parametric and water-balance models of the Budyko and Turc spaces. *Advances in Water Resources*, 134, 103435.

Dexter, A. (1985). Shapes of aggregates from tilled layers of some Dutch and Australian soils. *Geoderma*, 35(2), 91–107.

Dexter, A. R. (1988). Advances in characterization of soil structure. *Soil and Tillage Research*, 11(3-4), 199–238.

Dexter, A. R., Richard, G., Arrouays, D., Czyż, E. A., Jolivet, C., & Duval, O. (2008). Complexed organic matter controls soil physical properties. *Geoderma*, 144(3-4), 620–627.

Dietze, M., Bartel, S., Lindner, M., & Kleber, A. (2012). Formation mechanisms and control factors of vesicular soil structure. *Catena*, 99, 83–96.

Donohue, R. J., Roderick, M., & McVicar, T. R. (2007). On the importance of including vegetation dynamics in Budyko's hydrological model. *Hydrology and Earth System Sciences*, 11(2), 983–995.

Donohue, R. J., Roderick, M., & McVicar, T. R. (2010). Can dynamic vegetation information improve the accuracy of Budyko's hydrological model? *Journal of Hydrology*, 390(1-2), 23–34.

Donohue, R. J., Roderick, M. L., & McVicar, T. R. (2012). Roots, storms and soil pores: Incorporating key ecohydrological processes into Budyko's hydrological model. *Journal of Hydrology*, 436-437, 35–50.

Dooge, J., Bruen, M., & Parmentier, B. (1999). A simple model for estimating the sensitivity of runoff to long-term changes in precipitation without a change in vegetation. *Advances in Water Resources*, 23(2), 153–163.

Dorronsoro, C. & Alonso, P. (1994). Chronosequence in Almar River fluvial-terrace soil. *Soil Science Society of America Journal*, 58(3), 910–925.

Du, C., Sun, F., Yu, J., Liu, X., & Chen, Y. (2016). New interpretation of the role of water balance in an extended Budyko hypothesis in arid regions. *Hydrology and Earth System Sciences*, 20(1), 393–409.

Eden, M., Gerke, H. H., & Houot, S. (2017). Organic waste recycling in agriculture and related effects on soil water retention and plant available water: a review. *Agronomy for Sustainable Development*, 37(2), 11.

Fatichi, S., Or, D., Walko, R., Vereecken, H., Young, M. H., Ghezzehei, T. A., Hengl, T., Kollet, S., Agam, N., & Avissar, R. (2020). Soil structure is an important omission in Earth System Models. *Nature Communications*, 11(1), 522.

Feng, W., Plante, A. F., Aufdenkampe, A. K., & Six, J. (2014). Soil organic matter stability in organo-mineral complexes as a function of increasing C loading. *Soil Biology and Biochemistry*, 69, 398–405.

Fick, S. E. & Hijmans, R. J. (2017). WorldClim 2: new 1-km spatial resolution climate surfaces for global land areas. *International Journal of Climatology*, 37(12), 4302–4315.

Friedman, J., Hastie, T., & Tibshirani, R. (2010). Regularization paths for generalized linear models via coordinate descent. *Journal of Statistical Software*, 33(1), 1–22.

García-García, F., Calero, J., & Pérez-Valera, F. (2016). Morphological, pedological, and sedimentary evolution on the fringe of the southwestern European drylands during the Late Pleistocene and Holocene: Evidence of climate and land use changes. *Catena*, 143, 128–139.

Gentine, P., D'Odorico, P., Lintner, B. R., Sivandran, G., & Salvucci, G. (2012). Interdependence of climate, soil, and vegetation as constrained by the Budyko curve. *Geophysical Research Letters*, 39(19), L19404.

Gerrits, A. M. J., Savenije, H. H. G., Veling, E. J. M., & Pfister, L. (2009). Analytical derivation of the Budyko curve based on rainfall characteristics and a simple evaporation model. *Water Resources Research*, 45(4), W04403.

Ghezzehei, T. A. (2012). Soil structure. In P. M. Huang, Y. Li, & M. E. Sumner (Eds.), *Handbook of Soil Sciences: Properties and Processes* chapter 2, (pp. 2–1—2–17). Boca Raton, FL: CRC Press, 2nd edition.

Graham, R. C., Hirmas, D. R., Wood, Y. A., & Amrhein, C. (2008). Large near-surface nitrate pools in soils capped by desert pavement in the Mojave Desert, California. *Geology*, 36(3), 259–262.

Greve, P., Gudmundsson, L., Orlowsky, B., & Seneviratne, S. I. (2015). Introducing a probabilistic Budyko framework. *Geophysical Research Letters*, 42(7), 2261–2269.

Gu, B., Schmitt, J., Chen, Z., Liang, L., & McCarthy, J. F. (1994). Adsorption and desorption of natural organic matter on iron oxide: Mechanisms and models. *Environmental Science & Technology*, 28(1), 38–46.

Gulde, S., Chung, H., Amelung, W., Chang, C., & Six, J. (2008). Soil carbon saturation controls labile and stable carbon pool dynamics. *Soil Science Society of America Journal*, 72(3), 605–612.

Guo, Y., Gong, P., Amundson, R., & Yu, Q. (2006). Analysis of factors controlling soil carbon in the conterminous United States. *Soil Science Society of America Journal*, 70(2), 601–612.

Hall, R. D. & Shroba, R. R. (1995). Soil evidence for a glaciation intermediate between the Bull Lake and Pinedale glaciations at Fremont Lake, Wind River Range, Wyoming, USA. *Arctic and Alpine Research*, 27(1), 89–98.

Harden, J. W. (1982). A quantitative index of soil development from field descriptions: examples from a chronosequence in central California. *Geoderma*, 28(1), 1–28.

Harden, J. W. & Matti, J. C. (1989). Holocene and late Pleistocene slip rates on the San Andreas fault in Yucaipa, California, using displaced alluvial-fan deposits and soil chronology. *Geological Society of America Bulletin*, 101(9), 1107–1117.

Harden, J. W. & Taylor, E. M. (1983). A quantitative comparison of soil development in four climatic regimes. *Quaternary Research*, 20(3), 342–359.

Harden, J. W., Taylor, E. M., Hill, C., Mark, R. K., McFadden, L. D., Reheis, M. C., Sowers, J. M., & Wells, S. G. (1991). Rates of soil development from four soil chronosequences in the southern Great Basin. *Quaternary Research*, 35(3-Part1), 383–399.

Harrison, J. B. J., McFadden, L. D., & Weldon III, R. J. (1990). Spatial soil variability in the Cajon Pass chronosequence: implications for the use of soils as a geochronological tool. *Geomorphology*, 3(3-4), 399–416.

Hassink, J. (1996). Preservation of plant residues in soils differing in unsaturated protective capacity. *Soil Science Society of America Journal*, 60(2), 487–491.

Hettiaratchi, D. R. P. & O'Callaghan, J. R. (1980). Mechanical behavior of agricultural soils. *Journal of Agricultural Engineering Research*, 25(3), 239–259.

Hickel, K. & Zhang, L. (2006). Estimating the impact of rainfall seasonality on mean annual water balance using a top-down approach. *Journal of Hydrology*, 331(3-4), 409–424.

Hillel, D. (2004). *Introduction to environmental soil physics*. Amsterdam: Elsevier Academic Press.

Hirmas, D. R. & Allen, B. L. (2007). Degradation of pedogenic calcretes in West Texas. *Soil Science Society of America Journal*, 71(6), 1878–1888.

Hirmas, D. R. & Giménez, D. (2017). A geometric equation for representing morphological field information in horizons with compound structure. *Soil Science Society of America Journal*, 81(4), 863–867.

Hirmas, D. R., Giménez, D., Nemes, A., Kerry, R., Brunsell, N. A., & Wilson, C. J. (2018). Climate-induced changes in continental-scale soil macroporosity may intensify water cycle. *Nature*, 561(7721), 100–103.

Hoosbeek, M. R., Amundson, R. G., & Bryant, R. B. (2000). Pedological modeling. In M. E. Sumner (Ed.), *Handbook of Soil Science* (pp. E–77–E–116). Boca Raton, FL: CRC Press.

Hoosbeek, M. R. & Bryant, R. B. (1992). Towards the quantitative modeling of pedogenesis—a review. *Geoderma*, 55(3-4), 183–210.

Horn, R. & Peth, S. (2012). Mechanics of unsaturated soils for agricultural applications. In P. M. Huang, Y. Li, & M. E. Sumner (Eds.), *Handbook of Soil Sciences: Properties and Processes* chapter 3, (pp. 3–1—3–30). Boca Raton, FL: CRC Press, 2nd edition.

Huang, W.-S., Tsai, H., Tsai, C.-C., Hseu, Z.-Y., & Chen, Z.-S. (2010). Subtropical soil chronosequence on Holocene marine terraces in eastern Taiwan. *Soil Science Society of America Journal*, 74(4), 1271–1283.

Hudson, B. D. (1994). Soil organic matter and available water capacity. *Journal of Soil and Water Conservation*, 49(2), 189–194.

Istanbulluoglu, E., Wang, T., Wright, O. M., & Lenters, J. D. (2012). Interpretation of hydrologic trends from a water balance perspective: The role of groundwater storage in the Budyko hypothesis. *Water Resources Research*, 48(3), W00H16.

Janzen, H. H., Fixen, P. E., Franzluebbers, A. J., Hattey, J., Izaurralde, R. C., Ketterings, Q. M., Lobb, D. A., & Schlesinger, W. H. (2011). Global prospects rooted in soil science. *Soil Science Society of America Journal*, 75(1), 1–8.

Jarvis, N., Koestel, J., Messing, I., Moeys, J., & Lindahl, A. (2013). Influence of soil, land use and climatic factors on the hydraulic conductivity of soil. *Hydrology and Earth System Sciences*, 17(12), 5185–5195.

Jones, J. A., Creed, I. F., Hatcher, K. L., Warren, R. J., Adams, M. B., Benson, M. H., Boose, E., Brown, W. A., Campbell, J. L., Covich, A., et al. (2012). Ecosystem processes and human influences regulate streamflow response to climate change at long-term ecological research sites. *BioScience*, 62(4), 390–404.

Jorda, H., Bechtold, M., Jarvis, N., & Koestel, J. (2015). Using boosted regression trees to explore key factors controlling saturated and near-saturated hydraulic conductivity. *European Journal of Soil Science*, 66(4), 744–756.

Kabacoff, R. I. (2015). *R in Action: Data analysis and graphics with R*. Shelter Island, NY: Manning Publications Co., 2nd edition.

Kahle, M., Kleber, M., & Jahn, R. (2002). Carbon storage in loess derived surface soils from Central Germany: Influence of mineral phase variables. *Journal of Plant Nutrition and Soil Science*, 165(2), 141–149.

Kendrick, K. J. & McFadden, L. D. (1996). Comparison and contrast of processes of soil formation in the San Timoteo Badlands with chronosequences in California. *Quaternary Research*, 46(2), 149–160.

Kleber, M., Sollins, P., & Sutton, R. (2007). A conceptual model of organo-mineral interactions in soils: self-assembly of organic molecular fragments into zonal structures on mineral surfaces. *Biogeochemistry*, 85(1), 9–24.

Koop, A. N., Hirmas, D. R., Sullivan, P. L., & Mohammed, A. K. (2020). A generalizable index of soil development. *Geoderma*, 360, 113898.

Korkmaz, S., Goksuluk, D., & Zararsiz, G. (2014). MVN: An R package for assessing multivariate normality. *The R Journal*, 6(2), 151–162.

Koster, R. D. & Suarez, M. J. (1999). A simple framework for examining the interannual variability of land surface moisture fluxes. *Journal of Climate*, 12(7), 1911–1917.

Kurtay, T. & Reece, A. R. (1970). Plasticity theory and critical state soil mechanics. *Journal of Terramechanics*, 7(3-4), 23–56.

Langley Turnbaugh, S. J. & Evans, C. V. (1994). A determinative soil development index for pedo-stratigraphic studies. *Geoderma*, 61(1-2), 39–59.

Layzell, A. L., Mandel, R. D., Rittenour, T. M., Smith, J. J., Harlow, R. H., & Ludvigson, G. A. (2016). Stratigraphy, morphology, and geochemistry of late Quaternary buried soils on the High Plains of southwestern Kansas, USA. *Catena*, 144, 45–55.

Lebedeva, M. P., Golovanov, D. L., & Inozemtsev, S. A. (2009). Microfabrics of desert soils of Mongolia. *Eurasian Soil Science*, 42(11), 1204–1217.

Li, D., Pan, M., Cong, Z., Zhang, L., & Wood, E. (2013). Vegetation control on water and energy balance within the Budyko framework. *Water Resources Research*, 49(2), 969–976.

Logan, M. (2010). *Biostatistical Design and Analysis Using R: A Practical Guide*. Hoboken, NJ: Wiley-Blackwell, 1st edition.

Lybrand, R. A. & Rasmussen, C. (2015). Quantifying climate and landscape position controls on soil development in semiarid ecosystems. *Soil Science Society of America Journal*, 79(1), 104–116.

May, J.-H., Wells, S. G., Cohen, T. J., Marx, S. K., Nanson, G. C., & Baker, S. E. (2015). A soil chronosequence on Lake Mega-Frome beach ridges and its implications for late Quaternary pedogenesis and paleoenvironmental conditions in the drylands of southern Australia. *Quaternary Research*, 83(1), 150–165.

McAuliffe, J. R. (1994). Landscape evolution, soil formation, and ecological patterns and processes in Sonoran Desert bajadas. *Ecological Monographs*, 64(2), 111–148.

McCalpin, J. P. & Berry, M. E. (1996). Soil catenas to estimate ages of movements on normal fault scarps, with an example from the Wasatch fault zone, Utah, USA. *Catena*, 27(3-4), 265–286.

McFadden, L. D., McDonald, E. V., Wells, S. G., Anderson, K., Quade, J., & Forman, S. L. (1998). The vesicular layer and carbonate collars of desert soils and pavements: formation, age and relation to climate change. *Geomorphology*, 24(2-3), 101–145.

McFadden, L. D. & Weldon II, R. J. (1987). Rates and processes of soil development on Quaternary terraces in Cajon Pass, California. *Geological Society of America Bulletin*, 98(3), 280–293.

McFadden, L. D., Wells, S. G., & Dohrenwend, J. C. (1986). Influences of Quaternary climatic changes on processes of soil development on desert loess deposits of the Cima Volcanic Field, California. *Catena*, 13(4), 361–389.

Meixner, R. E. & Singer, M. J. (1981). Use of a field morphology rating system to evaluate soil formation and discontinuities. *Soil Science*, 131(2), 114–123.

Mezentsev, V. (1955). More on the calculation of average total evaporation. *Meteorologiya i Gidrologiya*, 5, 24–26.

Milborrow, S. (2021). rpart.plot: plot 'rpart' models: an enhanced version of 'plot.rpart'. R package version 3.1.0. http://www.milbo.org/rpart-plot/index.html.

Miller, D. C. & Birkeland, P. W. (1992). Soil catena variation along an alpine climatic transect, northern Peruvian Andes. *Geoderma*, 55(3-4), 211–223.

Milly, P. C. D. (1994). Climate, soil water storage, and the average annual water balance. *Water Resources Research*, 30(7), 2143–2156.

Minasny, B., McBratney, A. B., & Salvador-Blanes, S. (2008). Quantitative models for pedogenesis—A review. *Geoderma*, 144(1-2), 140–157.

Mohammed, A. K., Hirmas, D. R., Giménez, D., Mandel, R. D., & Miller, J. R. (2016). A digital morphometric approach for quantifying ped shape. *Soil Science Society of America Journal*, 80(6), 1604–1618.

Mohammed, A. K., Hirmas, D. R., Nemes, A., & Giménez, D. (2020). Exogenous and endogenous controls on the development of soil structure. *Geoderma*, 357, 113945.

Mount, J. & Zumel, N. (2020). vtreat: A Statistically Sound 'data.frame' Processor/Conditioner. https://github.com/WinVector/vtreat/, https://winvector.github.io/vtreat/.

Mu, Q., Heinsch, F. A., Zhao, M., & Running, S. W. (2007). Development of a global evapotranspiration algorithm based on MODIS and global meteorology data. *Remote Sensing of Environment*, 111(4), 519–536.

Mu, Q., Zhao, M., & Running, S. W. (2011). Improvements to a MODIS global terrestrial evapotranspiration algorithm. *Remote Sensing of Environment*, 115(8), 1781–1800.

Muggeo, V. M. R. (2003). Estimating regression models with unknown break-points. *Statistics in Medicine*, 22(19), 3055–3071.

Muggeo, V. M. R. (2008). segmented: An R package to fit regression models with broken-line relationships. *R News*, 8(1), 20–25.

Munroe, J. S. & Bockheim, J. G. (2001). Soil development in low-arctic tundra of the northern Brooks Range, Alaska, USA. *Arctic, Antarctic, and Alpine Research*, 33(1), 78–87.

Musick, H. B. (1975). Barrenness of desert pavement in Yuma County, Arizona. *Journal of the Arizona Academy of Science*, 10(1), 24–28.

Nemes, A., Rawls, W. J., & Pachepsky, Y. A. (2005). Influence of organic matter on the estimation of saturated hydraulic conductivity. *Soil Science Society of America Journal*, 69(4), 1330–1337.

Nesbitt, H. W. & Young, G. M. (1982). Early Proterozoic climates and plate motions inferred from major element chemistry of lutites. *Nature*, 299(5885), 715–717.

Noy-Meir, I. (1973). Desert ecosystems: Environment and producers. *Annual Review of Ecology and Systematics*, 4(1), 25–51.

Oades, J. M. (1984). Soil organic matter and structural stability: mechanisms and implications for management. *Plant and Soil*, 76(1), 319–337.

Oades, J. M. (1993). The role of biology in the formation, stabilization and degradation of soil structure. *Geoderma*, 56, 377–400.

Omernik, J. M. & Griffith, G. E. (2014). Ecoregions of the conterminous United States: Evolution of a hierarchical spatial framework. *Environmental Management*, 54(6), 1249–1266.

Padrón, R. S., Gudmundsson, L., Greve, P., & Seneviratne, S. I. (2017). Large-scale controls of the surface water balance over land: Insights from a systematic review and meta-analysis. *Water Resources Research*, 53(11), 9659–9678.

Panakoulia, S. K., Nikolaidis, N. P., Paranychianakis, N. V., Menon, M., Schiefer, J., Lair, G. J., Krám, P., & Banwart, S. A. (2017). Factors controlling soil structure dynamics and carbon sequestration across different climatic and lithological conditions. *Advances in Agronomy*, 142, 241–276.

Pawlowsky-Glahn, V. & Egozcue, J. J. (2006). Compositional data and their analysis: an introduction. In A. Buccianti, G. Mateu-Figueras, & V. Pawlowsky-Glahn (Eds.), *Compositional Data Analysis in the Geosciences: From Theory to Practice*, volume 264 (pp. 1–10). The Geological Society of London.

Phillips, J. D. (1990). Relative ages of wetland and upland surfaces as indicated by pedogenic development. *Physical Geography*, 11(4), 363–378.

Phillips, J. D. (1993). Progressive and regressive pedogenesis and complex soil evolution. *Quaternary Research*, 40(2), 169–176.

Porporato, A., Daly, E., & Rodriguez-Iturbe, I. (2004). Soil water balance and ecosystem response to climate change. *The American Naturalist*, 164(5), 625–632.

Potter, N. J. & Zhang, L. (2009). Interannual variability of catchment water balance in Australia. *Journal of Hydrology*, 369(1-2), 120–129.

Potter, N. J., Zhang, L., Milly, P. C. D., McMahon, T. A., & Jakeman, A. J. (2005). Effects of rainfall seasonality and soil moisture capacity on mean annual water balance for Australian catchments. *Water Resources Research*, 41(6), W06007.

PRISM Climate Group, Oregon State University (2021). Parameter-elevation Regressions on Independent Slopes Model. http://prism.oregonstate.edu.

Rabot, E., Wiesmeier, M., Schlüter, S., & Vogel, H.-J. (2018). Soil structure as an indicator of soil functions: A review. *Geoderma*, 314, 122–137.

Rawls, W. J., Brakensiek, D. L., & Saxton, K. E. (1982). Estimation of soil water properties. *Transactions of the American Society of Agricultural Engineers*, 25(5), 1316–1320.

Rawls, W. J., Giménez, D., & Grossman, R. (1998). Use of soil texture, bulk density, and slope of the water retention curve to predict saturated hydraulic conductivity. *Transactions of the ASAE*, 41(4), 983–988.

Rawls, W. J., Nemes, A., & Pachepsky, Y. A. (2004). Effect of soil organic carbon on soil hydraulic properties. *Developments in Soil Science*, 30, 95–114.

Rawls, W. J., Pachepsky, Y. A., Ritchie, J. C., Sobecki, T. M., & Bloodworth, H. (2003). Effect of soil organic carbon on soil water retention. *Geoderma*, 116(1-2), 61–76.

Regelink, I. C., Stoof, C. R., Rousseva, S., Weng, L., Lair, G. J., Kram, P., Nikolaidis, N. P., Kercheva, M., Banwart, S., & Comans, R. N. (2015). Linkages between aggregate formation, porosity and soil chemical properties. *Geoderma*, 247, 24–37.

Reheis, M. C., Harden, J. W., McFadden, L. D., & Shroba, R. R. (1989). Development rates of late Quaternary soils, Silver Lake Playa, California. *Soil Science Society of America Journal*, 53(4), 1127–1140.

Rivera, J. I. & Bonilla, C. A. (2020). Predicting soil aggregate stability using readily available soil properties and machine learning techniques. *Catena*, 187, 104408.

Robinson, D. A., Jones, S. B., Lebron, I., Reinsch, S., Domínguez, M. T., Smith, A. R., Jones, D. L., Marshall, M. R., & Emmett, B. A. (2016). Experimental evidence for drought induced alternative stable states of soil moisture. *Scientific Reports*, 6(1), 1–6.

Rodbell, D. T. (1990). Soil-age relationships on late Quaternary moraines, Arrowsmith Range, Southern Alps, New Zealand. *Arctic and Alpine Research*, 22(4), 355–365.

Rouholahnejad Freund, E. & Kirchner, J. W. (2017). A Budyko framework for estimating how spatial heterogeneity and lateral moisture redistribution affect average evapotranspiration rates as seen from the atmosphere. *Hydrology and Earth System Sciences*, 21(1), 217–233.

Sankarasubramanian, A. & Vogel, R. M. (2002). Annual hydroclimatology of the United States. *Water Resources Research*, 38(6), 19–1.

Sauer, D. (2010). Approaches to quantify progressive soil development with time in Mediterranean climate—I. Use of field criteria. *Journal of Plant Nutrition and Soil Science*, 173(6), 822–842.

Saxton, K. E. & Rawls, W. J. (2006). Soil water characteristic estimates by texture and organic matter for hydrologic solutions. *Soil Science Society of America Journal*, 70(5), 1569–1578.

Schaetzl, R. J., Barrett, L. R., & Winkler, J. A. (1994). Choosing models for soil chronofunctions and fitting them to data. *European Journal of Soil Science*, 45(2), 219–232.

Schaetzl, R. J. & Mokma, D. L. (1988). A numerical index of podzol and podzolic soil development. *Physical Geography*, 9(3), 232–246.

Schaetzl, R. J. & Thompson, M. L. (2015). *Soils: Genesis and Geomorphology*. New York: Cambridge University Press, 2nd edition.

Shao, Q., Traylen, A., & Zhang, L. (2012). Nonparametric method for estimating the effects of climatic and catchment characteristics on mean annual evapotranspiration. *Water Resources Research*, 48(3), W03517.

Six, J., Bossuyt, H., Degryze, S., & Denef, K. (2004). A history of research on the link between (micro) aggregates, soil biota, and soil organic matter dynamics. *Soil and Tillage Research*, 79(1), 7–31.

Six, J., Paustian, K., Elliott, E. T., & Combrink, C. (2000). Soil structure and organic matter I. Distribution of aggregate-size classes and aggregate-associated carbon. *Soil Science Society of America Journal*, 64(2), 681–689.

Soil Science Division Staff (2017). Soil survey manual. In C. Ditzler, K. Scheffe, & H. C. Monger (Eds.), *USDA Handbook 18*. Washington, D.C.: Government Printing Office.

Soil Survey Staff (2014a). Kellogg Soil Survey Laboratory Methods Manual. In R. Burt & Soil Survey Staff (Eds.), *Soil Survey Investigations Report No. 42, Version 5.0*. USDA Natural Resources Conservation Service.

Soil Survey Staff (2014b). *Keys to Soil Taxonomy*. USDA Natural Resources Conservation Service, 12th edition.

Sollins, P., Kramer, M. G., Swanston, C., Lajtha, K., Filley, T., Aufdenkampe, A. K., Wagai, R., & Bowden, R. D. (2009). Sequential density fractionation across soils of contrasting mineralogy: evidence for both microbial-and mineral-controlled soil organic matter stabilization. *Biogeochemistry*, 96(1), 209–231.

Sposito, G. (2017). Understanding the Budyko equation. *Water*, 9(4), 236.

Stamati, F. E., Nikolaidis, N. P., Banwart, S., & Blum, W. E. H. (2013). A coupled carbon, aggregation, and structure turnover (CAST) model for topsoils. *Geoderma*, 211-212, 51–64.

Stevenson, F. J. (1994). *Humus Chemistry. Genesis, Composition, Reactions*. New York, NY: John Wiley & Sons.

Stewart, C. E., Plante, A. F., Paustian, K., Conant, R. T., & Six, J. (2008). Soil carbon saturation: Linking concept and measurable carbon pools. *Soil Science Society of America Journal*, 72(2), 379–392.

Sullivan, P. L., Billings, S. A., Hirmas, D. R., Li, L., Zhang, X., Ziegler, S., Murenbeeld, K., Ajami, H., Guthrie, A., Singha, K., Giménez, D., Duro, A., Moreno, V., Flores, A., Cueva, A., Koop, A. N., Aronson, E. L., Barnard, H. R., Banwart, S. A., Keen, R. M., Nemes, A., Nikolaidis, N. P., Nippert, J. B., Richter, D., Robinson, D. A., Sadayappan, K., de Souza, L. F. T., Unruh, M., & Wen, H. (2022). Embracing the dynamic nature of soil structure: A paradigm illuminating the role of life in critical zones of the Anthropocene. *Earth-Science Reviews*, 225, 103873.

Swanson, D. K. (1985). Soil catenas on Pinedale and Bull Lake moraines, Willow Lake, Wind River Mountains, Wyoming. *Catena*, 12(4), 329–342.

Switzer, P., Harden, J. W., & Mark, R. K. (1988). A statistical method for estimating rates of soil development and ages of geologic deposits: A design for soil-chronosequence studies. *Mathematical Geology*, 20(1), 49–61.

Therneau, T., Atkinson, B., & Ripley, B. (2019). rpart: recursive partitioning and regression trees. R package version 4.1-15. https://cran.r-project.org/package=rpart.

Thompson, J. A. & Bell, J. C. (1996). Color index for identifying hydric conditions for seasonally saturated Mollisols in Minnesota. *Soil Science Society of America Journal*, 60(6), 1979–1988.

Tisdall, J. M. & Oades, J. M. (1982). Organic matter and water-stable aggregates in soils. *Journal of Soil Science*, 33(2), 141–163.

Torrent, J., Schwertmann, U., Fechter, H., & Alferez, F. (1983). Quantitative relationships between soil color and hematite content. *Soil Science*, 136(6), 354–358.

Trancoso, R., Larsen, J. R., McAlpine, C., McVicar, T. R., & Phinn, S. (2016). Linking the Budyko framework and the Dunne diagram. *Journal of Hydrology*, 535, 581–597.

Troch, P. A., Carrillo, G., Sivapalan, M., Wagener, T., & Sawicz, K. (2013). Climate-vegetation-soil interactions and long-term hydrologic partitioning: signatures of catchment co-evolution. *Hydrology and Earth System Sciences*, 17(6), 2209–2217.

Trumbore, S. (2000). Age of soil organic matter and soil respiration: Radiocarbon constraints on belowground C dynamics. *Ecological Applications*, 10(2), 399–411.

Tsai, H., Hseu, Z.-Y., Huang, W.-S., & Chen, Z.-S. (2007a). Pedogenic approach to resolving the geomorphic evolution of the Pakua river terraces in central Taiwan. *Geomorphology*, 83(1-2), 14–28.

Tsai, H., Hseu, Z.-Y., Kuo, H.-Y., Huang, W.-S., & Chen, Z.-S. (2016). Soilscape of west-central Taiwan: Its pedogenesis and geomorphic implications. *Geomorphology*, 255, 81–94.

Tsai, H., Huang, W.-S., & Hseu, Z.-Y. (2007b). Pedogenic correlation of lateritic river terraces in central Taiwan. *Geomorphology*, 88(3-4), 201–213.

Turk, J. K., Chadwick, O. A., & Graham, R. C. (2012). Pedogenic Processes. In P. M. Huang, Y. Li, & M. E. Sumner (Eds.), *Handbook of Soil Sciences: Properties and Processes* chapter 30, (pp. 30–1—30–29). Boca Raton, FL: CRC Press, 2nd edition.

Turk, J. K., Goforth, B. R., Graham, R. C., & Kendrick, K. J. (2008). Soil morphology of a debris flow chronosequence in a coniferous forest, southern California, USA. *Geoderma*, 146(1-2), 157–165.

Turk, J. K. & Graham, R. C. (2011). Distribution and properties of vesicular horizons in the western United States. *Soil Science Society of America Journal*, 75(4), 1449–1461.

Turk, J. K. & Graham, R. C. (2014). Analysis of vesicular porosity in soils using high resolution X-ray computed tomography. *Soil Science Society of America Journal*, 78(3), 868–880.

Turk, J. K. & Graham, R. C. (2020). Disturbance impacts on porosity and hydraulic properties of vesicular horizons. *Soil Science Society of America Journal*, 84(2), 543–555.

Valentin, C. (1994). Surface sealing as affected by various rock fragment covers in West Africa. *Catena*, 23(1-2), 87–97.

Valentin, C. & Casenave, A. (1992). Infiltration into sealed soils as influenced by gravel cover. *Soil Science Society of America Journal*, 56(6), 1667–1673.

Vereecken, H., Schnepf, A., Hopmans, J. W., Javaux, M., Or, D., Roose, T., Vanderborght, J., Young, M. H., Amelung, W., Aitkenhead, M., et al. (2016). Modeling soil processes: Review, key challenges, and new perspectives. *Vadose Zone Journal*, 15(5), 1–57.

Verheyen, K., Adriaens, D., Hermy, M., & Deckers, S. (2001). High-resolution continuous soil classification using morphological soil profile descriptions. *Geoderma*, 101(3-4), 31–48.

Vidic, N. J. (1998). Soil-age relationships and correlations: comparison of chronosequences in the Ljubljana Basin, Slovenia and USA. *Catena*, 34(1-2), 113–129.

Vidic, N. J. & Lobnik, F. (1997). Rates of soil development of the chronosequence in the Ljubljana Basin, Slovenia. *Geoderma*, 76(1-2), 35–64.

Walker, P. H. & Green, P. (1976). Soil trends in two valley fill sequences. *Australian Journal of Soil Research*, 14(3), 291–303.

Wang, D. & Wu, L. (2013). Similarity of climate control on base flow and perennial stream density in the Budyko framework. *Hydrology and Earth System Sciences*, 17(1), 315–324.

Wang, T., Istanbulluoglu, E., Lenters, J., & Scott, D. (2009a). On the role of groundwater and soil texture in the regional water balance: An investigation of the Nebraska Sand Hills, USA. *Water Resources Research*, 45(10), W10413.

Wang, T., Wedin, D., & Zlotnik, V. A. (2009b). Field evidence of a negative correlation between saturated hydraulic conductivity and soil carbon in a sandy soil. *Water Resources Research*, 45(7).

Wang, Y., Shao, M., Liu, Z., & Horton, R. (2013). Regional-scale variation and distribution patterns of soil saturated hydraulic conductivities in surface and subsurface layers in the loessial soils of China. *Journal of Hydrology*, 487, 13–23.

Watson, K. W. & Luxmoore, R. J. (1986). Estimating macroporosity in a forest watershed by use of a tension infiltrometer. *Soil Science Society of America Journal*, 50(3), 578–582.

Williams, C. A., Reichstein, M., Buchmann, N., Baldocchi, D., Beer, C., Schwalm, C., Wohlfahrt, G., Hasler, N., Bernhofer, C., Foken, T., et al. (2012). Climate and vegetation controls on the surface water balance: Synthesis of evapotranspiration measured across a global network of flux towers. *Water Resources Research*, 48(6), W06523.

Wood, Y. A., Graham, R. C., & Wells, S. G. (2005). Surface control of desert pavement pedologic process and landscape function, Cima Volcanic Field, Mojave Desert, California. *Catena*, 59(2), 205–230.

Wu, X., Wei, Y., Wang, J., Wang, D., She, L., Wang, J., & Cai, C. (2017). Effects of soil physico-chemical properties on aggregate stability along a weathering gradient. *Catena*, 156, 205–215.

Xu, X., Liu, W., Scanlon, B. R., Zhang, L., & Pan, M. (2013). Local and global factors controlling water-energy balances within the Budyko framework. *Geophysical Research Letters*, 40(23), 6123–6129.

Yaalon, D. H. (1975). Conceptual models in pedogenesis: can soil-forming functions be solved? *Geoderma*, 14(3), 189–205.

Yang, D., Sun, F., Liu, Z., Cong, Z., Ni, G., & Lei, Z. (2007). Analyzing spatial and temporal variability of annual water-energy balance in nonhumid regions of China using the Budyko hypothesis. *Water Resources Research*, 43(4), W04426.

Yang, H., Yang, D., Lei, Z., & Sun, F. (2008). New analytical derivation of the mean annual water-energy balance equation. *Water Resources Research*, 44(3), W03410.

Yokoo, Y., Sivapalan, M., & Oki, T. (2008). Investigating the roles of climate seasonality and landscape characteristics on mean annual and monthly water balances. *Journal of Hydrology*, 357(3-4), 255–269.

Zhang, L., Dawes, W. R., & Walker, G. R. (2001). Response of mean annual evapotranspiration to vegetation changes at catchment scale. *Water Resources Research*, 37(3), 701–708.

Zhang, L., Potter, N., Hickel, K., Zhang, Y., & Shao, Q. (2008). Water balance modeling over variable time scales based on the Budyko framework–Model development and testing. *Journal of Hydrology*, 360(1-4), 117–131.

Zhou, G., Wei, X., Chen, X., Zhou, P., Liu, X., Xiao, Y., Sun, G., Scott, D. F., Zhou, S., Han, L., & Su, Y. (2015). Global pattern for the effect of climate and land cover on water yield. *Nature Communications*, 6(1), 5918.

Zielhofer, C., Espejo, J. M. R., Granados, M. À. N., & Faust, D. (2009). Durations of soil formation and soil development indices in a Holocene Mediterranean floodplain. *Quaternary International*, 209(1-2), 44–65.

Zumel, N. (2016a). Principal Components Regression, Pt. 2: Y-Aware Methods. https://github.com/WinVector/Examples/blob/master/PCR/YAwarePCA.Rmd.

Zumel, N. (2016b). Principal Components Regression, Pt. 3: Picking the Number of Components. https://github.com/WinVector/Examples/blob/master/PCR/YAwarePCR_pickK.Rmd.

Zumel, N. & Mount, J. (2020). *Practical Data Science with R*. Shelter Island, NY: Manning Publications Co., 2nd edition.

Appendix A

Supplemental information for Chapter 2

Table A1: Description of the data used in this study.

Variable	Variable description/ explanation	Unit	Number of Obs.	Data Source
Horizon designation	Symbols used to designate layers within the soil (master horizons and suffix symbols)		57171	NRCS-NCSS
Top horizon depth	The distance from the soil surface to the upper boundary of the soil horizon		57171	NRCS-NCSS
Bottom horizon depth	The distance from the soil surface to the lower boundary of the soil horizon		57171	NRCS-NCSS
Munsell hue	Measure of the dominant wavelength of light using the Munsell notation system		53479	NRCS-NCSS
Munsell value	Measure of the lightness of soil color relative to neutral gray using the Munsell notation system		53473	NRCS-NCSS
Munsell chroma	Measure of the relative strength of a spectral color using the Munsell notation system		53206	NRCS-NCSS
Ped/void surface feature	Type of ped/void surface feature present (e.g., clay films)		19583	NRCS-NCSS
Ped/void surface feature percentage	Relative percent of the total surface area occupied by a ped/void surface feature (e.g., clay films) in a horizon	%	15049	NRCS-NCSS
Ped/void surface feature distinctness	Relative extent to which a ped/void surface feature (e.g., clay films) visually stand out from adjacent material; described as either faint, distinct, or prominent		10109	NRCS-NCSS
Fine clay	$<$0.0002 mm particle diameter mass fraction reported on a fine-earth ($<$2 mm) basis	%	12146	NRCS-NCSS
Total clay	$<$0.002 mm particle diameter mass fraction reported on a fine-earth ($<$2 mm) basis	%	57171	NRCS-NCSS

Variable	Variable description/ explanation	Unit	Number of Obs.	Data Source
Fine silt	0.002 to 0.02 mm particle diameter mass fraction reported on a fine-earth (<2 mm) basis	%	51005	NRCS-NCSS
Coarse silt	0.02 to 0.05 mm particle diameter mass fraction reported on a fine-earth (<2 mm) basis	%	51018	NRCS-NCSS
Total silt	0.002 to 0.05 mm particle diameter mass fraction reported on a fine-earth (<2 mm) basis	%	57171	NRCS-NCSS
Very fine sand	0.05 to 0.10 mm particle diameter mass fraction reported on a fine-earth (<2 mm) basis	%	53993	NRCS-NCSS
Fine sand	0.10 to 0.25 mm particle diameter mass fraction reported on a fine-earth (<2 mm) basis	%	53947	NRCS-NCSS
Medium sand	0.25 to 0.50 mm particle diameter mass fraction reported on a fine-earth (<2 mm) basis	%	53911	NRCS-NCSS
Coarse sand	0.50 to 1.0 mm particle diameter mass fraction reported on a fine-earth (<2 mm) basis	%	53854	NRCS-NCSS
Very coarse sand	1.0 to 2.0 mm particle diameter mass fraction reported on a fine-earth (<2 mm) basis	%	53669	NRCS-NCSS
Total sand	0.05 to 2.0 mm particle diameter mass fraction reported on a fine-earth (<2 mm) basis	%	57171	NRCS-NCSS
CCE	Calcium carbonate equivalent mass fraction on a <2 mm basis measured by CO_2 evolution after acid treatment	%	16786	NRCS-NCSS

Variable	Variable description/ explanation	Unit	Number of Obs.	Data Source
Al	Aluminum measured after total dissolution of the <2 mm fraction reported on an oxide basis	mg kg^{-1}	953	NRCS-NCSS
Ca	Calcium measured after total dissolution of the <2 mm fraction reported on an oxide basis	mg kg^{-1}	953	NRCS-NCSS
K	Potassium measured after total dissolution of the <2 mm fraction reported on an oxide basis	mg kg^{-1}	953	NRCS-NCSS
Na	Sodium measured after total dissolution of the <2 mm fraction reported on an oxide basis	mg kg^{-1}	947	NRCS-NCSS
Gibbsite	Identified on oriented clay slides by XRD; XRD peak height given as one of 5 semiquantitative classes: 5 = very large, 4 = large, 3 = medium, 2 = small, and 1 = very small		359	NRCS-NCSS
Halloysite	Identified on oriented clay slides by XRD; XRD peak height given as one of 5 semiquantitative classes: 5 = very large, 4 = large, 3 = medium, 2 = small, and 1 = very small		236	NRCS-NCSS
Illite	Identified on oriented clay slides by XRD; XRD peak height given as one of 5 semiquantitative classes: 5 = very large, 4 = large, 3 = medium, 2 = small, and 1 = very small		16	NRCS-NCSS
Kaolinite	Identified on oriented clay slides by XRD; XRD peak height given as one of 5 semiquantitative classes: 5 = very large, 4 = large, 3 = medium, 2 = small, and 1 = very small		5122	NRCS-NCSS

Variable	Variable description/ explanation	Unit	Number of Obs.	Data Source
Montmorillonite	Identified on oriented clay slides by XRD; XRD peak height given as one of 5 semiquantitative classes: 5 = very large, 4 = large, 3 = medium, 2 = small, and 1 = very small		3476	NRCS-NCSS
Vermiculite	Identified on oriented clay slides by XRD; XRD peak height given as one of 5 semiquantitative classes: 5 = very large, 4 = large, 3 = medium, 2 = small, and 1 = very small		2065	NRCS-NCSS
Argillic horizon	Binary value indicating the presence (1) or absence (0) of an argillic horizon within the depth of the morphological horizon		6283	NRCS-NCSS
Cambic horizon	Binary value indicating the presence (1) or absence (0) of a cambic horizon within the depth of the morphological horizon		1628	NRCS-NCSS
Soil order	Highest level of US Soil Taxonomy		57171	NRCS-NCSS
Drainage class	Natural drainage conditions of the soil; refers to the frequency and duration of wet periods (e.g., well drained)		366	NRCS-NCSS
MAP	Mean annual precipitation calculated as the sum of each mean monthly precipitation	mm	57171	WorldClim 2

Table A2: Example pedon data from the Burchard Series (Pedon ID = S19971A047014). Data taken from the USDA-NRCS NCSS Soil Characterization Data (https: // ncsslabdatamart.sc.egov.usda.gov/).

Horizon	**Depth**	**Color**[a]	**Particle-size distribution**[b]**(%)**								**CCE**[c]	**Clay films**[d]	
	(cm)		**C**	**fSi**	**coSi**	**vfS**	**fS**	**mS**	**coS**	**vcS**	**(%)**	**Amnt. (%)**	**Dist.**
A	0-20	10YR 3/2	33.7	17.9	20.9	5.5	10.2	8.0	2.9	0.9	0	NR	NR
AB	20-35	10YR 4/3	36.4	17.5	18.8	5.6	9.3	7.9	2.9	1.6	0	NR	NR
Bt	35-53	10YR 4/4	36.2	19.2	16.4	5.9	8.8	7.4	3.8	2.3	4	40	F
Btk	53-67	7.5YR 5/4	34.8	19.8	15.9	6.0	9.5	8.0	3.2	2.8	15	20	F
Bk1	67-97	7.5YR 5/4	34.9	21.1	15.1	6.2	9.4	8.0	3.7	1.6	15	NR	NR
Bk2	97-120	7.5YR 5/4	34.8	21.0	15.0	6.4	8.7	7.6	3.7	2.8	14	NR	NR
C	120-142	7.5YR 5/4	35.3	19.9	15.4	6.5	9.1	7.7	4.0	2.1	15	NR	NR

[a]Dominant moist matrix color.
[b]C, clay ($<$2 μm, d = 0.14 μm); fSi, Fine silt (2-20 μm, d = 6.34 μm); coSi, Coarse silt (20-50 μm, d = 31.63 μm); vfS, Very fine sand (50-100 μm, d = 70.72 μm); fS, Fine sand (100-250 μm, d = 158.12 μm); mS, Medium sand (250-500 μm, d = 353.56 μm); coS, Coarse sand (500-1000 μm, d = 707.12 μm); vcS, Very coarse sand (1000-2000 μm, d = 1414.22 μm).
[c]CCE, Calcium carbonate equivalent.
[d]Amnt., Amount; Dist., Distinctness; F, faint; NR, none recorded.

Table A3: HDI and PDI calculations for the example data given in Table A2.

Variable	**Horizon**							**Pedon**
	A	**AB**	**Bt**	**Btk**	**Bk1**	**Bk2**	**C**	
General								
i	1	2	3	4	5	6	7	
N								7
t (cm)	20	15	18	14	30	23	22	
Particle-size distribution								
h	E	E	I	I	I	I	I	
k	1	2						
g			1	2	3	4	5	
n								2
p								5
$D_i/D_k/D_g$ (μm)	6.49	5.70	5.82	6.39	6.04	6.24	6.14	
${}^{E}\overline{D}$ (μm)								6.15
${}^{I}\overline{D}$ (μm)								6.10
$\tilde{s}_D$ (μm)								0.29
$\tilde{z}_{D_i}$	1.32	-1.38	-1.14	0.81	-0.39	0.31	-0.05	
S_{D_i}	1.32	0	1.14	0	0.39	0	0.05	
$\max(S_D)$[a]								1.46
$\min(S_D)$[a]								-1.06
HDI_{D_i}	0.47	0	0.44	0	0.26	0	0	
Calcium carbonate equivalent (CCE)								
h	E	E	E	I	I	I	I	
k	1	2	3					
g				1	2	3	4	
n								3
p								4
$\mathrm{CCE}_i/\mathrm{CCE}_k/\mathrm{CCE}_g$ (%)	0	0	4	15	15	14	15	
${}^{E}\overline{\mathrm{CCE}}$ (%)								1.36
${}^{I}\overline{\mathrm{CCE}}$ (%)								14.66
$\tilde{s}_{\mathrm{CCE}}$ (%)								1.43
$\tilde{z}_{\mathrm{CCE}_i}$	-10.23	-10.23	-7.44	9.52	9.52	8.82	9.52	
S_{CCE_i}	10.23	10.23	7.44	9.52	9.52	8.82	9.52	
$\max(S_{\mathrm{CCE}})$[a]								1.54
$\min(S_{\mathrm{CCE}})$[a]								-0.45
$\mathrm{HDI}_{\mathrm{CCE}_i}$	0.73	0.73	0.67	0.72	0.72	0.70	0.72	

Variable	Horizon							Pedon
	A	**AB**	**Bt**	**Btk**	**Bk1**	**Bk2**	**C**	
Soil color								
h	*A*	*A*	*EBC*	*EBC*	*EBC*	*EBC*	*EBC*	
k	1	2						
g			1	2	3	4	5	
n								2
p								5
$L^*_i/L^*_k/L^*_g$	60.06	67.81	67.62	74.55	74.55	74.55	74.55	
$a^*_i/a^*_k/a^*_g$	2.27	2.42	2.71	4.48	4.48	4.48	4.48	
${}^{A}\overline{L^*}$								63.38
${}^{EBC}\overline{L^*}$								73.39
${}^{A}\overline{a^*}$								2.33
${}^{EBC}\overline{a^*}$								4.18
$\tilde{s}_{L^*}$								3.19
$\tilde{s}_{a^*}$								0.62
S_{c_i}	4.18	1.75	0.61	3.46	3.46	3.46	3.46	
$\max(S_c)$[a]								1.37
$\min(S_c)$[a]								−0.92
HDI_{c_i}	0.67	0.51	0.31	0.64	0.64	0.64	0.64	
Clay films								
F_{a_i} (%)			40	20				
F_{d_i}			10	10				
$\max(F_{a_i})$ (%)								100
$\max(F_{d_i})$								30
$S_{F_{a_i}}$			0.40	0.20				
$S_{F_{d_i}}$			0.33	0.33				
HDI_{F_i}	0	0	0.37	0.27	0	0	0	
Profile development index								
HDI_i	0.47	0.31	0.45	0.41	0.40	0.33	0.34	
PDI								0.39

[a]Determined for the whole dataset in this study.

Appendix B

Supplemental information for Chapter 4

B.0.1 Assessing relative importance of soil, root, and climate variables on EP

Table B1 shows β–weights for the soil, root, and climate variables used in the LASSO EP regression models for A, Ap, B, and Bp horizons across the ETF, GP, MC, NAD, and NWFM ecoregions considered in this study. The sign of each β–weight indicates either a positive $(+)$ or negative $(-)$ correlation between the respective variable and EP. The rescaled β–weights (i.e., rescaled by the maximum β–weight for each of the twenty ecoregion horizon models) are displayed in Fig. B.1. Additional information on the LASSO EP regression models for A, Ap, B, and Bp horizons across the ecoregions is included in Table B2. Results of an assessment of the relative importance of soil, root, and climate variables on EP is presented below. The proportion of variance in EP that could be predicted from these variables ranged from a R^2 of 0.217 (NAD Bp horizons) to 0.975 (NWFM Bp horizons), though the overall mean R^2 across all twenty models was 0.519. This indicated that these soil, root, and climate variables are generally important for predicting EP across ecoregions, though the degree of importance depended on both the ecoregion and the horizon type.

B.0.1.1 Eastern Temperate Forests

Across ETF A horizons, clay $(-)$, WSA $(+)$, and SCF $(+)$ were the most important predictors of EP (Fig. B.1). The textural control of clay (the strongest predictor) explained 1.27 times the variation in EP compared to WSA as determined by the squares of the β weights in Table B1. Clay also explained 3.84 times the variation compared to SCF, whereas the role of aggregation as indicated

Table B1: β–weights and intercepts (Int.) for soil, root, and climate variables used in the LASSO EP regression models for A, Ap, B, and Bp horizons across the ETF, GP, MC, NAD, and NWFM ecoregions. The number of horizons (n) used in each model are also included below. One asterisk indicates $0.001 < p < 0.01$ and two asterisks indicate $p < 0.001$. (SCF is sand and coarse fraction, CCSOC is complexed clay and SOC, and VFFR is very fine and fine roots.)

Horizon	n	SCF	Clay	SOM	CCSOC	WSA	Ped Size	VFFR	MAP	MAT	Int.
Eastern Temperate Forests (ETF)											
A	55	0.0814**	-0.160**	0	0	0.142**	0	0	0	0	-1.65**
Ap	176	0	−0.256**	0	0	0.211**	−0.0554**	0.0311**	0	4.04**	−24.6**
B	81	0.413**	−0.445**	0	0.290*	0	−0.0803**	0.0543**	1.03**	0	−9.40**
Bp	316	0.0982**	−0.369**	0.238**	0	0.289**	−0.137**	0.0604**	−0.178**	−0.698**	4.40**
Great Plains (GP)											
A	159	0.0547**	−0.210**	0	0	0.116**	−0.0278**	0	−0.510**	0	2.10**
Ap	149	0	−0.580**	0	0	0	−0.108**	−0.00610**	−0.359**	1.37**	−6.71**
B	140	−0.0982**	−1.10**	0.0940**	0	0.356**	−0.000252*	0	−0.695**	0	4.39**
Bp	220	−0.370**	−1.38**	−0.319**	0	0.107**	−0.0244**	0.000536**	−0.784**	1.54**	−4.59**
Mediterranean California (MC)											
A	59	0.250**	0	0.654**	0.0133**	0.00624**	−0.153**	0.00122**	−0.600**	−17.8**	104**
Ap	25	0.00668**	−0.573**	0	−0.0966	0.471**	−0.100**	0.129**	−0.510**	−30.1**	173**
B	52	0	−0.854**	0	0.199**	0.0642**	0	0	0	−21.9**	123**
Bp	37	0	−0.802**	0	0.378**	0	−0.171**	−0.0246**	−0.0694**	−46.2**	262**
North American Deserts (NAD)											
A	198	0.147**	0	0.154**	0.0473**	0.150**	−0.00635**	−0.0113**	−0.120**	0.105**	−0.716**
Ap	68	0	−0.791**	0	0	0	−0.0729**	−0.0973**	0.661**	−1.25**	2.33**
B	120	0.126**	−0.531**	0.198**	0	0	0	0.0194**	0	0.0149**	−1.11**
Bp	63	0	0	0.107**	0.257**	0.0474**	0	0	0	0	−1.43**
Northwestern Forested Mountains (NWFM)											
A	92	0.0481**	0	0	−0.0196**	0.190**	−0.0799**	0	0	−8.25**	45.4**
Ap	11	0.257**	−0.0805**	0	0	0	0	0	0	0	−1.42*
B	107	0	−0.709**	0.265**	0	0.298**	0	0	−0.191**	0	0.809**
Bp	14	0.0325**	−2.25**	0.482**	−1.58**	−0.339	0.117**	0.118**	1.06**	−40.8**	222**

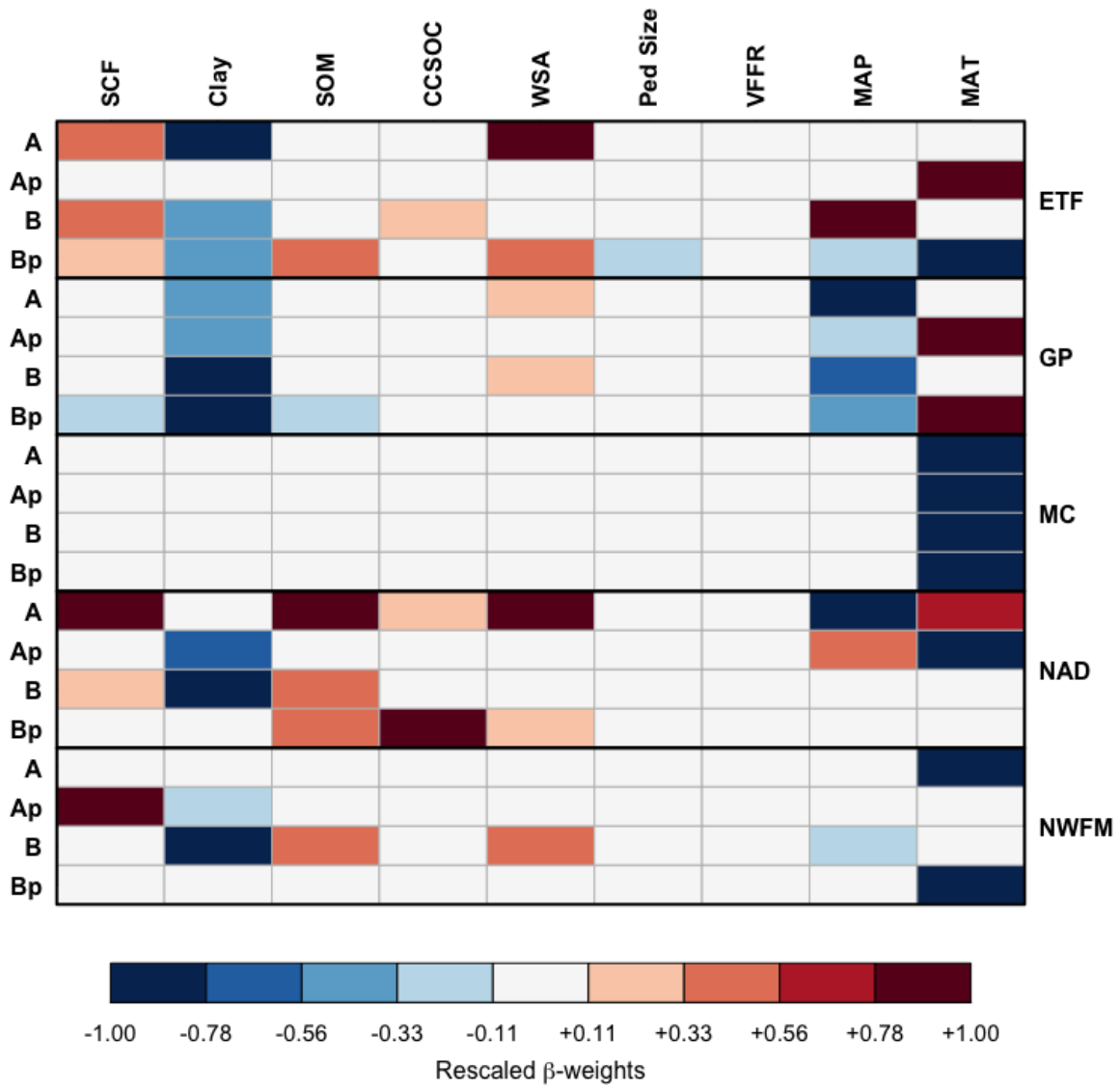

Figure B.1: Rescaled β–weights for soil, root, and climate variables comprising LASSO EP regression models for A, Ap, B, and Bp horizons across the ETF, GP, MC, NAD, and NWFM ecoregions. β–weights were rescaled by the maximum β–weight for each of the twenty ecoregion horizon models.

Table B2: λ min and intercept values from the LASSO EP regression models for A, Ap, B, and Bp horizons across the ETF, GP, MC, NAD, and NWFM ecoregions. Residual standard errors (RSE) and R^2 values for each model are also included below. All models are significant at $p < 0.001$ except for the NWFM Ap horizon model is significant at $p < 0.005$.

Horizon	**λ Min**	**Intercept**	**RSE**	R^2
ETF				
A	1.21	0.297	0.514	0.387
Ap	1.06	0.105	0.447	0.392
B	1.03	0.0772	0.440	0.550
Bp	1.03	0.0648	0.507	0.293
GP				
A	1.10	0.137	0.345	0.458
Ap	1.08	0.142	0.381	0.388
B	1.01	0.0145	0.345	0.723
Bp	1.02	0.0328	0.347	0.603
MC				
A	1.05	0.0748	0.406	0.628
Ap	1.02	0.0346	0.381	0.620
B	1.19	0.409	0.392	0.675
Bp	1.07	0.152	0.401	0.697
NAD				
A	1.03	0.0391	0.343	0.329
Ap	1.12	0.190	0.389	0.412
B	1.09	0.154	0.464	0.454
Bp	1.71	1.40	0.509	0.217
NWFM				
A	1.15	0.163	0.391	0.422
Ap	1.43	0.615	0.298	0.615
B	1.07	0.130	0.427	0.552
Bp	1.01	0.0139	0.0893	0.975

by WSA explained 3.02 times the variation in EP compared to SCF (Table B1). However, for ETF Ap horizons, the climate variable of MAT (+) was by far the most important and predominant predictor of EP explaining 250 and 366 times the variation compared to clay (−) and WSA (+), respectively (Table B1; Fig. B.1). When considering ETF B horizons, the climate variable MAP (+) was the strongest predictor of EP explaining 5.33, 6.17, and 12.6 times the variation compared to the textural controls of clay (−) and SCF (+), and the aggregating influence of CCSOC (+), respectively (Table B1; Fig. B.1). Clay explained 1.16 and 2.36 times the variation in EP compared to SCF and CCSOC, respectively, while SCF explained 2.04 times the variation compared to CCSOC (Table B1). Lastly, for ETF Bp horizons, a number of variables emerged as important predictors of EP where the strongest predictor—the climate variable of MAT (−)—explained 3.58, 5.84, 8.58, 15.4, 25.9, and 50.5 times the variation compared to the textural influence of clay (−), aggregation represented by WSA (+) and SOM (+), MAP (−), ped size (−), and SCF (+), respectively (Table B1; Fig. B.1).

B.0.1.2 Great Plains

For GP A horizons, MAP (−), clay (−), and WSA (+) were the most important predictors of EP with the climatic control of MAP explaining 5.91 and 19.3 times the variation compared to the textural influence of clay and the aggregating influence of WSA, respectively (Table B1; Fig. B.1). Clay explained 3.27 times the variation in EP compared to WSA across GP A horizons (Table B1). A shift to MAT (+) as the strongest predictor of EP occurred across GP Ap horizons with this climate variable explaining 5.56 and 14.5 times the variation compared to clay (−) and MAP (−), respectively (Table B1; Fig. B.1). The textural control of clay explained 2.61 times the variation in EP compared to the climatic influence of MAP (Table B1). With respect to GP B horizons, clay (−) emerged as the strongest predictor of EP explaining 2.49 and 9.52 times the variation compared to MAP (−) and WSA (+), respectively (Table B1; Fig. B.1). The climatic control of MAP explained 3.82 times the variation in EP compared to the role of aggregation as indicated by WSA (Table B1). Finally, for GP Bp horizons, MAT (+) emerged as the strongest predictor

of EP amongst a number of other important variables explaining 1.25, 3.85, 17.3, and 23.3 times the variation compared to clay (−), MAP (−), SCF (−), and SOM (−), respectively (Table B1; Fig. B.1).

B.0.1.3 Mediterranean California

With respect to the MC ecoregion, MAT (−) was the most important predictor of EP across all horizon types (Table B1; Fig. B.1). The climatic control of MAT was predominant as the strongest predictor of EP explaining $>$ 655 times the variation compared to each of the second strongest predictors for A, Ap, B, and Bp horizons (Table B1). However, for purposes of discussion in the next section, we mention several of these second and in some cases third and fourth strongest predictors that provide indications of the effect of MAT on soil controls of EP. Across MC A horizons, the predominant climatic control of MAT (−) on EP was followed in order of importance by the aggregating influence of SOM (+), the climatic influence of MAP (−), and the textural control of SCF (+) (Table B1). When considering MC Ap horizons, the strong role of MAT (−) on EP was followed by the textural control of clay (−), the climatic influence of MAP (−), and the aggregating influence of WSA (+) (Table B1). For MC B horizons, the predominant climatic control of MAT (−) on EP was followed by the textural influence of clay (−) and the aggregating influence of CCSOC (+) (Table B1). Lastly, across MC Bp horizons, the strong climatic influence of MAT (−) was followed by the textural control of clay (−) and the aggregating influence of CCSOC (+) (Table B1).

B.0.1.4 North American Deserts

Across NAD A horizons, SOM (+), WSA (+), SCF (+), MAP (−), MAT (+), and CCSOC (+) were the most important predictors of EP (Fig. B.1). The aggregating control of SOM (the strongest predictor) explained 1.06, 1.10, 1.64, 2.16, and 10.6 times the variation in EP compared to the additional aggregating influence of WSA, the textural influence of SCF, the climatic controls of MAP and MAT, and the additional aggregating role of CCSOC, respectively (Table B1; Fig. B.1).

With respect to NAD Ap horizons, shifts in the direction of the relationship with EP occurred for the climate variables with MAT (−), clay (−), and MAP (+) becoming the most important predictors (Fig. B.1). The climatic control of MAT explained 2.51 and 3.60 times the variation in EP compared to the textural influence of clay and the climatic influence of MAP, respectively; clay explained 1.43 times the variation compared to MAP (Table B1). For NAD B horizons, clay (−), SOM (+), and SCF (+) were the most important predictors of EP with the textural control of clay explaining 7.21 and 17.8 times the variation compared to SOM and SCF, respectively (Table B1; Fig. B.1). The role of aggregation indicated by SOM explained 2.47 times the variation in EP compared to the textural influence of SCF (Table B1). Finally, when considering NAD Bp horizons, CCSOC (+), SOM (+), and WSA (+) were the most important predictors of EP (Fig. B.1). All three of these variables provided an aggregating influence with CCSOC explaining 5.79 and 29.3 times the variation in EP compared to SOM and WSA, respectively, whereas SOM explained 5.07 times the variation compared to WSA (Table B1).

B.0.1.5 Northwestern Forested Mountains

When considering NWFM A horizons, MAT (−) was predominant as the most important predictor of EP (Fig. B.1). The climatic control of MAT was by far the strongest predictor of EP explaining 1,884 times the variation compared to aggregation as indicated by WSA (+) (Table B1). Across NWFM Ap horizons, SCF (+) and clay (−) were the most important predictors of EP with the textural control of SCF explaining 10.2 times the variation compared to the textural influence of clay (Table B1; Fig. B.1). For NWFM B horizons, clay (−), WSA (+), SOM (+), and MAP (−) were the most important predictors of EP (Fig. B.1). The textural control of clay explained 5.66, 7.17, and 13.8 times the variation in EP compared to the aggregating controls of WSA and SOM and the climatic influence of MAP, respectively (Table B1). Lastly, with respect to NWFM Bp horizons, MAT (−) was by far the most important and predominant predictor of EP explaining 327, 664, and 1,487 times the variation compared to texture (clay, −), aggregation (CCSOC, −), and MAP (+) (Table B1; Fig. B.1).